Density Fluctuations in π^+/K^+p Interactions at 250 GeV/c

F.P.M. Botterweck

Density Fluctuations in π^+/K^+p Interactions at 250 GeV/c

Density Fluctuations in π^+/K^+p Interactions at 250 GeV/c

Een wetenschappelijke proeve op het gebied
van de natuurwetenschappen, in het bijzonder de fysica.

Proefschrift

ter verkrijging van de graad van doctor
aan de Katholieke Universiteit Nijmegen,
volgens besluit van het College van Decanen
in het openbaar te verdedigen
op dinsdag 3 november 1992,
des namiddags te 3.30 uur precies,

door

Franciscus Petrus Maria Botterweck

geboren op 28 december 1963 te Geleen.

Krips Repro, Meppel
1992

Promotor: Prof. Dr. E.W. Kittel

CIP-DATA KONINKLIJKE BIBLIOTHEEK, DEN HAAG

Botterweck, Franciscus Petrus Maria

Density Fluctuations in π^+/K^+p Interactions at 250 GeV/c
Franciscus Petrus Maria Botterweck. -[S.1. : s.n.]
(Meppel : Krips Repro). - Ill.
Thesis Nijmegen. - With bibliogr. - With summary in Dutch.
ISBN 90-9005189-9
Subject headings: intermittency / density fluctuations / meson-proton interactions.

Mijn dank gaat uit naar velen:

Lex Scholten, Paul van Hal, Frans Meijers, Albert DeRoeck en alle andere NA22 participanten van het eerste uur, voor de datareconstructie en het raamwerk van het analyseprogramma.

Tom Haupt for the introduction to the NA22 experiment and the intermittency topic.

Eddi De Wolf voor de zeer verhelderende discussies en het zorgvuldig lezen van het manuscript.

Martine Charlet voor de onschatbare hulp bij het schrijven van dit proefschrift. Haar tomeloze inzet, sluwheid bij grafiese manipulaties en kennis van statistiek en fitprogramma's hebben mij menigmaal uit mijn lijden verlost.

Hans Eggers and Peter Lipa for the long-distance co-operation concerning the empty-bin paper and the inspiration I got from their work.

Wolfram Kittel: zijn enthousiasme voor lage p_T fenomenen kent geen grenzen.

Edmar Markhorst en Ernest den Bekker, die de eerste stappen op weg naar de NA22 bijdrage aan het intermittency gebeuren hebben gezet.

Annelies Mey voor de detector plaatjes en de prettige conversaties. Erna Dikmans en Marjo van Wees voor de doortastende wijze waarop zij dingen weten te regelen.

Wes Metzger, die het werken met VM/CMS tot iets moois maakt.

EHEF astronauten.

The NA22 collaboration for all the unforgettable meetings.

De operators van het U.C.I.

De portiers.

Alle medewerkers van de afdeling experimentele hoge-energiefysica voor de aangename samenwerking.

De medewerkerkers van de afdeling theoretische hoge-energiefysica, in het bijzonder Rob Timmermans en Caspar Terheggen.

Al mijn vrienden.

Jopie en Mathieu.

Vuijr der Pa en de Ma.
In al der tied dè ig nuujdig
houw vuijr ut proefsjrift,
haat der mig winnig gezieje,
mèr ig han ummer an ug gedaat.
Ig hauwp dat der ut e sjun bukske vingkt.

Contents

Introduction

The present-day situation in high-energy physics can be roughly described as follows. At the one hand there is the very successful Standard Model (S.M.), giving a perfect description of the electroweak interactions between leptons, quarks, and gauge bosons. Electron-positron experiments, as those performed at the high-energy electron-positron collider LEP, confirm the S.M. continuously. Some problems, as the existence of the Higgs and the top-quark, still remain, but at least for the latter, the expectation is that it will be found in the future.

On the other hand, there is the theory of strong (color) interactions, quantum chromodynamics (QCD). For large squared momentum transfer Q^2, corresponding to small distances and to a small value of the strong coupling constant α_s, the interactions between quarks and gluons can be described perturbatively. Experimentally, the predictions of QCD can be tested by studying collective phenomena, such as jet production (jets can be considered as the hadronic realization of the underlying parton setup). Indeed, experiments also seem to confirm QCD predictions.

However, hadronization, the transition of colored partons to color-neutral hadrons, cannot be described by perturbative QCD because of the small Q^2 (of the order of 1GeV^2) and the large α_s. Therefore, phenomenological models have to be developed. In the LUND JETSET model, most commonly used to describe hadron production in e^+e^- interactions, strings are stretched between quarks and gluons at the end of the parton evolution. These strings, in turn, produce mesons and baryons according to a certain fragmentation function.

In hadron-hadron collisions as studied in this thesis, the situation is even more complicated. Contrary to e^+e^- annihilation, there is no good understanding of the interaction between the incoming hadrons. Thus, not only is there no good theory for the multiparticle production at the end, but also the initial interaction itself needs to be understood. However, models are available, as FRITIOF and DPM and, for higher energies, PYTHIA. Also these models use the LUND fragmentation scheme for hadron production. The models describe the inclusive data (inclusive means that one studies the behavior of one particle, irrespective of the other particles) rather well, but in general fail to reproduce (the tail of) multiplicity distributions or the two- and three-particle correlations. So, detailed experimental investigations are needed to improve our understanding.

In this thesis, factorial moments F_q of the multiplicity distribution in phase-space intervals δ of decreasing size are studied. From chapter 1 it will become clear that the factorial moments are related to multiparticle density distributions (or multiparticle correlations). If these density distributions become singular for $\delta \to 0$, this shows up as a power-law behavior of the factorial moments, $F_q(\delta) \sim \delta^{-f_q}$. Białas and Peschanski have called this phenomenon 'intermittency' and have connected it to a self-similar cascading mechanism.

Nowadays, intermittency is well established experimentally for various types of high-energy interactions, but theoretically the effect is still far from being understood. The models for hadronic interactions mentioned before fail to describe the phenomenon QCD-inspired parton-shower models are able to describe the e^+e^- data, but the fundamental reason for this success is still not completely clear

The first chapter of this thesis is an introduction to the phenomenon of intermittency The original idea to use factorial moments as a way to eliminate trivial statistical fluctuations is explained The connection with fractal dimensions and density distributions is made and some related topics are discussed

The setup of the NA22/EHS experiment, the data of which are used here, is described in chapter 2

Chapter 3 deals with the 'empty-bin effect', a problem especially the higher-order factorial moments may suffer from, and which cannot be corrected for

To measure the intermittency strength, the experimentally found factorial moments have to be fitted by a power law The method used and the limitations of the method are described in chapter 4

The quality criteria an event should satisfy in order to be used in the analysis are given in chapter 5 Also studied is the influence of these event-selection criteria on the one-dimensional factorial moments

A more detailed analysis of the one-dimensional factorial moments is presented in chapter 6

Not only because of the complexity, but also because of chronological considerations, the multidimensional analysis is kept for the last chapter Though the one-dimensional factorial moments are still widely used, the general opinion nowadays is that the only correct way to study intermittency is to do the analysis in three-dimensional momentum space A very recent improvement in the study of correlations is presented in the last section of this chapter

1

Dynamical density fluctuations

This work is devoted to an investigation of dynamical density fluctuations in multiparticle production. It is based on two premises advanced by Białas and Peschanski [BPNP86] [BPNP88]:

1. Dynamical density fluctuations can be studied by calculating (bin-averaged) normalized moments of the density distribution in a domain of phase space. However, in experiments the normalized *factorial* moments of the multiplicity distribution should be measured to remove the influence of the purely statistical fluctuations.
2. If the normalized factorial moments increase according to a power law for decreasing size of the phase-space domains, this indicates the existence of self-similar fluctuations on all scales, referred to as *intermittency.*

These ideas will be illuminated in the following sections, in addition to a discussion of more conventional ways of describing the behavior of the data in terms of short-range correlation effects.

1.1 Measuring fluctuations

To allow a systematic study of dynamical density fluctuations in a multiparticle production process, Białas and Peschanski have borrowed from hydrodynamics the idea of normalized moments and the variation of these moments with the length of scale.

In their first paper on this topic [BPNP86], the authors considered events with large fixed multiplicity and tried to investigate the statistical significance of the density fluctuations in a particular JACEE event [JAPR83]. Even though this event contains about 1000 particles, they were faced with the problem of trivial, statistical fluctuation. To model these purely statistical fluctuations they opted for a multinomial distribution.

The second paper [BPNP88] on this topic contained an extension of the analysis to more general inclusive and semi-inclusive spectra. A method was developed to study fluctuations in events at lower energies, with a considerably smaller average number of particles. Here, the line of arguments will be followed as presented in this second paper.

Assume, for the moment, the phase-space variable used to be one-dimensional, for example rapidity $y = 0.5\ln((E+p_L)/(E-p_L))$ (see appendix to this chapter). In order to avoid constraints following from energy-momentum and charge conservation, take not too small a central rapidity interval Δ. Divide this interval into M bins of size $\delta = \Delta/M$. The event spectrum is now characterized by a set of M particle densities, $\rho_1, \dots, \rho_m, \dots, \rho_M$. Note that these are the asymptotic densities in the following sense. Assume an infinite number of N particles in the distribution, then the probability to find a particle in bin m is defined by

$$p_m = \lim_{N\to\infty} \frac{n_m}{N} = \lim_{N\to\infty} \frac{\rho_m \delta}{N}. \tag{1.1}$$

The event-to-event realization of a certain set of densities is described by the multivariate probability density

$$P(\rho_1, \dots, \rho_m, \dots, \rho_M). \tag{1.2}$$

The moments of the density distribution in bin m are given by the average over the distribution P

$$\langle \rho_m^q \rangle_P = \int_0^\infty \cdots \int_0^\infty \mathrm{d}\rho_1 \cdots \mathrm{d}\rho_M P(\rho_1, \dots, \rho_m, \dots, \rho_M) \rho_m^q \tag{1.3}$$

and the normalized moments of order q in bin m are

$$Z_q^{(m)} = \frac{\langle \rho_m^q \rangle_P}{\langle \rho_m \rangle_P^q}. \tag{1.4}$$

After bin averaging one obtains

$$Z_q^{(M)} = \frac{1}{M} \sum_m Z_q^{(m)} \ . \tag{1.5}$$

It is useful to note, that in case of a flat averaged density distribution, the average probability of finding a particle in a bin is just $1/M$, and therefore the bin-averaged normalized moments in terms of probabilities are

$$C_q^{(M)} = \frac{1}{M} \sum_{m=1}^{M} \langle (M p_m)^q \rangle = \left\langle \frac{1}{M} \sum_{m=1}^{M} (M p_m)^q \right\rangle . \tag{1.6}$$

Both definitions are identical in the limit of (1.1) for a flat averaged density distribution

$$\langle \rho_m \rangle = \frac{N}{\Delta} \ , \ \forall m \ .$$

1.1.1 Factorial moments

Now consider a real event realization in terms of particle numbers. Suppose n_m particles are found in bin m. Białas and Peschanski suggest to interpret this as if there have been n_m independent realizations of the probability of finding a particle in that particular bin, which may then be described by a Poisson distribution with average $\rho_m \delta$. Then, the most general form of the particle number distribution can be written as [BPNP88, RPSF90]

$$Q(n_1, \dots, n_M) = \int P(\rho_1, \dots, \rho_m, \dots, \rho_M) \prod_{m=1}^{M} \mathrm{d}\rho_m \frac{(\rho_m \delta)^{n_m}}{n_m!} e^{-\rho_m \delta} \delta(constraints) \ . \tag{1.7}$$

This is a convolution of the asymptotic, underlying, dynamical density distribution and a statistical distribution described by multi-Poissonian noise.

Note the additional delta function in formula (1.7) containing (physical) constraints, an important one being a fixed multiplicity, $\delta(N-\sum_m n_m)$.

Of course, modelling the statistical noise by a multi-Poissonian is a strong assumption, but, once accepted, the strength of the *factorial* moment method follows immediately. It will be shown that the *factorial* moments of distribution Q are related to the moments of distribution P.

Factorial moments are easily calculated from their generating functions (see appendix). The generalization to M bins yields the following generating function of the multivariate distribution Q

$$\begin{aligned} F(s_1,\ldots,s_M) &= \langle s_1^{n_1}\cdots s_M^{n_M}\rangle_Q && (1.8)\\ &= \left\langle \prod_{m=1}^{M} e^{\delta\rho_m(s_m-1)}\right\rangle_P . && (1.9)\end{aligned}$$

From (1.90) of the appendix it is clear that this is the moment generating function of the distribution P.

For the so-called vertical moment analysis one is interested in the event-to-event fluctuations in one bin. Taking the q-th order derivative of F with respect to s_m at $s_1=\cdots=s_M=1$, one obtains the q-th order factorial moment in bin m. Using also (1.9), the following identities are found

$$\begin{aligned} \xi_q(m) = \left\langle n_m^{[q]}\right\rangle_Q &= \langle n_m(n_m-1)\cdots(n_m-q+1)\rangle_Q && (1.10)\\ &= \frac{\partial^q \langle s_1^{n_1}\cdots s_M^{n_M}\rangle_Q}{\partial s_m^q}\Big|_{\text{all } s=1} \\ &= \frac{\partial^q \left\langle e^{\rho_1\delta\lambda_1}\cdots e^{\rho_m\delta\lambda_m}\cdots e^{\rho_M\delta\lambda_M}\right\rangle_P}{\partial\lambda_m^q}\Big|_{\text{all } \lambda=0} \\ &= \delta^q\langle\rho_m^q\rangle_P . && (1.11)\end{aligned}$$

The bin size δ can be eliminated by defining vertically normalized factorial moments in bin m

$$F_q^{(m)} = \frac{\langle n_m\cdots(n_m-q+1)\rangle_Q}{\langle n_m\rangle_Q^q} = \frac{\xi_q}{\xi_1^q} = \frac{\langle\rho_m^q\rangle_P}{\langle\rho_m\rangle_P^q} = Z_q^{(m)} . \qquad (1.12)$$

In an experiment, these normalized moments are in general averaged over the bins,

$$\langle F_q\rangle_V^{(M)} = \frac{1}{M}\sum_{m=1}^{M} F_q^{(m)} . \qquad (1.13)$$

Due to a bin-dependent normalization, this bin-average is automatically corrected for a possibly non-flat rapidity density.

In further chapters, another, so-called horizontal normalization will be considered. Assuming a flat rapidity density

$$\langle n_m\rangle = \frac{1}{M}\langle n\rangle \ , \ \forall m=1,\ldots,M \qquad (1.14)$$

where $\langle n \rangle$ is the event averaged multiplicity in the initial interval Δ, one obtains

$$\langle F_q \rangle_H^{(M)} = M^{q-1} \sum_{m=1}^{M} \frac{\langle n_m(n_m-1)\cdots(n_m-q+1)\rangle}{\langle n \rangle^q} \quad . \tag{1.15}$$

Since the horizontally normalized moments are affected by a non-flat rapidity distribution, inducing an extra increase of these moments with decreasing bin size, sometimes an additional correction factor is applied [BPNP88, FWAP89]. This will be briefly discussed in chapter 6. Another way to correct for these artificial 'correlations', is to make an appropriate change of variables. This is unavoidable in the multidimensional intermittency study discussed in chapter 7.

In their 1986 paper, Białas and Peschanski did not consider event-to-event fluctuations in a fixed bin of phase space, but instead studied bin-to-bin fluctuations in a single event. To do so, one needs knowledge of the average around which fluctuations occur. This needs some theoretical prejudice on the distribution.

Since in this thesis the one-event analysis is not so important, a generalized horizontal analysis of events with fixed multiplicity will be discussed. This is useful for some forthcoming Monte Carlo studies.

If in (1.7) the particle number is fixed, the following formulae are obtained

$$Q_N(n_1,\ldots,n_M) = Q(n_1,\ldots,n_M)\delta(N-\sum_m n_m) \tag{1.16}$$

$$\begin{aligned} F_{Q_N}(s_1,\ldots,s_M) &= \sum_{n_1,\ ,n_M} \int P(\rho_1,\ldots,\rho_m,\ldots,\rho_M) \prod_{m=1}^{M} \mathrm{d}\rho_m \frac{(\rho_m \delta s_m)^{n_m}}{n_m!} e^{-\rho_m \delta} \,. \\ &\quad \delta(N-\sum_m n_m) \\ &= \int \prod_m \mathrm{d}\rho_m P(\rho_1,\ldots,\rho_M) e^{-\rho\Delta} \frac{(\rho\Delta)^N}{N!} \left(\sum_m s_m \frac{\rho_m}{M\rho}\right)^N \\ &= \int \prod_m \mathrm{d}\rho_m P_N(\rho_1,\ldots,\rho_M) \left(\sum_m s_m \frac{\rho_m}{M\rho}\right)^N \end{aligned} \tag{1.17}$$

$$\rho = \frac{1}{M}\sum_m \rho_m \tag{1.18}$$

Then, using (1.1), the following normalized factorial moment is found

$$\langle F_q \rangle_{Q_N} = M^{q-1} \frac{\sum_m \left\langle n_m^{[q]} \right\rangle}{N^{[q]}} = \langle C_q \rangle_{P_N} \quad . \tag{1.19}$$

1.2 Intermittency

The method of normalized moments described above was used by Białas and Peschanski [BPNP86] to study the JACEE spike event [JAPR83]. The remarkable property they found was that the moments seemed to be rising with decreasing bin-size according to a power law

$$F_q(\delta) \sim \delta^{-f_q}, \quad f_q > 0. \tag{1.20}$$

This power-law behavior, possibly an indication for a new scaling law, had already been found in hydrodynamics, where it was called **intermittency**.

Intermittency occurs in hydrodynamics in the onset of turbulence. In liquid flows with a Reynolds number near the critical value, laminar phases alternate with short turbulent (chaotic) bursts, so-called temporal intermittency. For Reynolds numbers $R_e \gg R_{crit}$, fully developed turbulence occurs with energy dissipation at ever-decreasing regions of space, called spatial intermittency.

It is not possible to find closed analytical solutions to the problem of turbulence using the first principle Navier-Stokes equation [PVPR87]. Therefore, statistical models for intermittency in hydrodynamics were developed [KOJF62] [MAJF74] [FSNJ78]. Two successful models [LSTS83, MSPR87] are described below. All these models possess (multi-)fractal properties, since the eddies, the regions of dissipation, do not cover the whole space uniformly, but cover only a fraction of it.

In high-energy experiments intermittency, leading to a singular behavior of the normalized factorial moments at infinitesimally small intervals, has been searched for since 1986. The strength of the intermittency, determined by f_q, varies from strong to weak with increasing complexity of the interaction. A large number of experiments have produced data on these moments, and a large number of theoretical papers on this topic have been written.

The theoretical work can be divided into two parts. One group tries to find explanations in terms of self-similar cascading, phase transitions, or other exotic phenomena. The more conservative group (this is not a value judgment) tries to explain the data by more conventional approaches, like standard short-range correlations, long-range correlations (for hadronic interactions), and Bose-Einstein interference correlations.

In the following, a number of aspects of intermittency will be described. First, the connection between intermittency indices f_q and fractal dimensions will be clarified. Then a model explicitly leading to intermittency will be described. After that, the more conventional approach will be reviewed.

1.3 Moments, slopes, and fractality

It was first realized by Lipa [LIPATH, LBPL89], that a connection must exist between fractal dimensions, defined in the context of fractal objects, and intermittency indices, since both measure properties of objects with spikes and valleys, resulting from a self-similar process.

The generalized (or Renyi) dimensions D_q, measuring scaling behavior of probabilities p_m in the intervals $m = 1, \ldots, M$ with respect to the interval length δ, are defined by

$$\left\langle p^{q-1}(\delta)\right\rangle = \sum_{m=1}^{M} p_m^q = \left(\frac{1}{\delta}\right)^{(1-q)D_q} \tag{1.21}$$

at $\delta \to 0$. So one obtains [1]

$$D_q = \frac{1}{q-1} \lim_{\delta\to 0} \frac{\ln \sum_m p_m^q}{\ln \delta} \quad . \tag{1.22}$$

One may define an infinite set of such generalized dimensions. D_0 is called the fractal dimension and measures simply the geometrical properties of the fractal. D_1 is the information

---

[1] If the probabilities are uniformly distributed ($p_m = 1/M$ for all m) and the interval size is simply $\delta = 1/M$, then $D_q = 1$. Thus $D_q \neq 1$ measures the deviation from these assumptions.

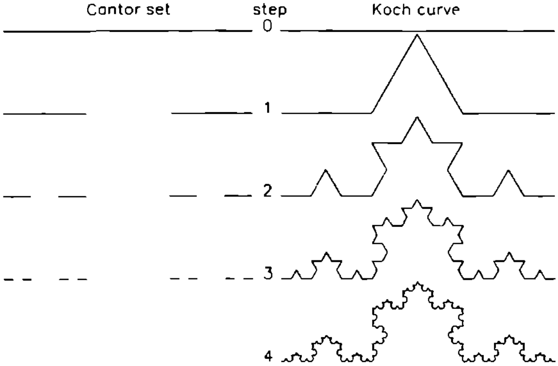

Figure 1.1 *The Cantor set and the Koch curve*

dimension [JFZN82], obtained by letting $q \to 1$. Then

$$D_1 = \lim_{\delta \to 0} \frac{\sum_m p_m \ln p_m}{\ln \delta}$$

D_2 is the correlation dimension [HPPH83].

From the definition it can be deduced that positive values of q stress the importance of large values of p_m (peaks), negative q-values stress the importance of very small p_m's (dips).

Two distinct cases can be considered depending on the variation of D_q with q: the *monofractal*, and the *multifractal*.

Monofractal

First, the simple fractal is considered, which might be a Cantor set or a Koch curve (fig. 1.1). The Cantor set describes a stepwise cascade of a line of length 1. At the first step, $\nu = 1$, the line piece is divided into 3 intervals and the middle one is taken out. Repeating this procedure for the resulting line pieces leads to a self-similar pattern. At each scale a copy of the preceding step is produced. After several steps one is left with a distribution of almost point-like objects which have dimension smaller than 1 (a line) but larger than 0 (a point). This dimension can be measured by means of the so-called box-counting method which is equivalent to setting $q = 0$ in (1.22). The number of intervals M after ν steps is 3^ν. Defining $p_1 = p_3 = 1/2$ and $p_2 = 0$, the sum over the intervals can be written as

$$\sum_{m=1}^{M} p_m^q = (p_1^q + p_2^q + p_3^q)^\nu = (2\left(\frac{1}{2}\right)^q)^\nu \tag{1.23}$$

Using (1.22), one obtains

$$D_q = \frac{\ln 2}{\ln 3} \tag{1.24}$$

for all values of q.

In the case of the Koch curve the length δ of a line piece varies with the number of steps as $\delta = \left(\frac{1}{3}\right)^\nu$ and the number of pieces M as $M = 4^\nu$. Defining the probability by $p_m = 1/M$ for all m one finds for the generalized dimensions

$$D_q = \lim_{\nu \to \infty} \frac{1}{q-1} \frac{\ln(4^\nu 4^{-\nu q})}{-\nu \ln 3} = \frac{\ln 4}{\ln 3} > 1 \tag{1.25}$$

for all values of q.

Multifractal
An example of a multifractal is the Cantor density. Here, instead of removing the middle interval, one gives it a different (non-zero) probability. The generalized dimensions then become

$$D_q = \frac{1}{1-q} \lim_{\nu \to \infty} - \frac{\ln(2p_1^q + p_2^q)^\nu}{\ln \lambda^\nu} \quad \text{with} \quad \lambda = 3. \tag{1.26}$$

Now the fractal dimension D_0 is 1, which can be understood from the fact that the support for the densities is a line.

In general, for a multifractal, the following relations hold [HPPH83]

$$D_{q'} < D_q \text{ , for } q' > q \ . \tag{1.27}$$

Now, from formula (1.6), the connection between the generalized dimensions D_q and the intermittency indices f_q becomes clear if the generalized dimensions are assumed to characterize an 'averaged' spectrum [LIPATH]

$$\left\langle \sum_m p_m^q \right\rangle \sim M^{(1-q)D_q} \ , \tag{1.28}$$

$$\langle C_q \rangle = \frac{1}{M} \left\langle \sum_m (M p_m)^q \right\rangle \sim M^{f_q} \ , \tag{1.29}$$

$$\Rightarrow D_q = 1 - \frac{f_q}{q-1} = 1 - d_q \ . \tag{1.30}$$

The last equation also defines the *anomalous* dimension d_q, measuring the deviation from the support dimension.

Since the moments are measured in the form of factorial moments, there is a limitation to positive integer q values. But, as already mentioned, the multifractal spectrum also consists of non-integer, and even negative q values. Hwa and collaborators have been strong advocates of this line of research [HWPR41, CHPR43], but only very recently a procedure for subtracting statistical noise has been developed [HWOI91]. Early work done by the author on this subject is not included in this thesis, but will be subject of future analysis.

1.4 Models for intermittency

Recalling the formula for the q-th order density moment (1.3) and assuming there are no dynamical fluctuations, the probability density can be taken as a product of M delta functions,

$$P(\rho_1, \ldots, \rho_M) = \prod_m \delta(\rho_m - c_m) \tag{1.31}$$

and the moments turn out to be

$$\langle \rho_m^q \rangle = c_m^q = \langle \rho_m \rangle^q \ , \tag{1.32}$$

yielding normalized moments independent of δ and equal to one. Absence of dynamical fluctuations means that there is only statistical noise. Indeed, using factorial moments with Poissonian noise leads to the same trivial result.

The question what kind of model is able to describe intermittency, has been answered by Białas and Peschanski in [BPNP86]. From hydrodynamics they borrowed the idea of a (weighted) curdling model and constructed from that their so-called α-model .

The α-model is a special case of the self-similar random-cascade model. First the most general form of such model will be described.

1.4.1 The random-cascade model

For convenience, consider a cascade to take place in one-dimensional rapidity space. The idea is to start with an initial rapidity interval Δ. At the first step in the cascade the interval is split into λ parts. Each part is attributed a random weight W, according to a distribution $r(W)$, such that the ensemble average $\{W\}$ is unity

$$\{W\} = \int r(W) W \mathrm{d}W = 1 \; . \tag{1.33}$$

After that, each part is again divided into λ parts, each of which is given a weight.

After ν steps in the cascade, this results in $M = \lambda^\nu$ intervals of size $\delta = \Delta/M$. Each interval m of M can be marked with a sequence of ν numbers $m = \{\alpha_\nu, \ldots, \alpha_1\}$, where $\alpha_i = 1, \ldots, \lambda$. As an illustration, two representations of the α-model ($\lambda = 2$, see below) are shown in fig. 1.2. In the block diagram the shaded boxes indicate a certain path, leading to bin 6, $m = \{1, 2, 1, 2\}$, corresponding to the same path (thick lines) in the Cayley tree representation. Due to the random nature of the process, it suffices to study one branch of the tree only, allowing the bin indices to be omitted [2].

The density in an interval after ν steps of the cascade is, starting from an initial density $\rho(\Delta)$

$$\rho(\delta) = W_\nu W_{\nu-1} \cdots W_1 \rho(\Delta) \; . \tag{1.34}$$

Again, due to the independence of the W's, the event average can be written as a product of ν ensemble averages, yielding in general for the moments of $\rho(\delta)$

$$\langle \rho^q(\delta) \rangle = \{W^q\}^\nu \langle \rho^q(\Delta) \rangle \tag{1.35}$$

and for the normalized ones, using $\{W\} = 1$

$$\langle Z_q(\delta) \rangle = \frac{\langle \rho^q(\delta) \rangle}{\langle \rho(\delta) \rangle^q} = \{W^q\}^\nu \frac{\langle \rho^q(\Delta) \rangle}{\langle \rho(\Delta) \rangle^q} \sim M^{\frac{\ln\{W^q\}}{\ln \lambda}} \tag{1.36}$$

The similarity sign at the right-hand side indicates the power law behavior, and the intermittency strength is determined by the exponent.

For weakly fluctuating W one can write $W = 1 + \tau$, with $\{\tau\} = 0$. Then, up to second order in τ,

$$\ln\{W^q\} = \ln\{(1+\tau)^q\} \approx \frac{q(q-1)}{2}\{\tau^2\} \tag{1.37}$$

$$\text{and } f_q = \frac{q(q-1)}{2} f_2 . \tag{1.38}$$

---

[2] The random-cascade model can also be used to make predictions on the correlated moments. This is beyond the scope of this thesis. Results on factorial correlators are published in [CHPL91], and will be extensively discussed in [CHARTH].

This is the result obtained in [BPNP88], and the relation hints to a Gaussian distribution. Indeed, if the product of the ν random variables is rewritten as a sum of logarithms, such that $(\rho(\Delta) = 1)$

$$\ln \rho(\delta) = \sum_{i=1}^{\nu} \ln W_i \ , \tag{1.39}$$

it follows from the central limit theorem that, for a large number of steps

$$P_{LN}(\ln \rho) \mathrm{d} \ln \rho = \frac{1}{\sqrt{2\pi\nu\sigma^2}} \exp\left[-\frac{(\ln \rho - \nu\mu)^2}{2\nu\sigma^2}\right] \frac{1}{\rho} \mathrm{d}\rho \ , \tag{1.40}$$

$$\text{where} \quad \mu = \{\ln W\} \ , \quad \sigma^2 = \{(\ln W)^2\} - \mu^2 \ . \tag{1.41}$$

Calculating the moments from this Log-Normal distribution (P_{LN}) the relation (1.38) is recovered. This relation is only exact if the W's are themselves Log-Normally distributed [BPNP88, PVPR87].

An essential feature of these kinds of models is that the total density (or multiplicity) fluctuates from event to event. In reference [BPPL88] it was shown that a specific choice of $r(W)$ can lead to a Negative Binomial form of the total multiplicity distribution. The link between global variables, such as the total multiplicity, and local intermittency patterns has been studied in more detail in [BSZP89], where a phase diagram for the random-cascade model has been constructed. Tests of these predictions are outside the scope of this thesis.

1.4.2 The α-model

The α-model of [BPNP86] has branching parameter $\lambda = 2$ and the random-variable distribution $r(W)$ only allows for two values $\beta_- < 1$ and $\beta_+ > 1$ with probabilities a and b, such that the normalization criterion leads to

$$\{W\} = a\,\beta_- + b\,\beta_+ = 1 \ , \quad a + b = 1 \tag{1.42}$$

$$r(W) = a\ \delta(W - \beta_-) + b\ \delta(W - \beta_+). \tag{1.43}$$

The intermittency exponents f_q can be expressed in terms of these parameters as

$$f_q = \frac{\ln(a\beta_-^q + b\beta_+^q)}{\ln 2} \ . \tag{1.44}$$

Fig. 1.2 shows a graphic representation of the α-model .

1.4.3 The p-model

A model used in hydrodynamics and describing the data surprisingly well is the so-called p-model [MSPR87]. It conserves energy and momentum. Translated into the language of the α-model , this means that the total density does not fluctuate, or the sum of probabilities per bin is 1. The left and right intervals are no longer independent. This is due to the fact that, when the step to the left on the Cayley tree gets a weight β_+ with probability 1/2, the step to the right gets a weight $\beta_- = 2 - \beta_+$, and vice versa. The intermittency slopes are then calculable from the weight distribution

$$r(W) = \frac{1}{2}\ \delta(W - \beta_-) + \frac{1}{2}\ \delta(W - \beta_+) \ , \ \{W\} = 1. \tag{1.45}$$

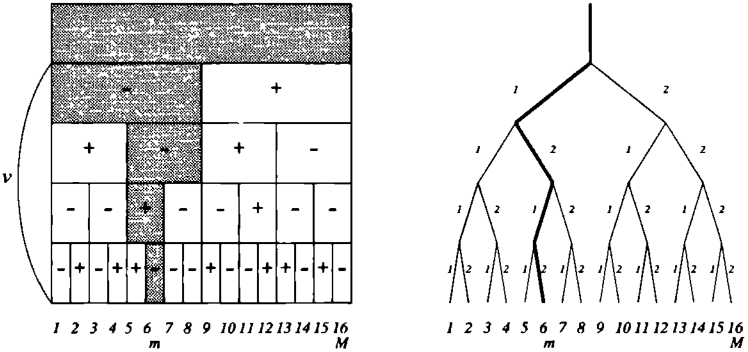

Figure 1.2: *The α-model of intermittency. At each step of the cascade the interval is divided into two pieces. The density in each part is increased or decreased by a factor (β_+ or β_-, with probabilities a and b respectively), indicated by a + or a − sign. A typical path is marked in grey. It corresponds to the dark path in the so-called Cayley tree. The bin, $m = 6$, is represented by the sequence $\{\alpha_1, \alpha_2, \alpha_3, \alpha_4\} = \{1, 2, 1, 2\}$.*

The density after ν steps in the cascade is again a product of ν independent random numbers

$$X = W_\nu W_{\nu-1} \cdots W_2 W_1 \ . \tag{1.46}$$

The probability to find a certain configuration after ν steps is then

$$P(\beta_+^k \beta_-^{\nu-k}) = \binom{\nu}{k} \left(\frac{1}{2}\right)^k \left(\frac{1}{2}\right)^{\nu-k} \tag{1.47}$$

giving an average weight of order q

$$\{X^q\} = \sum_{k=1}^{\nu} (\beta_+^k \beta_-^{\nu-k})^q P(\beta_+^k \beta_-^{\nu-k}) = \left(\frac{1}{2}\beta_+^q + \frac{1}{2}\beta_-^q\right)^\nu \tag{1.48}$$

After substituting $p = \beta_+/2$ the intermittency indices become

$$f_q = q - 1 + \frac{\ln(p^q + (1-p)^q)}{\ln 2} \ . \tag{1.49}$$

1.4.4 Remarks on random-cascade models

The simplicity of the α-model has made it possible to study the quality of the log-normal approximation in (1.38) [ABZP91]. It was found to fail badly. Applying the theory of Bernoulli trials [FELLV1] [3], the authors of [ABZP91] found an expansion of the probability distribution valid for a large number of steps and converging to the true value only slowly.

This expansion was also used by Alberty and Peschanski as a test function to study the empty-bin effect [APZP91]. This empty-bin effect is studied in more detail in a subsequent

---

[3] The probability to find a density $\beta_-^k \beta_+^{(\nu-k)}$ in a ν-steps cascade is equal to the number of k successes in ν Bernoulli trials with probabilities a and b.

chapter using different tools. It derives from the fact that due to limited statistics (a finite number of events) the tail of the probability distribution is truncated. Simulating truncated data by the test function, the authors have found that the Negative Binomial distribution describes well the moments in the case of not too long a cascade, and with rather large truncation (small statistics).

The urge to relate the intermittency indices of different orders to each other has led Brax and Peschanski to a description of the random-cascade models in terms of Lévy-stable laws [BPPL91]. The theory of Lévy-stable distributions is described in [FELLV2]. In short, the idea is to find a class of distributions of random variables such that the sum of n independent identically distributed random variables, scaled by a factor $n^{1/\mu}$, are distributed according to the same distribution. This is in fact a generalization of the central limit theorem. The parameter $\mu \in (0,2]$ is the Lévy index, characterizing the distribution. For $\mu = 2$, the Gaussian distribution is recovered. Also the Cauchy distribution belongs to this class, and has $\mu = 1$. Except for these cases, no closed analytical expressions for these distributions are known, but only their characteristic function [KPAM83]. However, it is possible to give a general expression for the intermittency indices [BPPL91]

$$f_q = f_2 \frac{q^\mu - q}{2^\mu - 2} . \tag{1.50}$$

In the multidimensional analyses of chapter 7 this formula will be used to fit the intermittency indices of several experiments.

As a final remark, it might be good to mention that in [ZAJU90] it was proven that also non-random cascade models are able to show intermittent behavior, if $\beta_+ + \beta_- = 2$ is fulfilled.

1.4.5 Phase transitions

From statistical physics it is known that a system undergoing a second-order phase transition shows a scale-invariant behavior at the critical point. Then, the correlation length at the transition is larger than the size of the largest system produced [BHPL91]. It has been shown by Satz [SANP89], that those systems exhibit intermittent behavior at the critical point, only. First numerical calculations by Wosiek [WOAP88] indeed have shown an effect for the two-dimensional Ising model. However, in [NOBR89] Novak could show that this effect might be due to violation of the Z(2) (global spin-flip) symmetry and a different definition for the spin multiplicity satisfying the symmetry has been proposed. Novak also introduced new moments to correct for the finite size effects of the lattice. Applying these modifications to the finite-size Ising model (64^2 to 1024^2 sites), Gupta et al.[GUBI90] found clear evidence for the existence of intermittency in this model.

It turns out that for the case of second-order transitions the anomalous fractal dimensions are independent of q (monofractal). Therefore, such a behavior of the anomalous dimensions could be an indication for a transition from a quark-gluon plasma (in thermodynamic equilibrium) to a hadronic phase. Note, however, that a monofractal model, like the β-model from hydrodynamics [FSNJ78] also shows this behavior [4]. This is in contrast with the random-cascade models where $d_{q+1} > d_q$.

---

[4] First-order transitions with short correlation length will not exhibit self-similarity at all scales, and, therefore, the anomalous dimensions are zero.

Non-thermal, or spin-glass phase transitions have been investigated in [RPNP89] and it turns out that this type of transitions occurs if

$$\lambda_q = \frac{f_q + 1}{q} \tag{1.51}$$

has a minimum for a certain critical value of q. This kind of phase transition can occur in random-cascading models. They are characterized by a hierarchy of critical indices, contrary to the thermal phase transitions, where only one unique critical value appears [RPCE90]. The meaning of these non-thermal phase transitions is that there may be different kinds of intermittency, as there are different phases in a spin-glass system. This could then possibly explain the observation of two completely different spike events: The famous JACEE event [JAPR83] with a lot of spikes and holes, and the NA22 event with only one spike [SPIK87].

As stated earlier, the α-model may possess a non-thermal phase transition. A very interesting study of this phenomenon is published by Brax and Peschanski [BPNP90], who constructed a phase diagram consisting of four regions, each region exhibiting a different phase-transition behavior.

A study of multifractality in the α-model has led Białas and Zalewski to state [BZPL90] that there might not be a phase *transition* at a certain critical value q_c (related to (1.51) by $\partial\lambda_q/\partial q = 0$), but that two phases, a 'liquid' and a 'dusty' one, are coexistent. Beyond the critical value of q, the measurement is more sensitive to the 'dusty' phase.

Of course, there are also cascade models that exhibit no phase transition [RPNP89]. Currently used models in e^+e^- physics, as QCD parton shower models, have no phase transitions, but are clearly quite successful in describing the data. Purely hadronic cascading models are also found to show intermittent behavior [OWPL88]. Thus, intermittency does not automatically signal a phase transition.

1.5 Factorial moments and correlations

A link exists between factorial moments and the well-known inclusive density distributions for identical particles

$$\begin{aligned} \rho(y_1, \ldots, y_q) &= \frac{1}{\sigma_I} \frac{d^q \sigma_{incl}}{dy_1 dy_2 \cdots dy_q} & (1.52) \\ &= \left\langle \sum_{n_1 \neq n_2 \neq \;\neq n_q}^{n} \delta(y_1 - y_{n_1})\delta(y_2 - y_{n_2}) \cdots \delta(y_q - y_{n_q}) \right\rangle & (1.53) \end{aligned}$$

where $\langle\rangle$ stands for the event average, as usual, n is the number of particles in one event, and σ_I is the total inelastic cross section.

Integrating (1.53) over q identical ranges, for example a rapidity bin m, yields the factorial moment of order q

$$\xi_q^{(m)} = \langle n_m(n_m - 1) \cdots (n_m - q + 1) \rangle = \int_{\Omega_m} \rho(y_1, \ldots, y_q) \mathrm{d}y_1 \cdots \mathrm{d}y_q \tag{1.54}$$

and thus for $q = 1$

$$\xi_1^{(m)} = \langle n_m \rangle = \bar{\rho}_m \delta \; . \tag{1.55}$$

Thus, the vertically normalized factorial moments expressed in terms of the density distributions are

$$\begin{aligned}\langle F_q\rangle_V^{(M)} &= \frac{1}{M}\sum_{m=1}^{M}\frac{\int_{\Omega_m}\rho(y_1,\ldots,y_q)\prod_{i=1}^{q}\mathrm{d}y_i}{(\int_{\Omega_m}\rho(y)\mathrm{d}y)^q}\\ &= \frac{1}{M\delta^q}\sum_{m=1}^{M}\int_{\Omega_m}\frac{\rho(y_1,\ldots,y_q)\prod_{i=1}^{q}\mathrm{d}y_i}{\bar{\rho}_m^q}\end{aligned} \tag{1.56}$$

There is a standard way to decompose a higher-order density function into a sequence of lower-order density and correlation functions, the so-called Mayer and Mayer cluster decomposition [HUSM63]:

$$\begin{aligned}\rho_1(y_1) &= C_1(y_1)\\ \rho_2(y_1,y_2) &= C_2(y_1,y_2)+\rho_1(y_1)\rho_1(y_2)\\ \rho_3(y_1,y_2,y_3) &= C_3(y_1,y_2,y_3)+\rho_1(y_1)C_2(y_2,y_3)+\rho_1(y_2)C_2(y_3,y_1)+\\ &\quad \rho_1(y_3)C_2(y_1,y_2)+\rho_1(y_1)\rho_1(y_2)\rho_1(y_3)\ .\end{aligned} \tag{1.57}$$

Since, in order to obtain the factorial moments, the integration of the density function is over q identical intervals, terms in the expansion only differing in permutation give the same contribution. Denoting the integral form of the q-th order correlation function, also called the factorial cumulant moment of order q, in bin m by

$$k_q^{(m)} = \int_{\Omega_m}\prod_{i=1}^{q}\mathrm{d}y_i C_q(y_1,\ldots,y_q) \tag{1.58}$$

the expansion of the factorial moments in terms of factorial cumulants is (leaving out the bin index for the moment)

$$\begin{aligned}\xi_1 &= k_1\\ \xi_2 &= k_2+k_1^2\\ \xi_3 &= k_3+3k_2k_1+k_1^3\\ \xi_4 &= k_4+4k_3k_1+3k_2^2++6k_2k_1^2+k_1^4\\ \xi_5 &= k_5+5k_4k_1+10k_3k_2+10k_3k_1^2+15k_2^2k_1+10k_2k_1^3+k_1^5\ .\end{aligned} \tag{1.59}$$

In [KSATS] these relations are explicitly given up to order 10. In [MUPR71] a general formula is given for the expression of factorial moments in terms of factorial cumulant moments and vice versa. These formulae can be obtained from the link between their respective generating functions (see appendix).

The vertically normalized factorial moments can now be expressed in their cumulant counterpart [CEPL91]

$$\begin{aligned}K_q^{(m)} &= \frac{k_q^{(m)}}{(k_1^{(m)})^q}\\ \langle K_q\rangle_V^{(M)} &= \frac{1}{M}\sum_m K_q^{(m)}\\ \langle K_aK_b\rangle_V^{(M)} &= \frac{1}{M}\sum_m K_a^{(m)}K_b^{(m)}\end{aligned} \tag{1.60}$$

by

$$\begin{aligned}
\langle F_2\rangle_V^{(M)} &= 1+\langle K_2\rangle_V^{(M)} \\
\langle F_3\rangle_V^{(M)} &= 1+3\,\langle K_2\rangle_V^{(M)}+\langle K_3\rangle_V^{(M)} \\
\langle F_4\rangle_V^{(M)} &= 1+6\left\langle K_2^2\right\rangle_V^{(M)}+4\,\langle K_3\rangle_V^{(M)}+\langle K_4\rangle_V^{(M)} \quad ,
\end{aligned} \tag{1.61}$$

and so on. These equations are exact, but often only the bin-averaged factorial moments are known, and then translation invariance, that is bin-independence, has to be assumed for terms such as

$$\left\langle K_2^2\right\rangle_V^{(M)} \simeq \left[\langle K_2\rangle_V^{(M)}\right]^2 \tag{1.62}$$

The usefulness of the expressions listed above will become clear in the following section.

1.5.1 Factorial cumulants

Although factorial cumulants are not discussed in this thesis, it is instructive to mention some features.

Equivalently to the normalized factorial moments, the normalized factorial cumulants are defined by

$$\langle K_q\rangle_V^{(M)} = \frac{1}{M\delta^q}\sum_m \frac{\int_{\Omega_m} C_q(y_1,\dots,y_q)\prod_{i=1}^q \mathrm{d}y_i}{(\bar\rho_m)^q} \quad . \tag{1.63}$$

Therefore, the normalized cumulant moments are a better measure of higher-order particle correlations than the factorial moments themselves. However, a disadvantage is that the k_q's can only be obtained from the ξ_q's and this means that their errors increase very rapidly with the order q.

An approximation of the contribution of second-order correlations to the third- and higher-order factorial moments can be obtained by explicitly setting $K_q = 0$, for $q > 2$, and replacing K_2 by $F_2 - 1$. A similar procedure can be followed to study the combined contribution of second- and third-order correlations to F_4 and F_5 [CEPL91].

Linked-Pair Approximation and the NBD

Since little is known experimentally about correlations higher than third order and since it is well-known that third-order correlations are much weaker than second-order ones, several groups have tried to express the higher-order correlations in terms of (known?) two-particle correlations. To avoid problems with normalization, the connection is made between the reduced correlation functions

$$c_q(y_1,\dots,y_q) = \frac{C_q(y_1,\dots,y_q)}{\rho_1(y_1)\cdots\rho_1(y_q)} \quad . \tag{1.64}$$

If the rapidity distribution does not change considerably within a bin interval, it is possible to express the correlation function in a reduced form by [CEPL91]

$$\int_{\Omega_m} C_q(y_1,\dots,y_q)\prod_{i=1}^q \mathrm{d}y_i = (\bar\rho_m)^q \int_{\Omega_m} c_q(y_1,\dots,y_q)\prod_{i=1}^q \mathrm{d}y_i \quad , \tag{1.65}$$

such that,

$$K_q^{(m)} = \frac{1}{\delta^q} \int_{\Omega_m} c_q(y_1, \ldots, y_q) \prod_{i=1}^{q} \mathrm{d}y_i \ . \tag{1.66}$$

The *Linked-Pair Approximation* (LPA) of [CSPR89] for the reduced correlation functions is then (writing y_i as i)

$$c_3(1,2,3) = \frac{A_3}{3}[c_2(1,2)c_2(2,3) + c_2(2,3)c_2(3,1) + c_2(3,1)c_2(1,2)] \tag{1.67}$$

$$c_q(1,\ldots,q) = \frac{A_q}{q!/2}[c_2(1,2)c_2(2,3)\cdots c_2(q-1,q) + \text{ permutations}]. \tag{1.68}$$

After integration all $q!/2$ permutations give the same contribution, such that it suffices to write

$$K_q^{(m)} = \frac{A_q}{\delta^q} \int_{\Omega_m} c_2(y_1,y_2)c_2(y_2,y_3)\cdots c_2(y_{q-1},y_q) \prod_{i=1}^{q} \mathrm{d}y_i. \tag{1.69}$$

Using a convenient change of variables and applying a so-called *strip approximation* [5], Carruthers, Sarcevic, and Eggers [CSPR89] were able to find a recursive relation between the normalized factorial cumulants, leading to

$$K_q^{(m)}(\delta) = A_q \left[K_2^{(m)}(\delta)\right]^{q-1}, \quad \forall\ m = 1,\ldots,M. \tag{1.70}$$

with A_q a constant for all binnings M. De Wolf [DWAP90] has found that, in the limit of small δ (where the strip approximation is valid), the Linked-Pair approximation yields a NB distribution if the originally free parameter A_q is taken to be $A_q = (q-1)!$ [6].

To see this, it is sufficient to look at the generating function of the NBD (appendix)

$$\begin{aligned} F_{NB}(s) &= (1-(s-1)\frac{\bar{n}}{k})^{-k} \quad \Rightarrow & (1.71)\\ F_q &= \prod_{i=1}^{q}(1+\frac{i-1}{k}) \Rightarrow & (1.72)\\ F_2 &= 1+\frac{1}{k} & (1.73)\\ K_{NB}(s) = \ln F_{NB}(s) &= -k\ln(1-(s-1)\frac{\bar{n}}{k}) \quad \Rightarrow & (1.74)\\ K_q = (q-1)!\left(\frac{1}{k}\right)^{q-1} &= (q-1)!\,(F_2-1)^{q-1} \ . & (1.75) \end{aligned}$$

From these formulae the k parameter of the NBD can be interpreted as a measure of the integrated two-particle correlation function

$$\frac{1}{k} = \int_{\Omega_m} \mathrm{d}y_1 \mathrm{d}y_2 k_2(y_1,y_2) \ , \tag{1.76}$$

---

[5] The strip approximation, for two variables y_1 and y_2 in bin $y_{m-1} < y_1, y_2 < y_{m-1} + \delta$ consists of a transformation with Jacobian one: $\zeta = y_2 - y_1$ and $Y = (y_1 + y_2)/2$, and an area conserving rotation of 45°, such that $-\delta/2 < \zeta < \delta/2$ and $y_{m-1} < Y < y_{m-1} + \delta$.

[6] In the same paper, De Wolf has shown that a slightly different linked-pair ansatz derived from a Random-Phase Approximation scheme, using stationarity, makes the A_q an obsolete parameter.

under the condition that the integral exists.

If the NBD is valid in small intervals, with the same parameter k and $\bar{n}$ for all bins, the combined distribution will be NBD, too.

Corollary, for the usual bin-averaged factorial moments, a deviation from the NBD approximation can be expected, since the k parameter depends on rapidity and is thus not constant for all the bins.

It follows from the formulae above that if the NBD indeed holds, there is no additional information from higher than second-order factorial moments. This implies, that it is sufficient to have a good parametrization of F_2, or of the second-order correlation function.

1.5.2 Parametrization of F_2

Scaling density distribution

If, indeed, there is an intermittency signal in the data, it follows from the definition of F_q in terms of the density distribution, that the latter should be singular for $\delta \to 0$. This is best seen for F_2 using a reduced function

$$r_2(y_1, y_2) = \frac{\rho_2(y_1, y_2)}{\rho_1(y_1)\rho_1(y_2)} = \left|\frac{y_1 - y_2}{L}\right|^{-f_2} \Rightarrow \tag{1.77}$$

$$F_2 = \frac{1}{\delta^2}\int_{\Omega_m} \mathrm{d}y_1 \mathrm{d}y_2 r_2(y_1, y_2) \sim \text{Constant } \delta^{-f_2} \ . \tag{1.78}$$

The integral can be solved exactly or using the strip approximation, the only difference lies in the constant.

Scaling cumulants

If one assumes, instead, that the factorial cumulant scales: $K_q = c_q\, \delta^{-\phi_q}$, and the NBD (linked-pair) holds, it is possible to express F_q as a sum of unity and terms with a power of δ. Eggers [EGGETH] derives the behavior of F_4

$$\begin{aligned} F_4(\delta) &= 1 + 6c_2\, \delta^{-\phi_2} + 11c_2^2\, \delta^{-2\phi_2} + 6c_2^3\, \delta^{-3\phi_2} \\ &\approx \text{Constant } \delta^{-f_4}. \end{aligned} \tag{1.79}$$

He finds that, for small values of ϕ_2, the largest term is the one with coefficient $11c_2^2$ from the term quadratic in K_2, giving an approximate power law for F_4. For large values, typically ϕ_2 =0.5-1, the most singular term contributes mainly in small intervals, giving a 'more than linear rise' in a log-log plot.

Short-range correlations

A more standard approach is to parametrize K_2 using an exponential or a Gaussian form for the (reduced) two-particle correlations

$$\text{exponential} \quad c_2(y_1, y_2) = \gamma_2 e^{-|y_1-y_2|/L} \tag{1.80}$$

$$\text{Gaussian} \quad c_2(y_1, y_2) = \frac{\beta}{\sqrt{2\pi}\sigma} e^{-(y_1-y_2)^2/2\sigma^2}. \tag{1.81}$$

The Gaussian form turns out to be valid at high energies (UA5) The exponential form has been used by Capella et al [CFPL89], who calculated the integral exactly [7] In [CSPR89] the strip approximation has been used to calculate the integral This gives

$$F_2 = 1 + \gamma_2 \frac{1 - e^{-\delta/(2L)}}{\delta/(2L)} \tag{1 82}$$

Note, that for $\delta \ll L$ F_2 saturates, and thus there is no intermittency! The claim of, among others, Carruthers is that the present data on factorial moments can be described by these standard short-range correlations, without assuming any real new physics The question of the origin of these short-range correlations has not yet been unambiguously answered, but is usually attributed to the production of clusters (resonances)

1.6 Some properties of factorial moments

Before proceeding to the experimental data, it is instructive to recall some features of the factorial moments [LIPATH, EGGETH]

For Monte-Carlo simulations the p-model is particularly suited, since it is easy to program and the intermittency indices can be exactly calculated (equation (1 49)) After a certain number of steps ν, the initial (rapidity) interval (e g chosen to be $-2 < y < 2$) is split in 2^ν intervals For each event, a (fixed) number of particles is distributed among these intervals, using a multinomial distribution with probabilities given by the p-model

1.6.1 Finite multiplicity

To see that the method of factorial moments really works, the p-model has been used to calculate the normalized moments (fig 1 3)

$$\langle C_q \rangle^{(M)} = M^{q-1} \sum_{m=1}^{M} \langle \tilde{p}_m^q \rangle \text{ with } \tilde{p}_m = \frac{n_m}{n} ,$$

and the normalized factorial moments for fixed multiplicity events (fig 1 4)

$$\langle F_q \rangle^{(M)} = M^{q-1} \sum_{m=1}^{M} \frac{\left\langle n_m^{[q]} \right\rangle}{n^{[q]}} \tag{1 83}$$

The number of events generated is 2000 and the event multiplicity n is 6, 10 and 50 The number of steps ν in the cascade is 7, and the weight β is taken to be 0 7

From fig 1 3 an overestimation of the normalized moments as compared to the expected values (straight lines) can be seen The situation improves when the particle multiplicity is increased from 6 to 50

In fig 1 4 the rise of the factorial moments for high multiplicity events (n=50) nicely follow the predicted line However, for very low multiplicity (n=6), alas a reality for the NA22

---

[7] Capella et al [CFPL89] also decomposed the higher-order correlation into two-particle correlations They evaluated the integrals exactly, but, using for each order a parameter, did not recognize the NB behavior The free parameter determining the strength of the correlation is, for each order, fitted to the data in $\delta = L$, to get correct normalization The correlation length L is taken to be 1

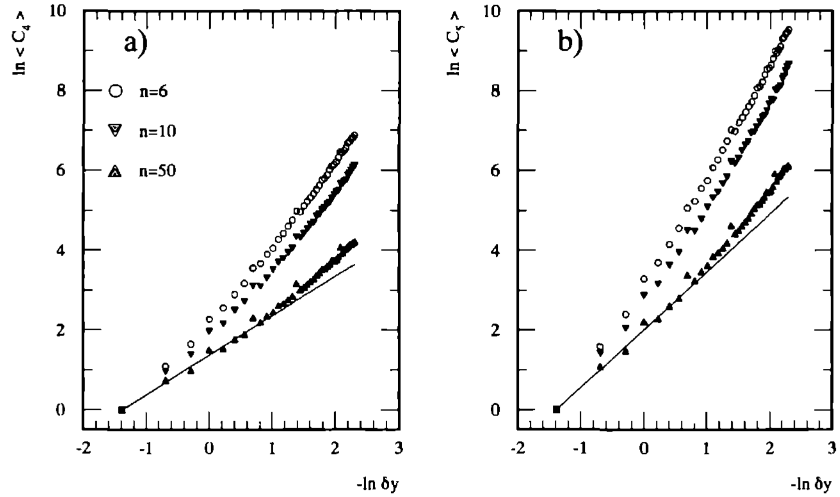

Figure 1.3: *The 4th and 5th order normalized moments for the p-model with* $p = 0.7$. *The points are from the Monte Carlo code. The multiplicities n are indicated. The lines give the analytical p-model prediction.*

experiment, the FM's bend down at small bin-sizes, even in this fully intermittent model. The points in the lower right angle of fig. 1.4 b, indicate bins without any contribution. Moments are in fact 0 for these bins, but they are plotted as an illustration. This effect, the so-called empty-bin effect, has been mentioned before, and will be studied further on.

1.6.2 Gaussian distributed particles

To see how factorial moments behave when there is a fixed correlation length, the following procedure has been proposed [LIPATH], in analogy to [BPNP86].

Choose, per event, the center of a spike randomly within the initial interval. Generate around this centre a number of particles, distributed according to a Gaussian with a certain width σ. The results, for three values of the width, are shown in fig. 1.5. The factorial moments rise steeply for $\delta > \sigma$, but saturate to a constant value for $\delta < \sigma$. The smaller the width, the larger the saturation value. The lines indicate the rise expected when all particles of the event are in the same bin. In that case (1.83) reduces to

$$\langle F_q \rangle^{(M)} = M^{(q-1)}.$$

The same saturation effect is observed for a real intermittent model (for example the p-model, see [LIPATH]), where the positions of the produced particles are smeared according to a Gaussian (or another realistic function) with a width corresponding to the experimental resolution. The experimental resolution, therefore, sets a lower limit to the region experimentally accessible for testing the FM's.

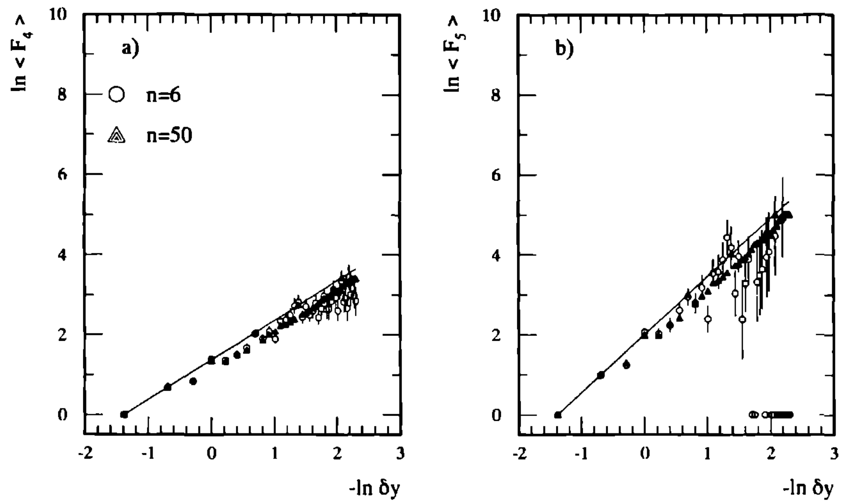

Figure 1.4: *The 4th and 5th order normalized factorial moments for the p-model. The points are from the Monte Carlo code. The multiplicities n are indicated. The lines give the analytical p-model prediction.*

1.6.3 Dead-zone

It was suggested by De Wolf [DENA91] that factorial moments might strongly suffer from the so-called dead-zone effect. This has an equivalent in photo-counting, where there is a dead time in the photo-tube after a photon has been detected. The dead time influences the measured photon multiplicity distribution. A correction scheme can be found in references [DEAD70].

Translated to hadron physics, dead-zone is the effect that two particles are so close together in rapidity (or any variable) that they cannot be distinguished and are taken to be one. In a distribution of rapidity gaps, this defect would show up as a dip in the distribution at small gap sizes. De Wolf has shown that even for very small dead-zones this would lead to a large underestimation of the factorial moments at small bin-sizes.

In the NA22 experiment fortunately, no sign of a dead-zone effect has been observed (chapter 5).

1.6.4 Moments from a single spike event

The NA22 anomalous event [SPIK87] is perfectly suited to demonstrate the effect of a density spike (that is almost all particles concentrated in one small interval of rapidity) on the behavior of the normalized factorial moments as a function of the bin-size. The formula relevant for the analysis of this event is the horizontal factorial moment definition (1.15)

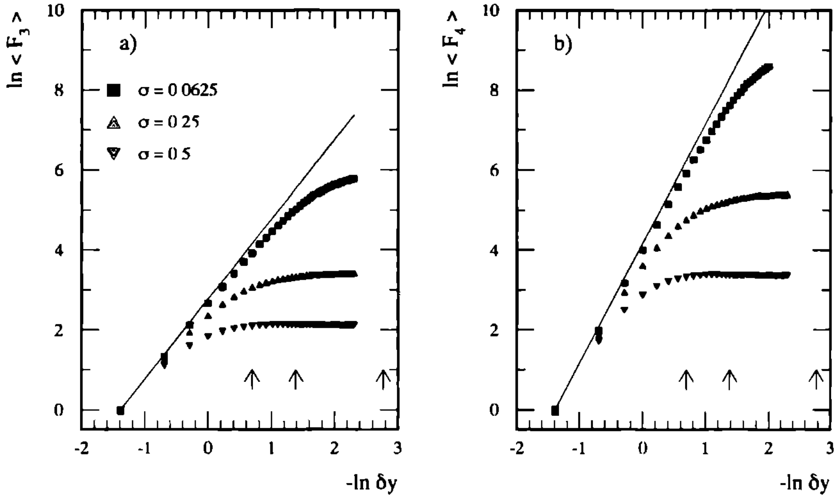

Figure 1.5: *The factorial moments F_3 and F_4 for a Gaussian distribution with three values of the width: σ = 0.0625, 0.25, and 0.5 (indicated by the arrows). The number of particles per event is 100 and the number of events is* 2000. *The solid lines indicate the expected rise for a spike event, see section below.*

with omission of the event averaging

$$F_q^{(M)} = M^{q-1} \sum_{m=1}^{M} \frac{n_m^{[q]}}{n^q} , \tag{1.84}$$

where n is the total number of particles inside the initial interval Δy.

Taking the logarithm on both sides, the formula naturally splits into a trivial δy dependent part and a non-trivial n_m dependent part

$$\ln F_q^{(M)} = (q-1)\ln M + \ln \sum_{m=1}^{M} n_m^{[q]}/n^q . \tag{1.85}$$

This suggests, in a log-log plot, a series of straight lines with slope (q-1), corresponding to a fixed number of particles n_m in the spike. In fig. 1.6, these are indicated as dashed lines, together with the corresponding particle number. The spike, though containing 10 particles in an interval of 0.098 rapidity units, does, at a binning of 40 and more intervals maximally contribute with 9 particles.

1.6.5 Superposition of intermittent sources

If there is intermittency in hadron-hadron interactions, it can also be expected in hadron-nucleus, or nucleus-nucleus interactions. Even more, there might in one event be a superposition of many intermittent sources. Also high multiplicity hadron-hadron events may have multiple intermittent sources.

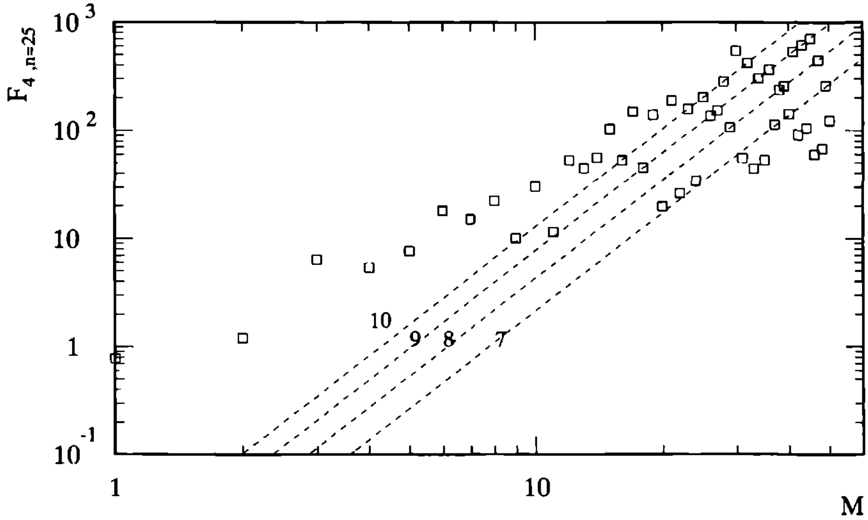

Figure 1.6: *The fourth-order factorial moment for the spike event. The dashed lines indicate possible trajectories expected from (1.85). The numbers correspond to the particle number* n_m.

The multiplicity dependence of the intermittency index has been studied first in [LBPL89]. In a so-called Białas plot (double logarithmic plot of the intermittency index versus the charged-particle density) evidence was found for a power law decrease of the intermittency strength with the multiplicity.

Analytically, such a power law has been derived by Capella et al. [CFPL89]. Assume there are N independent sources (the number of sources *could* be distributed according to a distribution $Q(N)$) with the same probability distribution $S(n)$. Then the total probability distribution $P(M)$ is a convolution, and the factorial moment generating function becomes

$$F_P(s) = \left\langle s^M \right\rangle_P = \langle s^n \rangle_S^N = F_S(s)^N \ . \tag{1.86}$$

The second order normalized factorial moment is then

$$F_2 = 1 + \frac{1}{N}(\mathcal{F}_2 - 1) \ . \tag{1.87}$$

If the $\mathcal{F}_2$ of the individual source is close enough to one, the intermittency slope can be estimated by

$$f_2 \approx \frac{1}{N}\phi_2 \ , \tag{1.88}$$

where ϕ_2 is the individual intermittency index. The dependence of higher-order slopes can be calculated, yielding the same N-dependence

$$f_q \approx \frac{1}{N}\phi_q \ . \tag{1.89}$$

1.6.6 Projection effect

Physical processes usually are three-dimensional in space or momentum. If a one-dimensional variable is studied, an integration over the remaining complementary variables has to be done (or they can be chosen in a specific region). In the case of intermittency it is proven, that this integration masks a lot of the original effect. Multidimensional analyses are, therefore, necessary to reveal the true aspects of the production process. Chapter 7 will be completely devoted to this rather recently developed topic.

1.7 The FRITIOF Monte Carlo

The complexity of present-day high-energy experiments makes it impossible to predict and calculate analytically the distributions in all measurable variables. Therefore, models are constructed that can be coded in the form of Monte Carlo [8] (MC) event generator programs. Simulating large numbers of events with these MC's allows to calculate distributions and to compare these to the experimental data.

Of course, in some cases, as in e^+e^- annihilation, it is possible to calculate analytically properties of outgoing e^+e^- or $\mu^+\mu^-$ pairs. Even then it is useful to have MC event generators at hand, since, in combination with MC detector simulation programs, it is possible to study detector efficiencies. In fact, present-day experiments are impossible without good MC generators.

In hadronic or leptonic interactions yielding hadrons in the final state, there is no theory that can be used to calculate the behavior of interactions from the beginning to the end. Of course, Quantum Chromodynamics (QCD) is assumed to be the underlying theory, but still, due to the large value of the strong-interaction coupling constant and to color confinement, it is impossible to describe the transition from the partonic (quark-gluon) state to the hadronic state. Therefore, phenomenological models based on educated guesses are necessary.

In the case of hadronic interactions at NA22 energies, one of these models converted to Monte Carlo code is FRITIOF. A complete description is given in [FRIT87]. A comprehensive introduction to this and other low-p_T models on the market, is given in [DRTH88].

In this thesis FRITIOF2.0 is used. It includes multiple soft gluon exchange to excite the incoming hadrons to larger masses, gluon radiation according to the color dipole approximation of [GUPL86] and a possibility of hard scattering. The hadronization at the end of the parton cascade makes use of the well-known LUND fragmentation scheme.

In the FRITIOF approach, low-p_T interactions are viewed as an exchange of many soft gluons between the incoming hadrons. Since no net color is transferred, the result of the interaction is an excitation of the colliding hadrons to larger masses M_1 and M_2, according to a probability distribution $\sim 1/M_1^2M_2^2$. The upper bound for the masses is determined by $M_1 + M_2 < \sqrt{s}$ and the lower bound by $M_i > m_i$ where m_i is the mass of the incoming particle. However, to avoid a too high yield of low mass 'strings' in the case of incoming π^+ and K^+ particles, in those cases the m_i are set to the mass of the ρ and $K^*(892)$, respectively.

The excited hadron can now be pictured as a longitudinally stretched string with the valence quarks (or di-quarks) at the end. If the string is an excited meson, the fragmentation is assumed to be the same as in e^+e^- annihilation. For an excited baryon, the fragmentation

---

[8] The principle of these programs is based on the use of pseudo-random numbers [JARP80], which explains the name Monte Carlo.

is taken to be equivalent to that of deep-inelastic lepton-hadron interactions. As in the case of the point-like interactions, the strings can radiate gluons, resulting in a gluon cascade. In FRITIOF this is done using the dipole approximation of [GUPL86]. Since hadron-hadron interactions are not point-like, it can be argued that the gluon emission should be softer than in e^+e^- interactions.

An additional feature of FRITIOF2.0 is that it also includes hard parton-parton scattering, resulting in a well-localized 'kink' on the string. The energy dependent cross-sections for these processes is calculated in [CSPR78] and for the Monte-Carlo implementation PYTHIA4.8 [PYTH87] is used.

The valence quarks of the incoming hadrons are given a primordial transverse momentum according to a gaussian distribution. The width of this distribution is set to 0.42 GeV/c.

The fragmentation of the final string setup is handled by JETSET version 6.3 [JETS63] of the LUND group. In short, the idea is that a string can break up by producing $q-\bar{q}$ or $qq-\bar{q}\bar{q}$ pairs according to an iterative scheme. A tunneling process is required if the (di-)quarks are assumed to have mass or transverse momentum. The function describing this process automatically leads to a suppression of heavy quark flavors and allows the quarks to obtain transverse momentum. The width of this fragmentation transverse momentum distribution is set to 0.44 GeV/c. The leading quark of the string couples to the anti-quark of the produced $q-\bar{q}$ pair, and forms a rank-one primary hadron with a certain longitudinal momentum defined by the fragmentation function. The energy of the remaining system is scaled down. The quark of the first produced $q-\bar{q}$ pair can combine with the anti-quark of a secondly produced $q-\bar{q}$ pair, forming a rank-two primary hadron. This goes on, until the mass of the string is below a certain cut-off value (the pion mass). The fragmentation function is left-right symmetric, meaning that it does not matter at which string end the fragmentation starts.

In the original version of the JETSET program, the primary hadrons are pseudo-scalar and vector mesons and baryons. The JETSET version used here also contains tensor mesons ($J^{PC}=2^{++}$) $f_2(1270)$, $a_2(1320)$ and $K_2^*(1430)$. The standard ratio for generating pseudo-scalar or vector mesons is changed from 50 : 50 to 50 : 35 : 15 for pseudo-scalar:vector:tensor. The decay of the unstable hadrons is also handled by JETSET.

The fragmentation of the di-quark, consisting of the leading L-quark and the 'held-back' J-quark, requires an additional distribution function. From the analysis of baryon production in NA22 meson-hadron interactions [NA22BA] it has been found that this distribution should be modified to $F(x_J) \sim x_J(1-x_J)^{10}$. The strangeness suppression factor λ is kept at its default value 0.3 giving a reasonable description of central K^0 production [NA22K0].

1.8 Appendix

1.8.1 Generating functions

In probability theory the method of generating functions is widely used. Here, some properties will be listed. The interested reader is advised to further consult [KSATS, VKSPPC, WMDICT].

The moment-generating function is defined as the expectation value of the (random) variable $\exp(xs)$

$$M(s) \equiv \langle e^{xs} \rangle \equiv \int e^{xs} P(x) \mathrm{d}x \tag{1.90}$$

For a discrete probability distribution [9]

$$P(x) = \sum_{n=0}^{\infty} P(n) \delta(x-n) \tag{1.91}$$

equation (1.90) can be rewritten

$$M(s) = \sum_{n=0}^{\infty} e^{sn} P(n) \tag{1.92}$$

Using a Taylor expansion for $M(s)$ around $s = 0$, rewriting $\exp(sn)$ as a sum of $(sn)^q/q!$ and exchanging the summations, it is easy to see that

$$\langle n^q \rangle = M^{(q)}(0) \tag{1.93}$$

In words The q^{th}-order moment is equal to the q^{th}-derivative of $M(s)$ with respect to s in $s = 0$

As an example, consider the (continuous) Gaussian distribution with average μ and dispersion σ According to (1.90)

$$M_{Gauss}(s) = \int e^{sx} \frac{1}{\sqrt{2\pi}\sigma} e^{-\frac{(x-\mu)^2}{2\sigma^2}} \mathrm{d}x = e^{\mu s + \frac{\sigma^2}{2} s^2} \tag{1.94}$$

For a (discrete) Poisson distribution with average α, the moment generating function is

$$M_{Poiss}(s) = \sum_{n=0}^{\infty} \frac{\alpha^n}{n!} e^{-\alpha} e^{ns} = e^{\alpha(e^s - 1)} \tag{1.95}$$

In certain cases, one is interested in the so-called cumulant moments Their generating function $C(s)$ is connected with the moment-generating function by

$$C(s) = \ln M(s) \tag{1.96}$$

Furthermore, the expectation value of s^x can be used as a probability-generating function as well as a factorial moment generating function In the first case, an expansion is made around $s = 0$

$$F(s) \equiv \langle s^x \rangle \equiv \sum_n s^n P(n) = \sum_n \frac{s^n}{n!} F^{(n)}(0) \tag{1.97}$$

Thus $F^{(n)}(0) = n! P(n)$

Expanding now around $s = 1$,

$$\begin{aligned} F(s) &= \sum_q \frac{(s-1)^q}{q!} F^{(q)}(s=1) \\ &= \sum_n s^n P(n) = \sum_n (s-1+1)^n P(n) \\ &= \sum_n \sum_{q=0}^{n} \binom{n}{q} (s-1)^q P(n) \\ &= \sum_q \frac{(s-1)^q}{q!} \sum_{n=q}^{\infty} n^{[q]} P(n) \quad , \end{aligned} \tag{1.98}$$

---

[9] Unless stated otherwise, the discrete case will be taken as default

it is clear that $F^{(q)}(s=1)$ can be identified with the factorial moment of order q, $\left\langle n^{[q]}\right\rangle$, where the notation $n^{[q]} = n(n-1)\cdots(n-q+1)$ has been used. In the following ξ_q will denote the q^{th}-order factorial moment.

It is interesting to see that the factorial moments of the Poisson distribution with $F(s) = e^{\alpha(s-1)}$ are

$$\xi_q = \frac{\partial^q F(s)}{\partial s^q}|_{s=1} = \alpha^q \quad , \tag{1.99}$$

leading to normalized factorial moments

$$\langle F_q \rangle = \frac{\xi_q}{\xi_1^q} = 1 \quad , \tag{1.100}$$

for all orders q.

In anology to cumulant moments, connected to normal moments, one defines factorial cumulant moments k_q, connected to the factorial moments ξ_q, via the relation

$$\begin{aligned} K(s) &= \ln F(s) \quad \Rightarrow \quad F(s) = e^{K(s)} & (1.101)\\ k_q &= \frac{\partial^q K(s)}{\partial s^q}|_{s=1} \quad . & (1.102) \end{aligned}$$

For a probability distribution that can be written as a Poisson transform

$$P_{PT}(n) = \int P(x) \frac{(zx)^n}{n!} e^{-(xz)} \mathrm{d}x \quad , \tag{1.103}$$

$F(s)$ is found to be

$$F_{PT}(s) = \sum_{n=0}^{\infty} \int P(x) \frac{(zx)^n}{n!} e^{-(zx)} s^n \mathrm{d}x = \int P(x) e^{xz(s-1)} \mathrm{d}x \quad . \tag{1.104}$$

Taking the q-th partial derivative with respect to s at $s=1$, one finds

$$\xi_q = \int P(x)(xz)^q \mathrm{d}x = z^q \langle x^q \rangle_P \quad . \tag{1.105}$$

This important result forms the basis of the papers by Białas and Peschanski [BPNP86, BPNP88]. From (1.104) it can be seen that the factorial-moment generating function of a Poisson transform is directly linked to the moment-generating function of the measure $P(x)$.

An intriguing property of the Negative Binomial distribution can now easily be obtained, realizing that the NBD is a Poisson transform of a conveniently defined Gamma distribution $g(x)$

$$g(x) = \frac{1}{\Gamma(k)} (\frac{\bar{n}}{k})^{-k} x^{k-1} e^{-xk/\bar{n}} \quad , \tag{1.106}$$

because in that case one finds for the factorial-moment generating function of the NBD

$$\begin{aligned} F_{NB}(s) &= \sum_{n=0}^{\infty} \int_0^{\infty} \frac{1}{\Gamma(k)} (\frac{\bar{n}}{k})^{-k} x^{k-1} e^{-xk/\bar{n}} s^n e^{-x} \frac{x^n}{n!} \mathrm{d}x \\ &= \int_0^{\infty} \frac{1}{\Gamma(k)} (\frac{\bar{n}}{k})^{-k} x^{k-1} e^{-x(k/\bar{n}-s+1)} \mathrm{d}x = (1-(s-1)\frac{\bar{n}}{k})^{-k}. \end{aligned} \tag{1.107}$$

From this it is clear that the normalized factorial moments are independent of $\bar{n}$

$$\langle F_q \rangle = \frac{\bar{n}^q \prod_{j=0}^{q-1}(1+\frac{j}{k})}{\bar{n}^q} = \prod_{j=0}^{q-1}(1+\frac{j}{k}) \ . \tag{1.108}$$

For a compound distribution with N independent sources, distributed according to $P(N)$, and with all sources having the same distribution $Q(n)$

$$P_{comp}(n) = \sum_{N=0}^{\infty} P(N) \sum_{n_1 \ldots n_N} \prod_{j=1}^{N} Q(n_j)\delta(n - \sum_{j=1}^{N} n_j) \tag{1.109}$$

the (factorial-moment) generating function is:

$$F_{comp}(s) = F_P(F_Q(s)) \ . \tag{1.110}$$

Assuming that the NBD is a compound distribution with the number of sources distributed according to a Poissonian, the probability distribution of emission of particles in each individual source can be found using (1.110) and (1.107). As stated in [GIZP86] it turns out to be a logarithmic distribution. In this reference a clan cascade model is described explaining the data in terms of aggregation of particles within a clan.

Alternatively, for a fixed number of sources k, the distribution of particles emitted from one source is the geometric (Bose-Einstein) distribution

$$P_{BE}(n) = \frac{\bar{m}^n}{(\bar{m}+1)^{n+1}}, \tag{1.111}$$

because in that case

$$F_{NBD}(s) = F_{BE}(s)^k \quad , \text{ with } \ F_{BE}(s) = (1-(s-1)\frac{\bar{n}}{k})^{-1} \tag{1.112}$$

and with $\bar{m} = \bar{n}/k$. This construction of the NBD has been known since 1924 when it was derived by Planck [PLAN32]. It was re-derived for photo-count distributions in optics by Mandel [MAND59] and was found to fit hadronic multiplicity data by Giovannini [GINC72]. In the eighties the interest in the NBD revived [CSPL83] and it has been used since then by many experiments to fit the data on multiparticle production in high-energy collisions.

1.8.2 Definition of variables

All of the analyses presented in this thesis have been done in a right-handed coordinate system, with the beam momentum along the x-axis. This axis will be called the longitudinal axis and the plane perpendicular to this the transverse plane. The momentum of a particle, measured in the laboratory (lab) frame then consists of a longitudinal component p_x and two transverse ones, p_y and p_z. Together they form a three vector $\bar{p} = (p_x, p_y, p_z)$. The kinematical description of the particle is completed, if besides the charge, also the mass m, and thus the energy E, is known.

The energy of a multiple production process

$$a + b \rightarrow h_1 + h_2 + \cdots + h_n$$

is determined by the mass and momenta of the incoming particles a and b. It is usually expressed in the Lorentz invariant, i.e. frame-independent, variable

$$\sqrt{s} = \sqrt{(E_{beam} + E_{target})^2 - (\bar{p}_{beam} + \bar{p}_{target})^2} \quad , \tag{1.113}$$

called the invariant mass. For a fixed target experiment this mass reduces to

$$\sqrt{s} = \sqrt{m_{beam}^2 + m_{target}^2 + 2E_{beam}m_{target}} \quad . \tag{1.114}$$

Though the momentum is measured in the lab frame, in most analyses the center-of-mass (c.m.) transformed momentum p_{cms}, also denoted as p^*, is used. Unless stated otherwise this will be the convention and all other variables will be expressed in the c.m. system, too.

In addition to the four-momentum $(E, \bar{p})$ the following variables are used in this thesis

- The *transverse momentum* p_T

$$p_T = \sqrt{p_y^2 + p_z^2} \ , \tag{1.115}$$

- The *azimuthal angle* φ

$$\varphi = \arctan\left(\frac{p_z}{p_y}\right) \ . \tag{1.116}$$

  Since there is no preferred transverse direction for unpolarized incoming particles the distribution in φ is uniform.

- The *rapidity* y, a longitudinal variable defined by

$$y = \frac{1}{2}\ln\left(\frac{E + p_x}{E - p_x}\right) . \tag{1.117}$$

  It can be easily seen that the c.m. rapidity

$$y^* = \frac{1}{2}\ln\left(\frac{1+\beta}{1-\beta}\right) + y_{lab}, \tag{1.118}$$

  where β is the parameter of the Lorentz transformation from the lab to the c.m.

$$\beta = \frac{-p_{beam}}{E_{beam} + m_{target}}. \tag{1.119}$$

  This implies that the shape of the rapidity distribution is invariant under a longitudinal Lorentz transformation. The reason to use rapidity in our analyses is that the region of small momenta is stretched, thus forming a plateau. This is contrary to

- The *Feynman variable* x_F

$$x_F = \frac{p_x}{p_{max}} \approx \frac{2p_x}{\sqrt{s}} \ , \tag{1.120}$$

  where the approximation is valid for $m \ll \sqrt{s}$ and p_{max} is the maximum momentum the particle can possibly have in the interaction. This variable is particularly well suited to study particles with momenta close to p_{max}, or with $x_F = \pm 1$. Small longitudinal momenta are compressed into a small region near $x_F = 0$.

- The last variable *pseudo-rapidity*

$$\eta = -\ln\tan(\theta/2) \approx -\ln\frac{p_T}{|\vec{p}| + p_x} \tag{1.121}$$

is a good approximation of rapidity for $p_x \gg p_T \gg m$. This variable is used in experiments where only the production angle θ but not the absolute value of the momentum can be measured.

In this thesis only so-called n-particle inclusive reactions are investigated. This means that one counts the number of particles in an event with a certain characteristic, irrespective of the other particles produced in that event. If an inclusive reaction is denoted by

$$a + b \longrightarrow c + X, \tag{1.122}$$

then the number of events with exactly n particles of type c is proportional to the topological cross-section:

$$N_n^c \propto \sigma_n^c \ . \tag{1.123}$$

The total cross section is then defined as the sum of all topological cross sections

$$\sigma_{Tot}^c = \sum_{n=1}^{\infty} \sigma_n^c \quad , \tag{1.124}$$

and is an indication for the total number of events in which at least one particle of type c is produced. Finally, a measure of the total number of particles c produced is the so-called inclusive cross section defined as

$$\sigma_{incl}^c = \sum_{n=1}^{\infty} n\sigma_n^c \quad , \tag{1.125}$$

and related to the average number of particles of type c by

$$\langle n_c \rangle = \frac{1}{\sigma_{Tot}^c} \sum_n n\sigma_n^c = \sum_n nP_c(n) \quad . \tag{1.126}$$

Bibliography

[ABZP91] J. Alberty and A. Białas, Z. Phys. C50 (1991) 315.

[APZP91] J. Alberty, R. Peschanski and A. Białas, Z. Phys. C52 (1991) 297.

[BHPL91] A. Białas and R. Hwa, Phys. Lett. B253 (1991) 436.

[BLMP89] B. Buschbeck and P. Lipa, Mod. Phys. Lett. A4 (1989) 1871.

[BPNP86] A. Białas and R. Peschanski, Nucl. Phys. B273 (1986) 703.

[BPNP88] A. Białas and R. Peschanski, Nucl. Phys. B308 (1988) 857.

[BPNP90] P. Brax and R. Peschanski, Nucl. Phys. B346 (1990) 65.

[BPPL88] A. Białas and R. Peschanski, Phys. Lett. B207 (1988) 59.

[BPPL91] P. Brax and R. Peschanski, Phys. Lett. B253 (1991) 225.

[BSZP89] A. Białas, A. Szczerba and K. Zalewski, Z. Phys. C46 (1990) 163.

[BZPL90] A. Białas and K. Zalewski, Phys. Lett. B238 (1990) 413.

[CEPL91] P. Carruthers, H. Eggers and I. Sarcevic, Phys. Lett. B254 (1991) 258.

[CFPL89] A. Capella, K. Fiałkowski and A. Krzywicki, Phys. Lett. B230 (1989) 149.
A. Capella, K. Fiałkowski and A. Krzywicki, Proc. Multi-Particle Dynamics La Thuile 1989, eds. A. Giovannini and W. Kittel (World Scientific 1990) p 413.

[CHARTH] M. Charlet, Ph.D. thesis Univ. of Nijmegen, in preparation.

[CHPL91] V. Aivazyan et al. (NA22 Collab.), Phys. Lett. B258 (1991) 487.

[CHPR43] C. Chiu and R. Hwa, Phys. Rev. D43 (1991) 100.

[CSPL83] P. Carruthers and C. Shih, Phys. Lett. 127B (1983) 242.

[CSPR78] R. Cutlers and D. Sivers, Phys. Rev. D17 (1978) 196.

[CSPR89] P. Carruthers and I. Sarcevic, Phys. Rev. Lett. 63 (1989) 1562.

[DEAD70] R. Chang, et al. , Phys. Rev. 178 (1969) 178.
B. Cantor and M. Teich, Jour. of the Optical Soc. of Am. 65 (1975), 786.
F. Johnson et al. , Phys. Rev. Lett. 16 (1966) 589.

[DENA91] E.A. De Wolf, paper presented at the CERN Workshop on Intermittency, January 1991.

[DRTH88] A. De Roeck, Inclusive particle production in hadron-proton interactions at 250 GeV/c, Ph.D. thesis Univ. of Antwerp 1988.

[DWAP90]	E.A. De Wolf, Acta Phys. Pol. B21 (1990) 611.
[EGGETH]	H. Eggers, Intermittency, moments and correlations in distributions of particles created in high energy collisions, Ph.D. thesis Univ. of Arizona 1991.
[FELLV1]	W. J. Feller, An introduction to probability theory and its applications, 3rd edn. Vol. 1, New York: Wiley 1968.
[FELLV2]	W. J. Feller, An introduction to probability theory and its applications, 1st edn. Vol. 2, New York: Wiley 1966.
[FRIT87]	B. Nilsson-Almqvist and E. Stenlund, Comput. Phys. Commun. 43 (1987) 387. B. Andersson, G. Gustafson and B. Nilsson-Almqvist, Nucl. Phys. B281 (1987) 289. B. Andersson, G. Gustafson and B. Nilsson-Almqvist, A high energy string dynamical model for hadronic interactions, LUND preprint LU-TP 87-6 (1987) unpublished.
[FSNJ78]	U. Frisch, P. Sulem and M. Nelkin, J. Fluid Mech. 87 (1978) 719.
[FWAP89]	K. Fiałkowski, B. Wosiek and J. Wosiek, Acta Phys. Pol. B20 (1989) 639.
[GINC72]	A. Giovannini, Nuovo Cimento 10A (1972) 713; ibid. 15A (1973) 543, ibid. , 24A (1974) 421, ibid. 34A (1976) 547.
[GIZP86]	A. Giovannini and L. Van Hove, Z. Phys. C30 (1986) 391.
[GUBI90]	S. Gupta, P. La Cock and H. Satz, The search for intermittency in the finite-size Ising model, BI-TP 90/21.
[GUPL86]	G. Gustafson, Phys. Lett. B175 (1986) 453. G. Gustafson and U. Petterson, Nucl. Phys. B306 (1988) 746.
[HPPH83]	H. Hentschel and I. Procaccia, Physica 8D (1983) 435.
[HSNP89]	H. Satz, Nucl. Phys. B326 (1989) 613.
[HUSM63]	K. Huang, Statistical Mechanics, John Wiley and Sons, 1963.
[HWOI91]	R. Hwa and C. Pan, preprint OITS-478 (1991).
[HWPR41]	R. Hwa, Phys. Rev. D41 (1990) 1456.
[JAPR83]	T.H. Burnett et al. (JACEE collab.), Phys. Rev. Lett. 50 (1983) 2062.
[JARP80]	F. James, Rep. Prog. Phys. 43 (1980) 1145.
[JETS63]	B. Andersson, G. Gustafson, G. Ingelman and T. Sjöstrand, Phys. Rep. 97 (1983) 33. T. Sjöstrand, Comput. Phys. Commun. 39 (1986) 347. T. Sjöstrand and M. Bengtsson, Comput. Phys. Commun. 43 (1987) 367.

[JFZN82] J. Doyne Farmer, Z. Naturf. 37a (1982) 1304.

[KOJF62] A. Kolmogorov, J. Fluid Mech. 13 (1962) 82.

[KPAM83] V. Koroliouk, N. Portenko, A. Skorokhod, A. Tourbine, Aide-mémoire de théorie des probabilités et de statistique mathématique, Editions Mir, Moskou, USSR (1983).

[KSATS] M. G. Kendall and A. Stuart, The Advanced Theory of Statistics, Vol. 1-3, Charles Griffin & Company Limited, London, 1967.

[LBPL89] P. Lipa and B. Buschbeck, Phys. Lett. B223 (1989) 465.

[LIPATH] P. Lipa, Intermittency in Antiproton-Proton Collisions, Ph.D. thesis Univ. of Vienna, HEPHY-PUB 542/90, 1990.

[LSTS83] D. Shertzer and S. Lovejoy, Selected papers from the 4th Int. Symp. on Turbulent Shear Flows, Univ. of Karlsruhe (1983), ed. L. Bradbury et al. (Springer 1984).

[MAJF74] B. Mandelbrot, J. Fluid Mech. 62 (1974) 331.

[MAND59] L. Mandel, Proc. Phys. Soc. 74 (1959) 233.

[MSPR87] C. Meneveau and K. R. Sreenivasan, Phys. Rev. Lett. 59 (1987) 1424.

[MUPR71] A. H. Mueller, Phys. Rev. D4 (1971) 150.

[NA22BA] I. Ajinenko et al. (NA22 collab.), Z. Phys. C44 (1989) 573.

[NA22K0] I. Ajinenko et al. (NA22 collab.), Z. Phys. C46 (1990) 525.

[NOBR89] I. Novak, Bratislava preprint (1989).

[OWPL88] W. Ochs and J. Wosiek, Phys. Lett. B214 (1988) 617.

[PLAN32] M. Planck, Sitzungsber. Deutsch. Akad. Wie. Berlin 33 (1932) 365.

[PVPR87] G. Paladin and A. Vulpiani, Phys. Rep. 156 (1987) 147.

[PYTH87] H.-U. Bengtsson and T. Sjöstrand, Comput. Phys. Commun. 46 (1987) 43.

[REYN83] O. Reynolds, Phil. Trans. Roy. Soc. London 174 (1883) 935.

[RPCE90] R. Peschanski, Intermittent signal of a quark-gluon plasma, Proc. Int. Workshop on Quark Gluon Plasma Signatures, Strasbourg 1990 eds. V. Bernard et al. (Editions Frontières 1991) p 81.

[RPNP89] R. Peschanski, Nucl. Phys. B237 (1989) 144.

[RPSF90] R. Peschanski, Why and How to Normalize the Factorial Moments of Intermittency, Contribution to the Santa Fe workshop on Intermittency in High energy Collisions, 1990, editors F. Cooper, R. C. Hwa, I. Sarcevic, World Scientific.

[SAJF59]	V.A. Sandborn, J. Fluid Mech. 6 (1959) 221.
[SANP89]	H. Satz, Nucl. Phys. B236 (1989) 613.
[SPIK87]	M. Adamus et al. (NA22 Collab.), Phys. Lett. B185 (1987) 200.
[VKSPPC]	N. G. van Kampen, Stochastic processes in physics and chemistry, North-Holland Physics Publishing, 1st edition, 1981.
[WMDICT]	W. J. Metzger, Statistical Methods in Data Analysis, Nijmegen preprint HEN-343, 1991.
[WOAP88]	J. Wosiek, Acta Phys. Pol. B19 (1988) 863.
[ZAJU90]	K. Zalewski, Acta Phys. Pol. B21 (1990) 501.

2

The NA22 experiment

In this chapter a short description will be given of the detector used for the NA22 experiment. Details on the setup and on the reconstruction of the data can be found in the theses of P.van Hal [VHTH87], F.Meyers [FMTH87], A.De Roeck [DRTH88] and L.Scholten [LSTH88]. These physicists were also deeply involved in developing quality selection criteria for reconstructed event vertices and particle tracks. A summary of their findings is given in the last part of this chapter.

2.1 NA22 experimental setup

The NA22 experiment (codename for the 22^{nd} experiment accepted to take data in the CERN North Area) made use of the European Hybrid Spectrometer (EHS) in combination with the Rapid Cycling Bubble Chamber (RCBC). The data were taken in two running periods: Run A during June-July 1982 and run B during July-August 1983. A general description of the EHS spectrometer can be found in the proposal [EHPR80] and in [ABNI83].

The setup of the NA22 experiment is shown in fig. 2.1. The abbreviations used in the figure stand for:

U1 U3 W2	Multi-Wire Proportional Chambers
D1 - D6	Drift Chambers
M1 M2	Magnets
RCBC	Rapid Cycling Bubble Chamber
SAD	Silica Aerogel Detector
ISIS	Identification of Secondaries by Ionization Sampling
FC	Forward Čerenkov
TRD	Transition Radiation Detector
IGD FGD	Intermediate/Forward Gamma Detector
INC FNC	Intermediate/Forward Neutral Calorimeter
ITH ITV	Horizontal and Vertical Trigger Hodoscopes

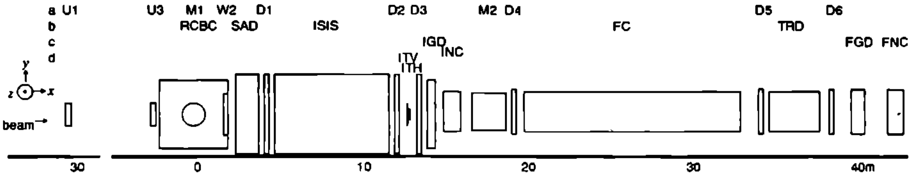

Figure 2.1: *The layout of the NA22 experiment. The top line (marked with a), indicates the devices used for charged-particle momentum reconstruction. Line b shows the charged-particle identification detectors, line c the neutral-particle detectors, and the last line, d, marks the trigger devices. The coordinate system, and the beam direction are indicated at the left.*

2.1.1 Beam

The NA22 beam is obtained from 400 GeV/c primary protons extracted from the CERN Super Proton Synchrotron and hitting a beryllium target about 600 meters upstream of EHS. Positively charged particles of 250 GeV/c momentum are selected by beam optics with a statistical spread of $\Delta p/p \approx 0.3\%$ and a relative uncertainty on the nominal value of 0.5%. The meson content is enriched by a 5.5 meter long polyethylene filter (the absorption length of this material is shortest for protons and longest for kaons). After filtering, the background consists of 27% muons (which is unfortunately increased due to this procedure); the hadronic component (73%) consists of protons (45.8%), π^+ (38.9%) and K^+ (15.3%).

The secondary beam is focussed in the horizontal (z) direction, such that the minimum width is obtained 12.5 meters behind RCBC.

Since some of the detectors perform badly when exposed to large intensities and in order to prevent irrelevant beam particles from confusing the RCBC pictures, two measures are taken to reduce the number of beam particles passing through the system:

- After the trigger has registered an event, a kicker magnet deflects the beam particles during the rest of the sensitive time of the bubble chamber (500 μs for run A and 1000 μs for run B).
- A 'chopper' (a disc with a sleeve in it), rotating at the running frequency of the RCBC (15 Hz) allows beam particles to pass only during the sensitive time of the chamber.

The identity of the beam particles is determined with two CEDARs (differential Čerenkov counters), one of them being adjusted to give a signal for a 250 GeV/c pion, the other for a kaon of same momentum (for a small part of the runs the pion counter has been adjusted to detect protons). The discrimination efficiency of the CEDARs was 100 percent, the detection efficiency about 75%. Two multi-wire proportional chambers (U1 and U3) were used to reconstruct the momentum direction of the beam particles. Further details on the beam can be found in [ATYR80].

diameter	85 cm
depth	40 cm
exit window	1.6 mm stainless steel
vacuum tank window	1 mm Al and 2 mm GRP (glass-reinforced-plastic)
sensitive time of RCBC	0.5 ms (Run A) 1.0 ms (Run B)
running frequency	15 Hz
average # of beam tracks/expansion	10
average bubble size	250 μm
two-track resolution	0.5 mm (2 bubbles)
average # of bubbles per cm	10
distance camera-RCBC	1.5 m
demagnification on film	16
separation of camera's (stereo base)	70 cm giving a 21° stereo angle

Table 2.1 *Bubble chamber characteristics*

2.1.2 RCBC: target and vertex detector

The bubble chamber has the form of a cylinder with a diameter of 85 cm (70 cm fiducial volume) and a depth of 40 cm. The axis is oriented along the z-direction. Three cameras positioned behind a glass shield, at 16° with respect to the z-axis, allow to take stereographic pictures.

At the beginning of the chamber sensitive time, a piston is moved outwards and the liquid hydrogen which before the expansion was maintained under an overpressure at a temperature of 25° K, is brought below its critical density (is superheated). Charged particles moving through the hydrogen ionize the atoms along their tracks and boiling starts around these ions. The resulting bubbles are allowed to grow during 1 ms and reach a size of about 250 μm. Then the stereo pictures are taken and the liquid is compressed again. This cycle is repeated 15 times per second.

The main target in the experiment are the nuclei of the hydrogen atoms contained in the chamber. In addition, two foils, one of gold and one of aluminum, are mounted inside RCBC at 15.5 cm from the entrance window. Interactions of beam particles with the nuclei of these foils are not discussed in this thesis. The interaction length in H_2 is 9.4 m for π^+, 11.4 m for K^+ and 5.7 m for p, corresponding to a total interaction cross-section of 24, 20 and 40 mb, respectively.

Due to the outgoing charged tracks it is possible to see the vertex and obtain a very precise knowledge of its position. The charged-track multiplicity and the track path can be determined exactly. This holds for the primary as well as for secondary interactions and decays.

The curvature of the track, caused by the the 2 Tesla magnet M1 surrounding RCBC, allows momentum measurement for charged particles with low momentum (sec. 2.1.4). Finally, the intensity of ionization makes it possible to distinguish protons from pions for $p_{lab} < 1.2$ GeV/c (sec. 2.1.5), or single from multiple tracks at high momentum.

In table 2.1.2 some RCBC characteristics are listed.

2.1.3 Trigger

The secondary beam intensity is about 20,000 particles/sec yielding an average of 10 particles per expansion. The weighted probability for a particle to collide with a proton in the RCBC is ≈ 14% . It is therefore possible that no interaction takes place during one expansion. To reduce the number of useless pictures, an interaction trigger [TRIG81] with 3 levels is used. The trigger layout is shown in fig. 2.2. Level 0 is the beam trigger. It checks whether the experiment is ready and whether a beam particle has entered the setup. For the latter, four scintillation counters, T1, T2, V1 and V2, are placed upstream of the RCBC. If no signal in V1 and V2, but a signal in both T1 and T2 is seen, the level 1 trigger has to be checked, otherwise level 0 is activated again.

The Level 1 trigger vetoes non-interacting beam tracks. If no track is seen in the central (ITV(2)) vertical scintillator strip of ITV or more than 1 track is seen in horizontal scintillator strips of ITH, the event is accepted on this level. ITV(2) is very efficient since only 5% of the non-interacting beam tracks fall outside its area. Both ITH and ITV are positioned 12 m downstream of RCBC. Because of the bending power of M1 the secondary tracks are spread out in the vertical direction and tracks reaching ITH give a signal. If no track gets that far, ITV(2) is not hit, and the event is accepted.

Level 2 of the trigger vetoes the interactions downstream the W2 wire chamber (at 1.6 meters behind the RCBC), for example in ISIS. If there are less than 3 hits in the planes 1 and 6 of W2, and more than 1 in ITH the event is rejected. Also the signal of the CEDARs is used in this part (their signal arrives too late for level 0 and 1). No signal means that the beam particle is a proton and the event is dropped.

The trigger is designed for maximum event acceptance and is, therefore, called a *minimum bias* trigger. However, levels 1 and 2 cause a bias, depending on the event shape, that has to be corrected for. The way each event obtains a trigger weight is described in [VHTH87] (and [DRTH88]).

For run A, in addition, an Optical Fiducial Volume Trigger (OFVT) [OFVT84] was used. It vetoes events with more than 20 beam tracks entering RCBC before the picture is taken and checks if the interaction is within the fiducial volume.

Summarized, the trigger logic looks like:

$$\begin{aligned}&\underbrace{T1\wedge T2\wedge(V1\vee\overline{V1)}\wedge Exp.Ready}_{Level\ 0}\wedge\underbrace{(IT\overline{V(2)}\vee ITH(n\geq 2))}_{Level\ 1}\wedge\\&\underbrace{\overline{ITH(n>1)\wedge\sum_{1,6}W2(n<3)}\wedge(C1\vee C2)}_{Level\ 2}\wedge\underbrace{(OFVT\vee RUNB)}_{Level\ 3}\end{aligned}\tag{2.1}$$

2.1.4 Momentum measurement

The momentum of charged particles is measured from the curvature of the tracks in a magnetic field. The field of the magnets is such that the track curvature is in the vertical plane. Very slow tracks (p_{lab} < 3 GeV/c) are curved enough in M1 to allow for measurement of their momentum.

Faster tracks, in general, enter the so-called first lever arm. This consists of the Multi-Wire Proportional Chamber (W2), and the three Drift Chambers D1, D2 and D3.

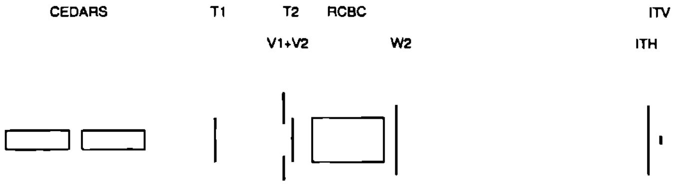

Figure 2.2: *The NA22 trigger components, seen from above.*

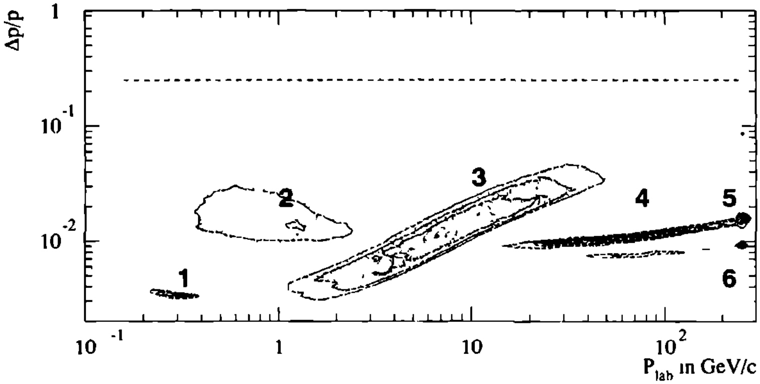

Figure 2.3: *Relative momentum resolution $\Delta p/p$ versus p_{lab}. The clusters correspond to different combinations of wire chambers, see text*

Tracks with momentum larger than 50 GeV/c pass through the gap in magnet M2 and thus enter the second lever arm with wire chambers D4, D5 and D6. The field of M2 in run A was 1.5 T parallel to the field in magnet M1. In run B the field was turned in the opposite direction and decreased to 0.75 T. This change slightly deteriorated the resolution of the momentum measurement, but improved the acceptance for tracks with $30 < p_{lab} < 80$ GeV/c.

The relative momentum resolution is plotted in figure 2.3. Six situations can be distinguished:

1: RCBC + M1 + range momentum relation (stopping protons)
2: RCBC + M1
3: RCBC + M1 + W2 + D1 + D2 + D3 (first lever arm)
4: RCBC + M1 + W2 + D1 + D2 + D3 + D4 (first and part of second lever arm)
5: RCBC + M1 + W2 + D1 + D2 + D3 + D4 + D5 + D6 (run B)
6: RCBC + M1 + W2 + D1 + D2 + D3 + D4 + D5 + D6 (run A)

The points outside the cluster regions are due to failures of the reconstruction program or to secondary interactions of outgoing tracks. The resolution in the angles ϕ and λ is limited to 0.05 mrad due to multiple scattering. ϕ is the angle between p_{xy} and the x-axis, where p_{xy} is the projection of $\bar{p}$ on the xy-plane. λ is the (dip) angle between $\bar{p}$ and the xy-plane.

2.1.5 Charged-particle identification in RCBC

Except for RCBC, in this thesis no use is made of the information from the particle identification devices The main reasons are that the majority of produced particles are pions, that these detectors only have a limited acceptance and that for the study of correlations they would have to be used on a track-to track basis The devices, however, are well suited for inclusive single-particle measurements [CPID91]

Using the momentum of a particle as measured from the track curvature in the magnetic field of magnet M1 and using a certain mass hypothesis, it is possible to calculate the expected energy loss from the Bethe-Bloch formula The energy loss is due to the electromagnetic interaction of the moving particle with the atoms in matter It results in an ionization of the atoms along its path, which in RCBC can be seen as a track with a bubble density depending on the rate of ionization Thus, comparing the predicted rates of ionization for the different mass hypotheses with the rate measured on the picture allows to discriminate between these hypotheses

The procedure of assigning mass to a particle from RCBC information is described in chapter 5

A further important use of the ionization was that (fast) tracks exactly overlapping in the bubble chamber appear as one track with ionization two or more In the scanning stage a fast track with heavy ionization was flagged and allowed to be matched with more than one track in the 40 m downstream spectrometer This advantage of visual detection and long lever arm has led to the particularly small two track resolution to be discussed in chapter 5

2.2 Data reconstruction

The reconstruction starts with three scan phases First, the interacting beam is searched, using predictions for the y and z position obtained from the information of the upstream wire chambers (program PREDIC)

The second step is to decide whether or not to measure the event Event rejection is caused by faint pictures or by too large a number of tracks in the neighborhood of the interacting beam (those tracks may be non-interacting beam particles or secondaries from a proton interaction having taken place before the triggering π^+, K^+ interaction)

In the third step, the event topology is determined That is, the number of secondary tracks, gammas, decays, and so on are counted and recorded At this stage, furthermore, the vertex position is measured precisely Scanning rules and formats are described in [SCAN83]

After scanning, the events are measured, either (semi-)automatically or manually, depending on the event topology and quality of the picture In principle, all three stereoscopic views are measured The rules are given in [MEAS84] On the average, 20 points are measured on each track In addition, the tracks are given an identification label (see chapter 5)

After measurement, the event is processed through a chain of reconstruction programs The first one is GEOHYB This program performs a geometrical reconstruction of the event It consists of several parts

-A- The vertex position in space is reconstructed from the 3 views The track image on each view is fitted to determine track curvature, RMS of measured points etc This is important to match the RCBC tracks with the spectrometer tracks (hooking of tracks) in a later stage

-B- The upstream part of the beam is reconstructed

-C- Downstream spectrometer tracks are reconstructed. This is a very involved procedure. It uses pattern recognition to form strings from the hits in the wire chambers. ISIS and TRD information is used to select strings. Accepted strings are coupled to RCBC tracks. If that succeeds for at least 2 views, a so-called hybrid track fit is performed. Ambiguities, for example due to hooking more spectrometer tracks to one RCBC track, are resolved in this procedure.

-D- Bubble chamber tracks without associated spectrometer hookings are reconstructed. To low momentum tracks ($p_{lab} < 2$ GeV/c) a mass dependent fit is applied. Stopping tracks get a momentum depending on their range (track length). Fits are obtained at several stages, each stage resolving ambiguities.

Non-associated tracks are extrapolated to the wire chambers in the first lever-arm of the spectrometer (swimming), and procedure C is repeated with larger tolerances.

Spectrometer tracks from procedure C that have no corresponding RCBC track, are called hanging tracks. The so-called 'rescue procedure' consists of an endeavor to associate the swimming tracks with the hanging tracks.

-E- A large part of the above procedure is repeated for tracks originating from a vertex outside RCBC. They are used in the HANG program to fit V^0's decaying outside RCBC [REVZ85]. V^0's are neutral particles (γ, π^0, K_L, Λ, $\bar{\Lambda}$) that convert or decay.

-F- The output of the program is cast into a specific format [GSTN84] and stored on tape (Geometry Summary Tape) for further processing.

The geometric reconstruction is not the last part of the chain. A special program to determine the event quality is described in the next sub-section.

Furthermore, a reconstruction program for the gamma detectors (IGD and FGD) had to be run. Kinematical fits for neutral and charged decays and for low topology primary vertices are handled by the program KINEM. This is described in detail in the thesis of L. Scholten [LSTH88].

Charged tracks passing through a particle identification device are assigned confidence levels according to several mass hypotheses. This procedure is described in [FMTH87].

At the end of the chain, the program DSTMAKER condenses the large GST into a smaller Data Summary Tape. Here, also the information from the so-called Ionization Scan [IONS84] is added.

The purpose of this last scan is two-fold: Predictions on the relative ionization based on various mass hypotheses can be compared with that seen on the picture. For tracks with momentum smaller than 1.2 GeV/c this leads to distinction between pions and protons.

At this phase, also a decision about the measurement can be made: The event can be flagged not measurable or doubtful, in which case it has to be remeasured. It might happen that at the previous scannings certain labels are not added correctly, or were overseen. This can be corrected during the ionization scan.

2.2.1 Quality assignment

After geometric reconstruction, a program named QUAL is run to determine the event quality and to take decisions left open by GEOHYB. This is described in [QUAL84].

Events may be improved in this stage to increase the number of acceptable events. For example, a very bad or suspicious track may be dropped in an event that has a number of reconstructed outgoing tracks larger than the number of measured tracks It might happen that an event has no charge balance The correct balance may be restored when the charge of a track can be flipped This can only be done, if the error on the curvature of the track allows for an ambiguous charge assignment

QUAL determines three qualities one for the beam, one for the vertex, and one for each track The vertex quality depends on the track qualities On the basis of these qualities, event samples can be selected Two of them, **p0bad** and **pMbad**, are described in chapter 5 and used throughout this thesis

2.2.2 Calibration

One of the most important tasks to be performed in an experiment is the calibration The detector has to be calibrated before all the programs can be actually run This means that the position of the detector components and their performance have to be determined accurately Also the shape of the magnetic fields has to be known very precisely for the determination of the momenta of the charged particles The calibration of the charged-particle identification detectors is described in [FMTH87], that of the γ-detectors in [VHTH87, BPNI82] and of the Neutral Calorimeters in [LSTH88] Finally, the calibration of the Magnetic fields is described in [DRTH88]

Bibliography

[ATYR80] H.W.Atherton et al. , Yellow Report CERN 80-07.

[ABNI83] M. Aguillar-Benitez et al. , Nucl. Instr. Meth. 205 (1983) 79.

[BPNI82] B. Powell et al. , Nucl. Instr. Meth. 198 (1982) 217.

[CPID91] I. Ajinenko et al. (NA22 collab.), Inclusive production of identified charged kaons, protons and anti-protons in K^+p, π^+p and pp interactions at 250 GeV/c, Nijmegen/Serpukhov draft HEN327 (1991).

[DRTH88] A. De Roeck, Inclusive particle production in hadron-proton interactions at 250 GeV/c, Ph.D. thesis Univ. of Antwerp 1988.

[EHPR80] CERN/SPSC/75-15, EHS proposal.
CERN/SPSC/76-43, Addendum Part A.
CERN/SPSC/79-117, Addendum Part B.
CERN/SPSC/78-91, Addendum Part C.
CERN/SPSC/80-50, Addendum Part D.

[FMTH87] F. Meijers, Multiplicities in Phase space intervals and Bose-Einstein correlations in hadronic interactions at 250 GeV/c, Ph.D. thesis Univ. of Nijmegen 1987.

[GSTN84] F. Crijns, The NA22 GEOHYB output structure, Nijmegen note HEN240 (1984).

[IONS84] P. van Hal, Note on the ionization scan, Nijmegen note (1984).

[LSTH88] L. Scholten, Neutral strange particle production in π^+ / K^+ p interactions at 250 GeV/c, Ph.D. thesis Univ. of Nijmegen 1988.

[MEAS84] H. Grässler and F. Crijns, NA22 measuring instructions, Nijmegen note (1984).

[OFVT84] B.H.Anders et al. , Nucl. Instr. Meth. 219 (1984) 16

[QUAL84] P. van Hal, F. Meijers, L. Scholten, Note on fixup/quality program, Nijmegen note (1984).

[REVZ85] F. Crijns and W. Friebel, Reconstruction of V^0's, decaying in the spectrometer, Nijmegen note HEN255 (1985).

[SCAN83] NA22 scanning instructions, Nijmegen note (1983). Y. Belokopytov, Scanload general rules, Update, Serpukhov note (1984).

[TRIG81] A. Bergire et al. , Triggering for experiments at EHS, CERN/EP/EHS/PH 81-14, 1981.

[VHTH87] P. van Hal, Particle production in hadron-proton interactions at 250 GeV/c incident beam momentum, Ph.D. thesis Univ. of Nijmegen 1987.

3

The empty-bin effect and uncertainty in factorial moments

Before proceeding to a description of the experimental data, some statistical properties of the factorial moments are tested using the well-known method of sampling distributions The work has been done in close collaboration with P Lipa and H C Eggers (Department of Physics, University of Arizona Tucson AZ 85721, USA) and M Charlet (University of Nijmegen) The paper [LEBC91] presented here has been slightly modified to accommodate some extra figures

3.1 Introduction

Factorial moments of particle distributions have become an important and popular topic of investigation ever since Białas and Peschanski suggested looking for intermittency in high-energy collisions [Bia86a] In the case of multiparticle dynamics intermittency is simply defined as scaling behavior of factorial moments as a function of decreasing window (bin) size of appropriate kinematic variables such as e g rapidity, azimuth or both More generally, factorial moments and related observables such as correlators and cumulants at different bin-sizes provide exciting tools for studying the anatomy of higher-order correlation functions [Car91], the latter previously unaccessible to current high-energy experiments

In the course of experimental measurement of these moments in small windows, it has become increasingly apparent that the latter are highly sensitive to a number of effects Summarized by e g Kittel [Kit90c], these include the effect of limited two-track resolution, track losses, double counting of tracks due to track match failures [Bus91, Lip90a], Dalitz decays and other resonance decays, and γ-conversion

Among the least understood is the so-called *empty-bin effect*, which arises when the bins reach a size where the average multiplicity per bin becomes significantly smaller than the order i of the factorial moment being determined In such a situation most of the events of a given event sample do not contribute to the factorial moment Thus the values of higher-order moments at small bin-sizes are determined only by a small fraction of the finite event sample of an experiment and consequently are subject to considerable sampling fluctuations

One might think that the effect of sampling fluctuations is sufficiently described by standard (gaussian) error estimation, but this is generally not true for higher-order moments and sufficiently small bin sizes several authors [Lip90a, Fri89, Des90a] observed in Monte Carlo simulations that factorial moments tended to flatten off and eventually decrease with smaller bin-sizes, even though the underlying distribution is explicitly intermittent and the true factorial moments are expected to increase with a power law The exact conditions, however, under which this effect occurs are not yet known Beset by such uncertainties, the comparison of experimental data with theoretical calculations has been controversial and a frequent source of confusion

In this paper, we investigate the sampling properties of factorial moments in detail and determine quantitatively the conditions for a noticeable empty-bin effect Moreover, we provide tools for a clear distinction between physical and purely statistical effects and thus, hopefully, clarify the interpretation of experimental data

Our general approach is the following we generate a sample of events, each one with a multiplicity chosen according to an assumed "true" theoretical distribution P_n, and then consider the behavior of a large number of such samples (experiments) each with a *fixed and finite* number of events N_{ev} From such an "ensemble of experiments", we then generate corresponding distributions of factorial moments, showing by way of the width and shape of these distributions how reliable a single measurement (corresponding to a single experiment) can be as an estimate of the true value

Section 2 explains the importance of the *tail* of multiplicity distributions in small bins for the measurement of factorial moments In Section 3, we discuss the 'ensemble of experiments" or, properly named, the "sampling distributions' of unnormalized experimental factorial moments in a single bin, followed by an extension to normalized factorial moments in Section 4 A specific example for the Negative Binomial Distribution with parameters typical of recent NA22 data is given in Section 5, while Section 6 extends the analysis to factorial moments averaged over M bins A practical method of estimating the true errors of experimental moments is discussed in Section 7, followed by a summary and discussion The appendices contain useful formulae for the actual calculation of the first moments of the sampling distributions

3.2 Truncated multiplicity distributions and incomplete factorial moments

Measuring factorial moments is equivalent to measuring the multiplicity distribution in each bin In a given experiment, the multiplicity distribution is found by counting the numbers $N_0, N_1,$ $N_n,$ of events with $0, 1,$ $, n,$ (charged) particles found within the selected (rapidity) window m [1] The *observed* multiplicity distribution $\hat{P}_n$ is then given by

$$\hat{P}_n = \frac{N_n}{N_{ev}}, \qquad (3\ 1)$$

where $N_{ev} = \sum_n N_n$ is the total number of events measured in this experiment Contrary to common misconception, the quantities $\hat{P}_n$ are not probabilities but frequencies, which

---

[1] We restrict the discussion in this and the next sections to the factorial moments in one bin only and omit the bin index m As kinematic variable we have mostly rapidity or pseudo rapidity in mind, but the results are of course valid for any set of kinematic variables

fluctuate around the (unobservable, theoretical) *true* probabilities

$$P_n = \lim_{N_{\rm ev}\to\infty} \frac{N_n}{N_{\rm ev}} . \tag{3.2}$$

For hadron-hadron collisions, which typically have total multiplicities less than 50, $\hat{P}_n$ and P_n drop rapidly with increasing n when the size δy of the rapidity window becomes small, so that the multiplicity of the observed events is bounded from above by a finite multiplicity $n_{\rm max}$ corresponding roughly to $P_{n_{\rm max}} \simeq 1/N_{\rm ev}$. As a consequence of finite $N_{\rm ev}$, the observed multiplicity distribution $\hat{P}_n$ is truncated, i.e. $\hat{P}_n = 0$ for all $n > n_{\rm max}$. Using the abbreviated notation for factorial products $n^{[\imath]} = n(n-1)\dots(n-\imath+1)$, the observed unnormalized factorial moments of $\imath$-th order

$$\hat{\xi}_\imath = \sum_{n=\imath}^{n_{\rm max}} \hat{P}_n n^{[\imath]} = \left\langle n^{[\imath]} \right\rangle_o \tag{3.3}$$

hence do not include information about the tail $n \geq n_{\rm max}$ of the *true* distribution P_n. Factorial moments, are designed, however, to pick out exactly this high-multiplicity tail, since all events with $n < i$ do not contribute to $\hat{\xi}_\imath$. Despite the small probabilities for large n, the truncation of the distribution to $n \leq n_{\rm max}$ can therefore affect the size of the factorial moments substantially, especially when $n_{\rm max}$ is small. In fact, the higher-order moments even vanish for all $i > n_{\rm max}$ whereas the true moments usually do not!

The question is therefore how much the uncertainties of the tail affect the experimentally observed factorial moments for a given finite number of events, i.e. how much do they differ from their true counterparts

$$\xi_\imath = \sum_{n=\imath}^{\infty} P_n n^{[\imath]} = \left\langle n^{[\imath]} \right\rangle_t . \tag{3.4}$$

Kittel [Kit90c] proposed the incomplete (or truncated) moments [Stu87a] as a simple measure for the relative importance of the high multiplicity tail. In our notation, the incomplete factorial moments are defined by

$$\xi_\imath^{\rm trunc} = \sum_{n=\imath}^{n_{\rm max}} P_n n^{[\imath]} . \tag{3.5}$$

Note that in this case the sum runs only to $n_{\rm max}$, cutting off the unobserved tail $n > n_{\rm max}$ of the assumed underlying true distribution P_n. Obviously, one has $\xi_\imath^{\rm trunc} \leq \xi_\imath$ and the quantity $1 - \xi_\imath^{\rm trunc}/\xi_\imath$ measures the relative contribution of the unobserved tail to the complete (true) factorial moment $\xi_\imath$. Since $n_{\rm max}$ depends on the sample size $N_{\rm ev}$ the incomplete moments provide an indirect measure for the uncertainty of the observed factorial moment due to the finite sample size. The actual procedure to determine the significance of the tail at a given sample size is then as follows: assume that the experimental data are a sample derived from the true distribution P_n, which is usually determined by fitting the free parameters of a suitably chosen family of distributions to the experimentally observed frequency distribution $\hat{P}_n$ in each analyzed rapidity bin. Secondly, the true distribution P_n is truncated at the experimentally found $n_{\rm max}$ of $\hat{P}_n$, i.e. the incomplete moments (3.5) are calculated and compared to the true ones (3.4).

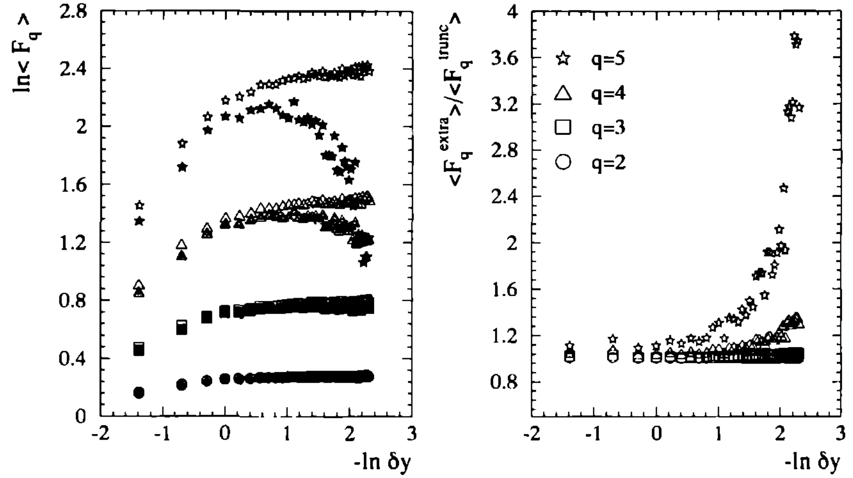

Figure 3.1: *a): $\langle F_q \rangle$ as a function of the bin-size δ from the truncated (filled) and complete (open) probability distribution, assuming a NBD with $\bar{n}$ and $1/k$ from the (bin-averaged) data. The symbols are explained in b).*
b): The ratio of the complete and truncated F_q. A large deviation from 1 is seen for F_5 in small intervals. F_2 to F_4 are not dramatically affected by the truncation.

This procedure is used in [Kit90c] to determine incomplete, bin-averaged and normalized factorial moments

$$F_i^{\text{trunc}} = \frac{1}{M} \sum_{m=1}^{M} \frac{\xi_i^{(m),\text{trunc}}}{(\xi_1^{(m),\text{trunc}})^i}, \tag{3.6}$$

where M is the number of analyzed bins at a given bin-size δy. Assuming that the true multiplicity distribution follows a Negative Binomial Distribution (NBD),

$$P_n^{\text{NBD}} = \frac{\Gamma(n+k)}{\Gamma(n+1)\Gamma(k)} \left(\frac{\bar{n}/k}{1+\bar{n}/k} \right)^n \left(\frac{1}{1+\bar{n}/k} \right)^k, \tag{3.7}$$

which has been found to be very successful in fitting high-energy multiplicity distributions (among them also those of the NA22 Collaboration [NA22-88b]), and taking a sample size of $N_{\text{ev}} \approx 60000$ one finds at NA22 energies ($\sqrt{s} = 22\,\text{GeV}$) sizeable deviations for the fifth moment at small bin-sizes $\delta y < 0.5$, but only small deviations for lower-order moments [Kit90c]. This is demonstrated in fig. 3.1. The $\bar{n}$ and $1/k$ are taken from the data. From this result we conclude that at this and higher energies the lower-order moments are well determined by the experimental accessible range of the multiplicity distributions even at the smallest bin-sizes $\delta y \approx 0.1$, whereas the fifth and higher moments depend strongly on the tail $n > n_{\text{max}}$, which is then obviously subject to strong sampling distortions. In this way the incomplete moments serve as sensitive indicators for conditions where sampling fluctuations of the observed moments become important.

Note, however, that a ratio $B_i = \xi_i/\xi_i^{\text{trunc}}$ significantly larger than 1 does unfortunately *not* allow one to conclude that the observed moments $\hat{\xi}_i$ are also systematically smaller than the true ones by the same factor B_i (which could then be used to correct for this bias via $\xi_i = B_i\hat{\xi}_i$); on the contrary, a detailed study of the sampling properties of the observed $\hat{\xi}_i$ in the next sections will show that the latter may also be *larger* than the true ones and that no general correction procedure for the empty-bin effect can be given.

3.3 The sampling distributions of observed factorial moments

We can quantify the uncertainty of the observed factorial moments $\hat{\xi}_i$ in terms of the true probabilities P_n by explicitly calculating their so called sampling distributions [Stu87a]. Imagine that we perform the same experiment again and again, each generating a sample of N_{ev} events. For each single sample one then calculates the corresponding $\hat{\xi}_i$ which may differ from sample to sample. After an infinite repetition of the experiment one is left with a distribution $\mathcal{P}(\hat{\xi}_i)$, the sampling distribution of the $\hat{\xi}_i$, which completely determines the sampling properties of the observed moments.

We first consider the sampling distribution of the set of multiplicity counts $(N_0, N_1, \ldots)$ and the corresponding frequencies $\hat{P}_n = N_n/N_{\text{ev}}$. Under the natural sampling condition that different events are statistically independent, the numbers of events N_n with multiplicity n follow a multinomial distribution around the set of true probabilities:

$$\mathcal{P}(N_0, N_1, \ldots, N_{n_c}, N_{n_t}) = \frac{N_{\text{ev}}!}{N_0!\ldots N_c! N_{n_t}!} P_0^{N_0} \ldots P_{n_c}^{N_{n_c}} P_{n_t}^{N_{n_t}} , \tag{3.8}$$

where we have compressed the histogram of $\hat{P}_n$ into a finite number of bins labeled by $n = 0, 1, \ldots, n_c, n_t$ by choosing a cutoff multiplicity $n_c \gg n_{\max}$, large enough for any given sample size to ensure that there are no events with multiplicity exceeding n_c since the probability $P_{n_t} = 1 - \sum_{n=0}^{n_c} P_n$ to find an event in the tail $n > n_c$ is orders of magnitude smaller than $1/N_{\text{ev}}$. Eq. (3.8) uniquely defines the distribution of experimental $\hat{P}_n$'s in terms of the theoretical P_n's.

The sampling distributions of the factorial moments $\hat{\xi}_i$ can now easily be written down in terms of $\mathcal{P}(N_0, \ldots, N_{n_t})$ (see Appendix A) but in this form they are difficult to manipulate. We rather use the generating function technique [Car87a] [Stu87a] to determine their first few moments which characterize the sampling distributions in a concise and much more illuminating way.

The moment generating function of the multinomially distributed variates $N_0, \ldots, N_{n_t}$ is given by

$$\begin{aligned} M(\lambda_0, \ldots, \lambda_{n_t}) &= \sum_{\substack{N_0,\ldots,N_{n_t}=0 \\ (\sum N_n = N_{\text{ev}})}}^{N_{\text{ev}}} \exp\left[-\sum_{n=0}^{n_t} \lambda_n N_n\right] \mathcal{P}(N_0, \ldots, N_{n_t}) \\ &= \left(\sum_{n=0}^{n_t} e^{-\lambda_n} P_n\right)^{N_{\text{ev}}} \end{aligned} \tag{3.9}$$

Using the fact that the moment generating function of any function $f(N_0, \ldots, N_{n_t})$ of the variates N_n is found by $M_f(\lambda) = \sum \exp[-\lambda f(N_0, \ldots, N_{n_t})] \mathcal{P}(N_0, \ldots, N_{n_t})$ [Stu87a], we obtain the desired moment generating function of the observed $\hat{\xi}_i$

$$M_{\hat{\xi}_i}(\lambda) = \left(\sum_{n=0}^{n_t} \exp\left[-n^{[i]}\lambda / N_{ev} \right] P_n \right)^{N_{ev}} \tag{3.10}$$

In the following we determine the first four cumulants $\kappa_p = (-\partial/\partial\lambda)^p \log M(\lambda)|_{\lambda=0}$ of $\mathcal{P}(\hat{\xi}_i)$ rather than its usual (central) moments since the former lead in the present case to shorter expressions. Denoting by $\{\}$ the average over the sampling distribution $\mathcal{P}(\hat{\xi}_i)$, we obtain from (3.10) the mean

$$\kappa_1^{(i)} = \{\hat{\xi}_i\} = \sum_{n=0}^{n_t} n^{[i]} P_n = \left\langle n^{[i]} \right\rangle_t = \xi_i \,. \tag{3.11}$$

Since n_c (and hence n_t) can be made arbitrarily large without changing this result, the above sum can be taken to run effectively to infinity. Hence the average over all samples of the measured factorial moment is equal to the factorial moment of the true probability distribution, independent of the sample size N_{ev}. Eq. (3.11) is just the defining property of an *unbiased* estimator of ξ_i.

Similarly, the second cumulant or equivalently the variance of $\mathcal{P}(\hat{\xi}_i)$ due to the sampling fluctuations of the frequencies $\hat{P}_n$ around the true P_n is found to be

$$\kappa_2^{(i)} = \mathrm{var}(\hat{\xi}_i) = \{(\hat{\xi}_i)^2\} - \{\hat{\xi}_i\}^2 = \frac{1}{N_{ev}} \left(\left\langle n^{2[i]} \right\rangle_t - \left\langle n^{[i]} \right\rangle_t^2 \right) , \tag{3.12}$$

where we used the abbreviated notation $n^{p[i]} = (n^{[i]})^p = n^p \cdots (n-i+1)^p$.

Note that (3.12) gives the *true* squared standard error $\sigma^2_{\hat{\xi}_i} = \mathrm{var}(\hat{\xi}_i)$ which may be quite different from the experimentally *observed* standard error $s_{\hat{\xi}_i}$ obtained from a particular sample

$$s^2_{\hat{\xi}_i} = \frac{1}{N_{ev} - 1} \left(\left\langle n^{2[i]} \right\rangle_o - \left\langle n^{[i]} \right\rangle_o^2 \right) , \tag{3.13}$$

since $s^2_{\hat{\xi}_i}$ is also subject to even stronger sampling fluctuations[2] than $\hat{\xi}_i$. As is well known, $s^2_{\hat{\xi}_i}$ is an unbiased estimator for $\sigma^2_{\hat{\xi}_i}$ and one can easily show that

$$\left\{ s^2_{\hat{\xi}_i} \right\} = \sigma^2_{\hat{\xi}_i} \tag{3.14}$$

holds independently of the sample size N_{ev}. However, as we shall demonstrate in a specific example in Section 5, the sampling distributions of the observed variances are much wider than the ones of the corresponding $\hat{\xi}_i$, i.e. just when the $\hat{\xi}_i$ are subject to sizeable sampling fluctuations their observed errors $s_{\hat{\xi}_i}$ do *not* provide a sufficient description of their uncertainty. Under such conditions one still obtains an estimate of the errors by assuming a suitable true distribution P_n and calculating variances according to eq. (3.12).

For the discussion of further properties of $\mathcal{P}(\hat{\xi}_i)$ we need their next two cumulants, which we obtain again directly from (3.10)

$$\kappa_3^{(i)} = \frac{1}{N_{ev}^2} \left(\left\langle n^{3[i]} \right\rangle_t - 3 \left\langle n^{[i]} \right\rangle_t \left\langle n^{2[i]} \right\rangle_t + 2 \left\langle n^{[i]} \right\rangle_t^3 \right) \tag{3.15}$$

---

[2] Eq (3.13) involves moments of order $2i$ (see Appendix B) which are obviously much more dependent on the uncertainties of the tail of P_n than the $\hat{\xi}_i$.

$$\begin{aligned}\kappa_4^{(i)} &= \frac{1}{N_{\mathrm{ev}}^3}\Big(\left\langle n^{4[i]}\right\rangle_t - 4\left\langle n^{[i]}\right\rangle_t\left\langle n^{3[i]}\right\rangle_t - 3\left\langle n^{2[i]}\right\rangle_t^2 \\ &\quad + 12\left\langle n^{[i]}\right\rangle_t^2\left\langle n^{2[i]}\right\rangle_t - 6\left\langle n^{[i]}\right\rangle_t^4\Big)\end{aligned}$$

and the useful coefficients β_1, β_2 and γ_1, γ_2 defined by the relations [Stu87a]

$$\begin{aligned}\gamma_1^2 &= \beta_1 = \frac{\kappa_3^2}{\kappa_2^3} \\ \gamma_2 &= \beta_2 - 3 = \frac{\kappa_4}{\kappa_2^2}\,.\end{aligned} \tag{3.16}$$

γ_1 and γ_2 are often called skewness and kurtosis respectively and provide well known measures for the deviation of $\mathcal{P}(\hat{\xi}_i)$ from a Gaussian which has $\gamma_1 = \gamma_2 = 0$. In particular, γ_1 takes the sign of κ_3 and a value $\gamma_1 \neq 0$ indicates that $\mathcal{P}(\hat{\xi}_i)$ is *asymmetric.*

The coefficients β_1 and γ_2 depend on the sample size N_{ev} in the same way as the variances σ^2

$$\beta_1^{(i)} = \frac{1}{N_{\mathrm{ev}}}\overline{\beta_1}^{(i)}, \quad \gamma_2^{(i)} = \frac{1}{N_{\mathrm{ev}}}\overline{\gamma_2}^{(i)} \tag{3.17}$$

with $\overline{\beta_1}$ and $\overline{\gamma_2}$ denoting the N_{ev} independent parts.

For a sufficient large sample size these coefficients are small and thus the sampling distributions approach a gaussian shape; the errors s and σ can then be interpreted as standard gaussian errors. On the other hand, eqs. (3.15)–(3.17) provide a sufficient description of the sampling peculiarities of smaller samples such as the empty-bin effect and the occurrence of non-gaussian errors.

Among different possibilities to quantify the size of the empty-bin effect we choose the mode rather than the coefficients β_1 and γ_2; a mode $\hat{\xi}_{i,0}$ of $\mathcal{P}(\hat{\xi}_i)$ is defined as the value of $\hat{\xi}_i$ where $\mathcal{P}(\hat{\xi}_i)$ has a local maximum and, if the distribution has only one mode (unimodal), coincides with the *most probable* value of $\hat{\xi}_i$. Since for asymmetric distributions the mode generally differs from the mean ($\gamma_1 > 0$ implies mode < mean), we define the difference $\Delta m =$ mean − mode as measure for the asymmetry of the sampling distribution $\mathcal{P}(\hat{\xi}_i)$. The size of the deviation $\Delta m > 0$ then indicates how far the *most probable* outcome $\hat{\xi}_{i,0}$ of an experiment is found below the true value ξ_i.

In this sense $\Delta m > 0$ quantifies the *tendency* of higher-order factorial moments to bend down from their expectation values; there exists no exact correction procedure for this kind of bias since such a tendency is only a statement about the ensemble of samples and does not allow a conclusion about a particular one.

With the assumption that the sampling distributions are reasonably approximated by the system of Pearson distributions[3] the asymmetry measure Δm can be expressed in terms

---

[3] The Pearson System of distributions is defined by the class of all continuous, unimodal (including J-shaped) and bimodal (U-shaped) distributions, which are uniquely determined by their first four moments or cumulants (all higher moments, if nonzero, are then given by recurrence relations) [Stu87a]. This system is designed to approximate all unimodal distributions whose first four moments are known. From our Monte Carlo simulations we observe that $\mathcal{P}(\hat{\xi}_i)$ may take nonzero values (spikes) at discrete values of $\hat{\xi}_i$ and thus may not be unimodal in the strict sense, but after smoothing such spikes one finds a continuous, unimodal distribution describing the gross sampling features we are interested in. We note that under extreme conditions (such as extreme broad sampling distributions or the case $i > n_{\mathrm{max}}$ giving $\hat{\xi}_i \equiv 0$) the approximation (3.18) can lead to meaningless results (e.g. mode < 0). As a rule of thumb one should have at least $0 < \sigma_{\hat{\xi}_i} < \hat{\xi}_i$ to assign the intended meaning to the measure Δm.

of the first four cumulants [Stu87a]

$$\Delta m = \sigma \frac{\sqrt{\beta_1}(\beta_2 + 3)}{10\beta_2 - 12\beta_1 - 18} . \tag{3.18}$$

In practice it is a rather tedious task to derive analytically the errors σ and asymmetries Δm for a given true distribution P_n. To facilitate the calculations we show in Appendix B expressions for $\left\langle n^{p[i]} \right\rangle$ in terms of usual factorial moments ξ_i up to order $p = 4$ and $i = 5$. Moreover, for the frequent case where P_n is well approximated by a Negative Binomial distribution, we provide tables for the N_{ev}-independent coefficients $\sigma = \sqrt{N_{\mathrm{ev}}}\sigma$, $\overline{\beta_1}$ and $\overline{\gamma_2}$ calculated from P_n^{NBD} using (3.12)–(3.17) and Mathematica [Wo88].

3.4 Normalized factorial moments

Frequently the normalized factorial moments $\hat{F}_i = \hat{\xi}_i / \hat{\xi}_1^i$ are used rather than the unnormalized versions. To estimate their sampling properties (again for one bin m only), we first note that $\hat{F}_i$, as a ratio of moments, is not an unbiased estimator any more and we have to consider the bias due to sampling a ratio of two correlated variates. Unlike the empty-bin effect, it is possible to correct for this kind of bias.

After expanding $\hat{F}_i(\hat{\xi}_1, \hat{\xi}_i)$ around the point (ξ_1, ξ_i) and neglecting terms of higher order than $O(1/N_{\mathrm{ev}})$ we obtain for the deviation of the expectation value of $\hat{F}_i$ from the true value $F_i = \xi_i / \xi_1^i$

$$\left\{\hat{F}_i\right\} = \left\{\frac{\hat{\xi}_i}{\hat{\xi}_1^i}\right\} = F_i \left(1 + \frac{i(i+1)}{2} \frac{\sigma^2_{\hat{\xi}_1}}{\xi_1^2} - i \frac{\mathrm{cov}(\hat{\xi}_1, \hat{\xi}_i)}{\xi_1 \xi_i}\right) \tag{3.19}$$

where the covariance between the first and i-th moment is

$$\mathrm{cov}(\hat{\xi}_1, \hat{\xi}_i) = \frac{1}{N_{\mathrm{ev}}} \left((i - \xi_1)\xi_i + \xi_{i+1}\right) . \tag{3.20}$$

Again we consider the special case of a Negative Binomial P_n^{NBD} as the true distribution and get

$$\left\{\hat{F}_i\right\} = F_i \left(1 - \frac{i(i-1)}{2N_{\mathrm{ev}}} \left(\frac{1}{\bar{n}} + \frac{1}{k}\right)\right) . \tag{3.21}$$

Obviously the bias due to normalization leads also to an underestimation of factorial moments, although for large samples it is much smaller than the empty-bin effect Estimating at small bin-sizes the magnitude of the factor $(1/\bar{n} + 1/k)$ in the order of 10 (for typical *hh* and e^+e^- experiments) we get a ~ 1% bias for the fifth moment with a sample size in the order of ~ 10000, increasing to ~ 10% for N_{ev} ~ 1000. For smaller sample sizes terms of $O(1/N_{\mathrm{ev}}^2)$ may also become important.

Eq. (3.21) should be viewed as a warning for heavy ion experiments which sometimes estimate normalized factorial moments from a sample of a few hundred events. Surely, eq. (3.21) might not be a proper description of the bias in such cases, but we mention that then the use of the jackknife method [KSb] for the removal of bias to any desired order in $1/N_{\mathrm{ev}}$ may be worth the effort.

3.5 An example: simulations for the NBD

To illustrate some of the above ideas, we now give an example. We generate, according to a Negative Binomial distribution (3.7), a sample consisting of a fixed number N_{ev} of simulated events and calculate the factorial moments $\hat{\xi}_i$ according to Eq.(3.3). [4] These are then divided by $\hat{\xi}_1^i = \langle n \rangle_o^i$, the i-th power of the observed mean multiplicity to give the normalized factorial moments $\hat{F}_i$. (For the parameters we shall use below, the difference between normalizing with $\langle n \rangle_t$ and $\langle n \rangle_o$ is less than 1%.) This procedure is repeated $\mathcal{N}_s$ times, until we have distributions $\mathcal{P}(\hat{F}_i)$ for every order.

Figure 3.2 shows the sampling distribution of normalized factorial moments $\mathcal{P}(\hat{F}_i)$ (a-d for $i = 2-5$ respectively) generated from the simulated samples for $N_{\text{ev}} = 60000$, $\mathcal{N}_s = 5000$ and NBD parameters $\bar{n} = 0.18$ and $1/k = 0.38$ for a single bin; these values are typical for distributions measured by NA22 for small bin-sizes $\delta y \simeq 0.1$ [NA22-88b], usually the smallest bin-size quoted by hadron-hadron experiments. For easier comparison, all distributions are rescaled and plotted as a function of $\hat{F}_i/F_i$, the *ratio* of sample factorial moment to true (untruncated NBD) factorial moment. Plotted in fig. 3.2(e-h) are the distributions $\mathcal{P}(\sigma(\hat{F}_i)/\sigma(F_i))$ of the ratios of factorial moment error for a given sample over the true error for $i = 2-5$; here, too, $\sigma(\hat{F}_i)/\sigma(F_i) = 1$ signifies agreement with the true value of the error. In plots i-l the correlation between the ratio of the factorial moments and the ratio of their errors is shown.

From the figures, we see that

1. the distribution for $\hat{F}_2/F_2$ is very narrow and centered around 1, i.e. there is very little deviation from the true moment value. With increasing order i, the distribution becomes wider and wider, with more and more samples yielding factorial moments deviating substantially from the true value. We note that for $i = 3, 4$ a sizable number of samples actually *overestimate* the true value.

2. for $i = 2, 3$, the distribution is relatively symmetric and of gaussian shape, centered around the mean corresponding to the "true" value $\{\hat{F}_i\} = F_i$, while for $i = 4, 5$ it becomes increasingly asymmetric, with more and more samples yielding zero or small factorial moments.

3. the same trends are amplified in the distributions of errors: narrow, almost symmetric distributions for $i = 2, 3$, widening and becoming increasingly asymmetric with higher orders $i = 4, 5$. Notice also the discrete nature of these latter distributions, which are due to the discrete values $n^{[i]}$ takes on, which are then broadened by the denominator $\langle n \rangle_o^i$. The same effect can be seen in fig. 3.2d for $\hat{F}_5$.

4. there is a strong correlation between the factorial moments and their errors. An under-(-over) estimation of the factorial moments results for lower order in a similar behavior of their errors. However, the errors on the fifth-order factorial moments are mostly underestimated.

---

[4] We do not restrict the multiplicity artificially by some arbitrary cutoff but rather allow the system to find its own maximum multiplicity due to the finite sample size. This maximum may of course change somewhat from sample to sample but is always smaller than the cutoff n_c.

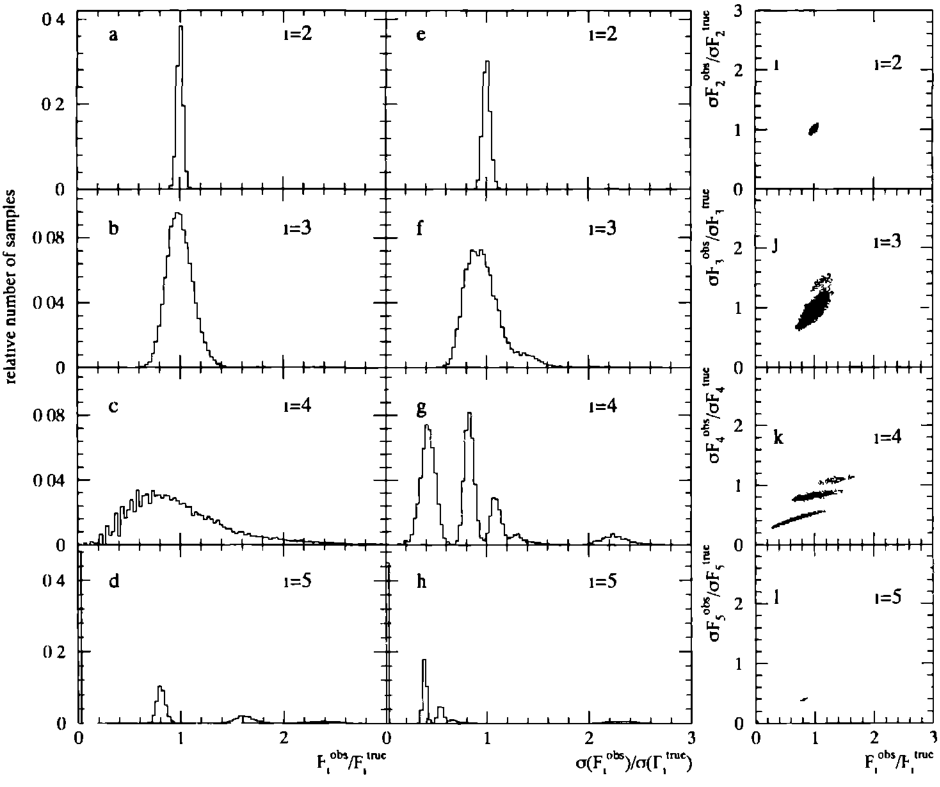

Figure 3.2 *Distribution of the ratios of the sample factorial moments in a single bin m, $\hat{F}_i^{(m)}$, over the true value $F_i^{(m)}$, plotted for orders $i = 2, 3, 4, 5$ in a-d. The NBD parameters are $\bar{n} = 0.18$ and $1/k = 0.38$. 60000 events per sample are generated. The width of the peak at (or the deviation of the peak from) the true value at 1 gives an idea of the reliability of one single sample in estimating the true value.*

Plots e-h show the distribution of the ratios of standard errors for sample factorial moments $\sigma(\hat{F}_i)$ over the true error $\sigma(F_i)$ for $i = 2, 3, 4, 5$.

The correlation between the sample factorial moments and their errors is plotted in i-l.

These simple results have important consequences. In performing an experiment, we are always only able to measure a *single* (event averaged) factorial moment $\hat{F}_i$ (one for each order i) rather than the whole distribution of such moments which we have calculated above. The probability that our particular experiment yields a certain value for $\hat{F}_i$ is given by the distribution shown in fig. 3.2(a-d), in other words, the results we would obtain in any particular experiment would be a random sampling of these distributions. The error would similarly be a random sample of the shown distributions in fig. 3.2(e-h).

The *asymmetry* of the sample distributions for the higher moments $\hat{F}_4/F_4$ and $\hat{F}_5/F_5$ is responsible for the empty bin effect. In our specific example (fig. 3.2), the maximum of $\mathcal{P}(\hat{F}_4/F_4)$ is found at ≈ 0.7 corresponding to a normalized asymmetry measure $\Delta m/F_4 \approx 0.3$. For $\hat{F}_5/F_5$ the maximum is obviously at $\hat{F}_5 = 0$. Moreover, the probability that a sample has $\hat{F}_5 = 0$ is as large as 0.45! Obviously, the measure $\Delta m/F_5$ takes its extreme value 1 in this case indicating extreme distortion of the observed moment (the probability to find a sample with $\hat{F}_5/F_5 < 1$ is ≈ 0.78). Summarizing, it is much more likely that at low average multiplicity in the bin under consideration, the higher-order factorial moments are found *below* their true values than above, this "downward tendency" obviously increases with decreasing average multiplicity per bin.

One might expect that such a bending down should be taken into account automatically by the increasing size of the observed errors. Unfortunately, this is only partly true: the asymmetry of the distributions in Figure 3.2(g,h) shows that the *observed* errors feel the empty-bin effect even more strongly since the probability to find a sample with observed error smaller than the true one $(\sigma(\hat{F}_5)/\sigma(F_5) < 1)$ is according to fig. 3.2h about 0.93. This indicates that in this case the observed errors are most likely underestimated. Moreover, we found for our example (fig. 3.2 i-l) that all factorial moments are strongly correlated with their respective errors, so that a sample with a $\hat{F}_4$ or $\hat{F}_5$ below the true value most likely also has an underestimated error $\sigma(\hat{F}_4)$ or $\sigma(\hat{F}_5)$.

3.6 Bin-averaged factorial moments

In the analysis of intermittency in particle physics, one commonly uses bin-averaged factorial moments

$$\hat{F}_i = \frac{1}{M} \sum_{m=1}^{M} \hat{F}_i^{(m)} \tag{3.22}$$

where $\hat{F}_i^{(m)}$ is the ith observed normalized factorial moment in bin m which we treated in Section 4, and M is the total number of bins [Bia86a].

This bin-averaging reduces the statistical error of the observed factorial moments substantially. In fact, for parameter values used in the above simulation, bin averaging cures most of the empty-bin effect encountered in the estimation of the single-bin factorial moments. In the best case — when all M bins are uncorrelated — the bin average acts as if the number of events were increased to an *effective* number of events $N_{\text{eff}} = MN_{\text{ev}}$. The variances σ^2 and coefficients β_1 and γ_2 of the bin-averaged moments are then reduced by a factor of order $1/M$ compared to the values for single-bin moments $\hat{F}_i^{(m)}$.

In general, the variances of the bin-averaged factorial moments can be written as

$$\begin{aligned}\mathrm{var}(\hat{F}_i) &= \frac{1}{M^2}\sum_{m=1}^{M}\mathrm{var}(\hat{F}_i^{(m)})\left(1+\frac{\sum_{m\neq m'=1}^{M}\mathrm{cov}(\hat{F}_i^{(m)},\hat{F}_i^{(m')})}{\sum_{m=1}^{M}\mathrm{var}(\hat{F}_i^{(m)})}\right)\\ &= \frac{R}{M}\left(\frac{1}{M}\sum_{m}\mathrm{var}(\hat{F}_i^{(m)})\right), \qquad (3.23)\end{aligned}$$

where the covariances between different bins can be absorbed into a correlation factor R, which reduces the number of M correlated bins to an *effective* number M/R of uncorrelated bins. R ranges from 1 for uncorrelated bins to M for perfectly positively correlated bins. In practice, we expect R to be close to 1, but the actual value should be determined by the experiment[5].

In the following, we demonstrate the effect of bin averaging on the shape of the sample distributions of the $\hat{F}_i$. The simulation of NBD in one bin, as described in the previous section, was repeated for $M = 40$ independent bins (we assume $R = 1$ throughout this study) and for each sample we measured the bin averaged factorial moment $\hat{F}_i$ according to Eq. (3.22). In analogy to fig. 3.2, we plot the sample distributions of the ratios $\hat{F}_i/F_i$ of 5000 samples in fig. 3.3.

Comparing fig. 3.3 with fig. 3.2, we summarize the effect of bin averaging as follows:

1. The width of the symmetric distributions for $\hat{F}_2/F_2$ and F_3/F_3 in fig. 3.2 are reduced in fig. 3.3 by a factor $1/\sqrt{M} \simeq 0.16$.

2. The asymmetric shape of the sample distribution for $\hat{F}_4/F_4$ becomes symmetric ($\Delta m = 0$) indicating that no empty bin effect is expected for $\hat{F}_4$ (for this particular choice of parameters).

3. The "spiky" distribution for $\hat{F}_5$ in fig. 3.2 becomes smoother with bin averaging and much more symmetric. Note that the huge spike at $\hat{F}_5 = 0$ vanishes after bin averaging.

4. Similar conclusions hold also for error distributions of bin-averaged factorial moments. The error distribution of F_4 becomes smooth and peaked around 1. However, the observed errors on F_5 still tend to be smaller than their 'true' counterparts. The correlation plot shows that there is a real improvement for orders up to 4.

The remaining asymmetry of the $\hat{F}_5$ distribution in fig. 3.3 is reduced to $\Delta m/F_5 \approx 0.1$ and leads now to a probability of 0.58 of finding a sample with $\hat{F}_5/F_5 < 1$ and a vanishing probability of finding a sample with $F_5 = 0$. In this sense, the empty-bin effect is almost cured and one can trust the experimentally observed statistical errors. This is valid, of course, only if our assumption $R \simeq 1$ can be justified by direct measurements.

3.7 Estimating errors of experimental moments

We recall that the Monte Carlo simulations above were performed for a specific distribution with a specific choice of parameters $\bar{n}$ and k for the assumed NBD, corresponding roughly

---

[5] We note that the covariances between different bins are simply related to the factorial correlators [Bia86a, NA22CO], but care has to be taken for different normalizations.

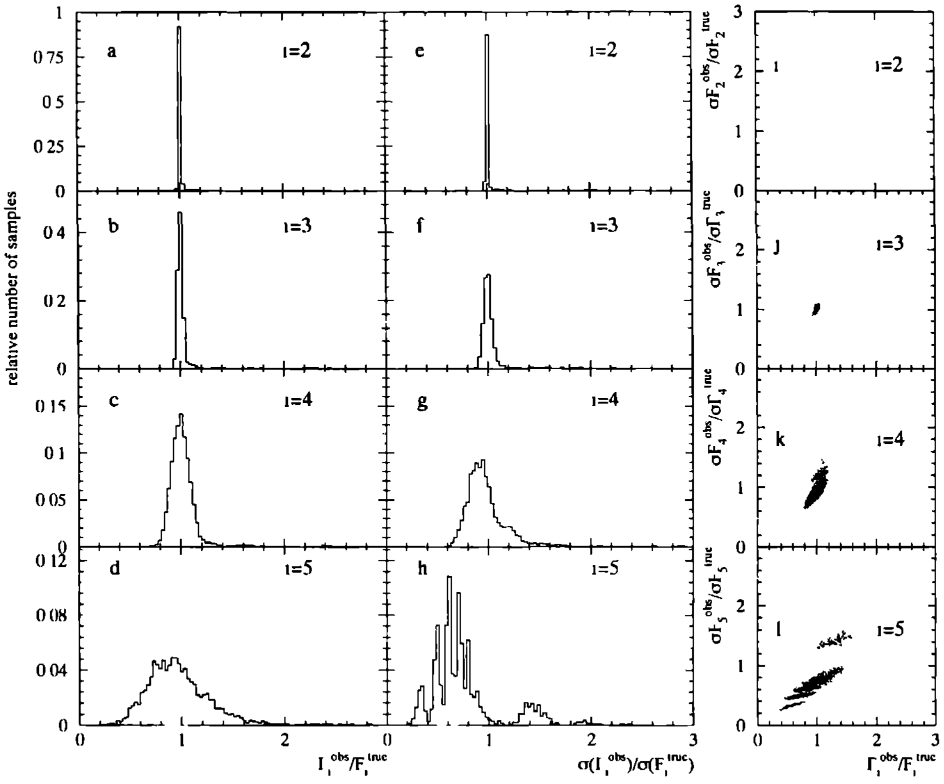

Figure 3.3: *The same as fig. 3.2, but now for the bin-averaged factorial moments ($M = 40$) of equation (3.22) The errors are obtained from (3.23) with $R = 1$. The distributions become much narrower and more symmetric about their true value at $\hat{F}_i/F_i = 1$. The error distribution of $\hat{F}_5$ still has its most probable value below 1 The correlation plots show the improvement obtained from the bin-averaging procedure.*

to a bin-size $\delta y = 0.1$ in hadronic collisions at 22 GeV. In principle, any given distribution and set of parameter values can be used to create similar sampling distributions and thereby estimate the uncertainties, but, in practice, an analytic estimate of errors via eqs. (3.12)–(3.18) is preferable.

Here, we concentrate on the single important case of the NBD (including the Poisson distribution as the limit $k \to \infty$), showing explicitly the dependence of the errors, skewness and kurtosis of the sampling distributions $\mathcal{P}(\hat{F}_i)$ up to order 5 on the parameters $\bar{n}$ and k (Tables 1–3). For greater generality, we exclude the trivial dependence of these coefficients both on the sample size $N_{\rm ev}$ and effective number of independent bins M/R.

Specifically, we show in Tables 1–3 the coefficients $\overline{\sigma}/\xi$ and β_1 and γ_2 calculated from $P_n^{\rm NBD}$ (3.7) via eqs. (3.12)–(3.17) for different parameters $\bar{n}$ and k. The relative errors and asymmetries of factorial moments for a particular experiment can then be estimated using these tables,

$$\frac{\sigma^{(i)}}{\xi_i} = \frac{1}{\sqrt{N_{\rm eff}}}\frac{\sigma^{(i)}}{\xi_i}, \quad \beta_1^{(i)} = \frac{1}{N_{\rm eff}}\beta_1{}^{(i)}, \quad \gamma_2^{(i)} = \frac{1}{N_{\rm eff}}\gamma_2{}^{(i)} \tag{3.24}$$

and eqs. (3.16) and (3.18). According to the discussion in the previous section the effective number of events can be estimated by

$$N_{\rm eff} = \frac{M}{R} N_{\rm ev} \tag{3.25}$$

As an example, take $\bar{n} = 0.1$, $k = 4$ for 60000 events and 40 bins. From Table 1, we read off for $i = 5$ the value 2109, which divided by $\sqrt{60000 \times 40/1}$ yields a normalized error $\sigma(\hat{F}_5)/F_5 \simeq 1.36$ (i.e. the error on $\hat{F}_5$ is larger than the moment!). For the same parameters with $\bar{n} = 0.4$ (corresponding to a bin-size $\delta y \simeq 0.2$ at NA22 energies), this drops to $\sigma(\hat{F}_5)/F_5 \simeq 0.1$, a 10% error, illustrating the strong dependence of fifth-order moment errors on the parameters. Similarly the relative asymmetry $\Delta m/F_5$ drops from $\simeq 1.2$ (indicating that the most probable value for $\hat{F}_5$ is 0!) to $\simeq 0.02$, i.e. a truly symmetric distribution $\mathcal{P}(\hat{F}_5)$, and the errors are gaussian.

3.8 Conclusions

The discussion of intermittency in high-energy physics relies on the interpretation of experimental data on factorial moments in very small bins, where at current collision energies the average multiplicity of charged particles is relatively small. It is therefore of crucial importance for any comparison of a theoretical distribution (such as the NBD) with experimental data to understand the reliability of the statistical errors determined by the experiments and the likelihood of purely statistical biases, which may obscure a proper interpretation of data. For example, if the bin-size is decreased sufficiently, the discussed empty-bin effect causes a bending down of the factorial moments which might naively be interpreted as a “scale breaking” phenomenon or spawn a misleading comparison with some theoretical model. We therefore argue that limits from the finite sample size should be estimated and well considered in the interpretation of experimental data.

Since the empty-bin effect increases dramatically with the order of the moment, the moments of lower order are limited mainly by experimental resolution and other background effects; the higher-order moments, on the other hand, are limited not so much by experimental resolution as by the present empty-bin effect.

In our present simulation, we assumed that multiplicity distributions in narrow rapidity bins are parametrized by Negative Binomial distributions. For this particular parametrization, we conclude that the finite sample size effects at a typical bin-size $\simeq 0.1$ are almost negligible for bin-averaged factorial moments up to $\hat{F}_5$ at NA22 energies. A direct comparison with theoretical models, as e.g. in [Car89c], is still possible in this case.

In this study we intended to simulate explicitly the situation for the "worst case", i.e. we chose parameters typical for a low energy experiment ($\sqrt{s} = 22\,\mathrm{GeV}$) with a comparatively small average multiplicity (< 10); we stress the fact that the statistical biases are obviously smaller at higher collision energies. For heavy ion experiments with their much larger multiplicities, the empty-bin effect can be expected to play only a negligible role compared to other sources of error, although care must be taken because of very small sample sizes (typically in the hundreds).

On the other hand, the situation might become drastically worse for the study of intermittency in two and more dimensions. In this case the average multiplicity per bin is further reduced by orders of magnitude and the effects of finite sample size become much more severe. Unfortunately, no direct measurements and parametrizations of multiplicity distributions in combined intervals of two or more variables have been reported so far, and so estimates of statistical biases analogous to the ones above are not yet possible. From present preliminary data we suspect that the tails of multiplicity distributions in two- and three-dimensional phase-space volumes are much more pronounced than in the one-dimensional case. According to the discussion in the previous section, this behavior might be crucial for the measurement of factorial moments in more dimensions.

Acknowledgements: We are indebted to P. Carruthers for continuous encouragement and making sure that this paper was written. We are grateful to B. Buschbeck for reading a first draft of this paper and suggesting many improvements. We would further like to thank W. Kittel for bringing up the question of truncated multiplicity distributions, and E.A. De Wolf and J. Rutherfoord for useful discussions.

3.9 Appendix

3.9.1 Appendix A

For completeness, we quote here the analytic expression for the sampling distributions of $\hat{\xi}_i$, discussed in Section 3.

Formally, the probability that a particular sample has a factorial moment $\hat{\xi}_i$ equal to some constant a is given by

$$\mathcal{P}(\hat{\xi}_i = a) = \sum_{N_0,\dots,N_{n_t}=0}^{N_{\mathrm{ev}}} \mathcal{P}(N_0,\dots,N_{n_t})\,\delta(N_{\mathrm{ev}} - \sum_{n=0}^{n_t} N_n)\,\delta(N_{\mathrm{ev}}a - \sum_{n} n^{[i]} N_n)\,. \tag{3.26}$$

We note the remarkable resemblance of this expression to the micro-canonical partition function, where the second restrictive condition would correspond to keeping the total energy of the system a constant (albeit with no weight function such as the $n^{[i]}$ we have here).

Since $n^{[i]} = 0\ \forall n < i$, we can sum out the first $i-1$ terms. With the help of Eq.(3.8) and $A_i \equiv \sum_{n=0}^{i-1} N_n$, the probability becomes

$$\mathcal{P}(\hat{\xi}_i = a) = \sum_{A_i, N_i, \ldots, N_{n_t}}^{N_{\mathrm{ev}}} \frac{N_{\mathrm{ev}}!}{N_i! \ldots N_{n_t}! A_i!} P_i^{N_i} \ldots P_{n_t}^{N_{n_t}} (P_0 + \ldots + P_{i-1})^{A_i} \tag{3.27}$$

where the sum has to be taken over all possible combinations satisfying $A_i + \sum_{n=i}^{n_t} N_n = N_{\mathrm{ev}}$ and $\sum_{n=i}^{n_t} n^{[i]} N_n = N_{\mathrm{ev}} a$; in particular $\mathcal{P}(\hat{\xi}_i = 0) = (P_0 + \ldots + P_{i-1})^{N_{\mathrm{ev}}}$. This probability is sampled (via the procedures described in sections 5 and 6) in the simulations shown in fig. 3.2. When averaging over many bins, corresponding averages of all values a_m in each bin have to be made.

3.9.2 Appendix B

We summarize useful formulae for the actual calculation of errors and asymmetry measure Δm via eqs. (3.12)–(3.17).

For the Negative Binomial Distribution (3.7) the factorial moments ξ_i are obtained by

$$\xi_i = \left\langle n^{[i]} \right\rangle_t = \frac{\bar{n}^i}{k^i} k(k+1)\cdots(k+i-1) = \bar{n}^i \prod_{j=0}^{i-1} \left(1 + \frac{j}{k}\right) . \tag{3.28}$$

The averages over powers of factorials used in eqs. (3.12)–(3.15) can be expressed in terms of the usual factorial moments ξ_i. In particular, $\left\langle n^{2[i]} \right\rangle$ can be written in closed form[6] [Eddil]

$$\left\langle n^{2[i]} \right\rangle_t = \sum_{j=0}^{i} j! \begin{pmatrix} i \\ j \end{pmatrix}^2 \xi_{2i-j} , \tag{3.29}$$

where $\begin{pmatrix} i \\ j \end{pmatrix}$ is the usual Binomial Coefficient symbol. The higher powers $\left\langle n^{3[i]} \right\rangle$ and $\left\langle n^{4[i]} \right\rangle$ are exhibited explicitly up to order $i = 5$:

$$\begin{aligned}
\left\langle n^{3[1]} \right\rangle_t &= \xi_1 + 3\,\xi_2 + \xi_3 \\
\left\langle n^{3[2]} \right\rangle_t &= 4\,\xi_2 + 32\,\xi_3 + 38\,\xi_4 + 12\,\xi_5 + \xi_6 \\
\left\langle n^{3[3]} \right\rangle_t &= 36\,\xi_3 + 540\,\xi_4 + 1242\,\xi_5 + 882\,\xi_6 + 243\,\xi_7 + 27\,\xi_8 + \xi_9 \\
\left\langle n^{3[4]} \right\rangle_t &= 576\,\xi_4 + 13824\,\xi_5 + 50688\,\xi_6 + 59904\,\xi_7 + 30024\,\xi_8 + \\
&\quad 7200\,\xi_9 + 856\,\xi_{10} + 48\,\xi_{11} + \xi_{12} \\
\left\langle n^{3[5]} \right\rangle_t &= 14400\,\xi_5 + 504000\,\xi_6 + 2664000\,\xi_7 + 4608000\,\xi_8 + 3501000\,\xi_9 + \\
&\quad 1350360\,\xi_{10} + 284800\,\xi_{11} + 33800\,\xi_{12} + 2225\,\xi_{13} + \\
&\quad 75\,\xi_{14} + \xi_{15}
\end{aligned} \tag{3.30}$$

---

[6] We are grateful to E.A. De Wolf for drawing our attention to this form and ref. [Eddil].

and

$$
\begin{aligned}
\left\langle n^{4[1]} \right\rangle_t &= \xi_1 + 7\,\xi_2 + 6\,\xi_3 + \xi_4 \\
\left\langle n^{4[2]} \right\rangle_t &= 8\,\xi_2 + 208\,\xi_3 + 652\,\xi_4 + 576\,\xi_5 + 188\,\xi_6 + 24\,\xi_7 + \xi_8 \\
\left\langle n^{4[3]} \right\rangle_t &= 216\,\xi_3 + 13608\,\xi_4 + 94284\,\xi_5 + 186876\,\xi_6 + 149580\,\xi_7 + \\
&\qquad 56808\,\xi_8 + 11025\,\xi_9 + 1107\,\xi_{10} + 54\,\xi_{11} + \xi_{12} \\
\left\langle n^{4[4]} \right\rangle_t &= 13824\,\xi_4 + 1714176\,\xi_5 + 21606912\,\xi_6 + 76317696\,\xi_7 + \\
&\qquad 110160576\,\xi_8 + 78451200\,\xi_9 + 30645504\,\xi_{10} + 6976512\,\xi_{11} + \\
&\qquad 953424\,\xi_{12} + 78400\,\xi_{13} + 3760\,\xi_{14} + 96\,\xi_{15} + \xi_{16} \\
\left\langle n^{4[5]} \right\rangle_t &= 1728000\,\xi_5 + 371520000\,\xi_6 + 7629120000\,\xi_7 + 42762240000\,\xi_8 + \\
&\qquad 97388280000\,\xi_9 + 110386900800\,\xi_{10} + 70137648000\ ,\xi_{11} + \\
&\qquad 26920728000\,\xi_{12} + 6548346000\,\xi_{13} + 1039382000\ ,\xi_{14} + \\
&\qquad 109180720\,\xi_{15} + 7585600\,\xi_{16} + 342225\,\xi_{17} + 9575\,\xi_{18} + \\
&\qquad 150\,\xi_{19} + \xi_{20}\,.
\end{aligned}
\tag{3.31}
$$

Table 3 1 *The N_{ev}-independent parts $\bar{\sigma}_{\xi_i}/\xi_i$ of the relative width of the sampling distributions $\mathcal{P}(\hat{\xi}_i)$ for Negative Binomial P_n^{NBD} and different parameters $\bar{n}$ and k The usage is explained in Section 7*

σ/ξ for $i = 2$						
$\bar{n}$	$k = 0\ 1$	$k = 0\ 5$	$k = 1$	$k = 4$	$k = 10$	$k = \infty$
0 01	51 4	85 7	103	128	136	143
0 04	19 1	24 4	27 9	33 5	35 3	36 7
0 1	12 4	12 0	12 9	14 5	15 0	15 5
0 4	8 86	5 61	5 12	4 81	4 76	4 74
1	8 12	4 24	3 46	2 74	2 57	2 45
4	7 75	3 52	2 56	1 55	1 27	1 06
10	7 68	3 37	2 37	1 26	0 934	0 648
40	7 64	3 29	2 27	1 11	0 727	0 318

$\bar{\sigma}/\xi$ for $i = 3$						
$\bar{n}$	$k = 0\ 1$	$k = 0\ 5$	$k = 1$	$k = 4$	$k = 10$	$k = \infty$
0 01	235	698	1060	1840	2170	2490
0 04	58 6	112	155	247	287	324
0 1	32 3	40 8	50 2	71 1	80 3	88 8
0 4	20 5	14 1	13 6	14 2	14 6	15 1
1	18 2	9 58	7 87	6 33	5 98	5 75
4	17 1	7 43	5 22	2 92	2 31	1 86
10	16 9	7 01	4 70	2 25	1 58	1 04
40	16 8	6 79	4 45	1 91	1 18	0 486

$\bar{\sigma}/\xi$ for $i = 4$						
$\bar{n}$	$k = 0\ 1$	$k = 0\ 5$	$k = 1$	$k = 4$	$k = 10$	$k = \infty$
0 01	1060	5640	$1\ 10 \times 10^4$	$2\ 81 \times 10^4$	$3\ 84 \times 10^4$	$5\ 00 \times 10^4$
0 04	177	515	874	1960	2600	3310
0 1	82 5	140	201	377	477	586
0 4	46 0	35 1	36 5	44 3	49 0	54 1
1	39 6	21 3	17 9	15 1	14 6	14 4
4	36 6	15 4	10 5	5 41	4 12	3 18
10	36 0	14 3	9 16	3 87	2 53	1 56
40	35 7	13 7	8 52	3 14	1 78	0 668

σ/ξ for $i = 5$						
$\bar{n}$	$k = 0\ 1$	$k = 0\ 5$	$k = 1$	$k = 4$	$k = 10$	$k = \infty$
0 01	4750	$4\ 54 \times 10^4$	$1\ 15 \times 10^5$	$4\ 52 \times 10^5$	$7\ 33 \times 10^5$	$1\ 12 \times 10^6$
0 04	531	2390	5010	$1\ 64 \times 10^4$	$2\ 54 \times 10^4$	$3\ 76 \times 10^4$
0 1	208	479	820	2110	3060	4320
0 4	102	87 7	99 4	146	177	214
1	85 0	47 4	41 0	37 5	38 0	39 3
4	77 0	31 7	21 1	10 2	7 49	5 53
10	75 5	28 9	17 9	6 70	4 06	2 27
40	74 7	27 5	16 3	5 17	2 63	0 872

Table 3.2 *The $N_{\rm ev}$-independent parts $\overline{\beta_1}^{(i)}$ of the (squared) skewness of the sampling distributions $\mathcal{P}(\hat{\xi}_i)$ for Negative Binomial $P_{\bar{n}}^{\rm NBD}$ and different parameters $\bar{n}$ and k. The usage is explained in Section 7*

$\overline{\beta_1}$ for $i = 2$

$\bar{n}$	$k = 0.1$	$k = 0.5$	$k = 1$	$k = 4$	$k = 10$	$k = \infty$
0.01	6780	1.03×10^4	1.31×10^4	1.84×10^4	2.04×10^4	2.20×10^4
0.04	1930	1460	1480	1630	1700	1760
0.1	1140	567	487	427	416	409
0.4	749	209	139	83.9	72.3	64.4
1	673	144	80.1	35.0	26.7	21.4
4	635	112	52.5	14.0	7.94	4.45
10	628	106	47.3	10.3	4.75	1.68
40	624	103	44.7	8.55	3.27	0.405

$\overline{\beta_1}$ for $i = 3$

$\bar{n}$	$k = 0.1$	$k = 0.5$	$k = 1$	$k = 4$	$k = 10$	$k = \infty$
0.01	3.81×10^5	1.15×10^6	1.97×10^6	4.45×10^6	5.84×10^6	7.30×10^6
0.04	5.40×10^4	7.72×10^4	9.68×10^4	1.41×10^5	1.62×10^5	1.82×10^5
0.1	2.25×10^4	1.83×10^4	1.91×10^4	2.07×10^4	2.12×10^4	2.17×10^4
0.4	1.13×10^4	3640	2610	1700	1470	1300
1	9430	1960	1060	421	304	229
4	8560	1300	524	97.5	46.7	22.6
10	8390	1180	438	59.2	21.7	6.49
40	8300	1120	397	43.4	12.5	1.32

$\overline{\beta_1}$ for $i = 4$

$\bar{n}$	$k = 0.1$	$k = 0.5$	$k = 1$	$k = 4$	$k = 10$	$k = \infty$
0.01	2.06×10^7	1.48×10^8	3.50×10^8	1.34×10^9	2.18×10^9	3.33×10^9
0.04	1.39×10^6	4.21×10^6	7.14×10^6	1.56×10^7	2.06×10^7	2.64×10^7
0.1	4.17×10^5	5.81×10^5	7.85×10^5	1.23×10^6	1.41×10^6	1.58×10^6
0.4	1.62×10^5	6.34×10^4	5.12×10^4	4.02×10^4	3.66×10^4	3.31×10^4
1	1.26×10^5	2.71×10^4	1.49×10^4	5850	4090	2930
4	1.11×10^5	1.53×10^4	5610	748	289	110
10	1.08×10^5	1.34×10^4	4350	364	96.3	20.3
40	1.06×10^5	1.25×10^4	3790	231	43.6	3.04

$\overline{\beta_1}$ for $i = 5$

$\bar{n}$	$k = 0.1$	$k = 0.5$	$k = 1$	$k = 4$	$k = 10$	$k = \infty$
0.01	1.07×10^9	2.03×10^{10}	6.91×10^{10}	4.74×10^{11}	9.89×10^{11}	1.94×10^{12}
0.04	3.47×10^7	2.28×10^8	5.48×10^8	2.02×10^9	3.23×10^9	4.91×10^9
0.1	7.52×10^6	1.83×10^7	3.30×10^7	8.26×10^7	1.12×10^8	1.44×10^8
0.4	2.26×10^6	1.11×10^6	1.04×10^6	1.06×10^6	1.06×10^6	1.03×10^6
1	1.65×10^6	3.79×10^5	2.18×10^5	9.21×10^4	6.49×10^4	4.55×10^4
4	1.39×10^6	1.83×10^5	6.33×10^4	6630	2110	618
10	1.35×10^6	1.54×10^5	4.58×10^4	2580	485	64.3
40	1.32×10^6	1.41×10^5	3.84×10^4	1410	165	6.14

Table 3.3: *The N_{ev}-independent parts $\overline{\gamma_2}^{(i)}$ of the kurtosis of the sampling distributions $\mathcal{P}(\hat{\xi}_i)$ for Negative Binomial P_n^{NBD} and different parameters $\bar{n}$ and k. The usage is explained in Section 7.*

$\overline{\gamma_2}$ for $i = 2$

$\bar{n}$	$k = 0.1$	$k = 0.5$	$k = 1$	$k = 4$	$k = 10$	$k = \infty$
0.01	1.21×10^4	1.43×10^4	1.67×10^4	2.13×10^4	2.30×10^4	2.44×10^4
0.04	3790.	2540.	2390.	2320.	2320.	2320.
0.1	2290.	1060.	865.	689.	646	615.
0.4	1540.	408.	260	145.	121.	105.
1	1390.	284.	152.	61.0	44.7	34.5
4	1320.	224.	101.	24.8	13.4	7.03
10	1300.	212.	91.2	18.4	8.10	2.63
40	1300.	206	86.3	15.3	5.64	0.634

$\overline{\gamma_2}$ for $i = 3$

$\bar{n}$	$k = 0.1$	$k = 0.5$	$k = 1$	$k = 4$	$k = 10$	$k = \infty$
0.01	9.61×10^5	2.37×10^6	3.57×10^6	6.53×10^6	8.00×10^6	9.47×10^6
0.04	1.47×10^5	1.90×10^5	2.23×10^5	2.80×10^5	3.01×10^5	3.18×10^5
0.1	6.33×10^4	4.72×10^4	4.67×10^4	4.58×10^4	4.48×10^4	4.37×10^4
0.4	3.25×10^4	9830.	6700.	3910.	3220.	2700.
1	2.73×10^4	5370.	2760.	963.	650.	458.
4	2.49×10^4	3570.	1370.	217.	94.5	41.1
10	2.44×10^4	3240.	1140.	130.	42.8	11.3
40	2.41×10^4	3090.	1040.	94.4	24.2	2.22

$\overline{\gamma_2}$ for $i = 4$

$\bar{n}$	$k = 0.1$	$k = 0.5$	$k = 1$	$k = 4$	$k = 10$	$k = \infty$
0.01	7.17×10^7	4.31×10^8	9.02×10^8	2.66×10^9	3.86×10^9	5.33×10^9
0.04	5.31×10^6	1.42×10^7	2.25×10^7	4.26×10^7	5.20×10^7	6.10×10^7
0.1	1.65×10^6	2.08×10^6	2.64×10^6	3.66×10^6	3.97×10^6	4.15×10^6
0.4	6.55×10^5	2.40×10^5	1.83×10^5	1.25×10^5	1.06×10^5	8.90×10^4
1	5.14×10^5	1.04×10^5	5.42×10^4	1.83×10^4	1.17×10^4	7540.
4	4.51×10^5	5.92×10^4	2.05×10^4	2250.	754	241.
10	4.39×10^5	5.18×10^4	1.59×10^4	1060.	235.	39.4
40	4.33×10^5	4.83×10^4	1.39×10^4	659	101.	5.35

$\overline{\gamma_2}$ for $i = 5$

$\bar{n}$	$k = 0.1$	$k = 0.5$	$k = 1$	$k = 4$	$k = 10$	$k = \infty$
0.01	5.11×10^9	8.01×10^{10}	2.44×10^{11}	1.28×10^{12}	2.32×10^{12}	3.93×10^{12}
0.04	1.85×10^8	1.05×10^9	2.33×10^9	7.36×10^9	1.08×10^{10}	1.48×10^{10}
0.1	4.17×10^7	9.07×10^7	1.52×10^8	3.28×10^8	4.14×10^8	4.87×10^8
0.4	1.29×10^7	5.87×10^6	5.17×10^6	4.52×10^6	4.12×10^6	3.58×10^6
1	9.45×10^6	2.05×10^6	1.11×10^6	3.97×10^5	2.50×10^5	1.52×10^5
4	7.99×10^6	9.97×10^5	3.26×10^5	2.76×10^4	7380.	1700.
10	7.72×10^6	8.42×10^5	2.36×10^5	1.04×10^4	1550.	145.
40	7.58×10^6	7.71×10^5	1.98×10^5	5530.	483.	11.4

Bibliography

[Bia86a] A. Bialas and R. Peschanski, Nucl. Phys. **B273**(1986)703; Nucl. Phys. **B308**(1988)857.

[Bus91] B. Buschbeck, Intermittency, a short experimental review, Proc. XXVI Rencontre de Moriond, Les Arcs, ed. J.Trân Thanh Vân (Edidtions Frontières 1991) 299.

[Car87a] P. Carruthers and C.C. Shih, Int. J. Mod. Phys. **A2**(1987)1447 .

[Car89c] P. Carruthers and I. Sarcevic, Phys. Rev. Lett. **63**(1989)1562; P. Carruthers, H.C. Eggers and I. Sarcevic, Phys. Lett. **254B**(1991)258.

[Car91] P. Carruthers, Phys. Rev. **A43**(1991)2632.

[Des90a] P. Desvalleés, R. Ouziel and R. Peschanski, Phys. Lett. **235B**(1990)317.

[Eddi1] E. Jakeman and E.R. Pike, J. Phys. (Proc. Phys. Soc.) **A1**(1968)690.

[Fri89] E.M. Friedlander, Mod. Phys. Lett. **A4**(1989)2457.

[Kit90c] W. Kittel, Intermittency, a review of experimental results, Proc. 20th Int. Symp. on Multiparticle Dynamics, Gut Holmecke/Dortmund, 1990, eds. R.Baier and D.Wegener (World Scientific 1991) 401.

[KSb] M. Kendall and A. Stuart, *The Advanced Theory of Statistics*, Vol.2, Fourth edition, London: Charles Griffin & Company Limited 1979.

[LEBC91] P. Lipa, H. Eggers, F. Botterweck, and M. Charlet, Z. Phys. **C54**(1992)115.

[Lip90a] P. Lipa, Ph.D. dissertation, U. Wien (1990), HEPHY-PUB 542/90.

[NA22CO] V.V. Aivazyan et al. (NA22 Collab.), Phys. Lett. **258B**(1991)487.

[NA22-88b] M. Adamus et al. (NA22 Collab.), Z. Phys. **C37**(1988)215.

[Stu87a] A. Stuart and J.K. Ord, *Kendall's Advanced Theory of Statistics*, Vol.1, Fifth edition, New York: Oxford University Press 1987.

[Wo88] S. Wolfram, *Mathematica: A System for Doing Mathematics by Computer*, New York: Addison-Wesley Publishing Company 1988.

4

Fitting factorial moments

In the following two chapters several aspects of the one-dimensional normalized factorial moments are studied Conclusions will be drawn from the fitted intermittency indices measuring the strength of the phenomenon In this chapter it will be shown that a number of problems arise in determining the intermittency index The errors on the factorial moments are calculated using some approximations The power law $F_q(\delta) = a_q \delta^{-f_q}$, typical for intermittency, can be fitted in several ways leading to different results The correct procedure of minimizing the χ^2, using the correlations between the factorial moments at different bin-sizes, may, nevertheless, produce doubtful results

In addition, it is well-known nowadays, that a real power-law behavior, if present in a 3-dimensional process, cannot be expected in a one- or two-dimensional projection (see chapter 7)

In spite of all this, the fitted power law does give an indication of the growth of the factorial moments with decreasing bin size The fit will be used in the following chapters to quantify some observations This chapter should, therefore, be understood as a discussion of the limits of the method

4.1 Error calculation

The vertically normalized factorial moments for bin-size $\delta = \Delta/M$ are defined by

$$\langle F_q\rangle_V^{(M)} = \frac{1}{M}\sum_{m=1}^{M} \frac{\frac{1}{W}\sum_{i=1}^{N} w_i n_{m,i}^{[q]}}{\left(\frac{1}{W}\sum_{i=1}^{N} w_i n_{m,i}\right)^q} \tag{4 1}$$

Here, w_i is the event weight, $W = \sum_{i=1}^{N} w_i$ the sum of the weights and $n_{m,i}$ is the number of particles in event i that fall in bin m The subscript V indicates the vertical average and the superscript M the number of bins Since the full region Δ is fixed, M is a measure for the bin-size δ Using $[\ ]_M$ and $\langle\ \rangle$ to indicate the bin and (weighted) event averaging, respectively, the formula can be rewritten as follows

$$\langle F_q\rangle_V^{(M)} = \left[\frac{\left\langle n_m^{[q]}\right\rangle}{\langle n_m\rangle^q}\right]_M = \left\langle\left[\frac{n_m^{[q]}}{\langle n_m\rangle^q}\right]_M\right\rangle = \left\langle \tilde{F}_q^{(M)}\right\rangle \quad , \tag{4 2}$$

where the bin index m is maintained, but the event index is dropped.

Before continuing the discussion on error calculation, it should be remarked that the weighted factorial moments need special care. In the appendix at the end of this chapter, the formula for the error on weighted moments will be given. In the following only the unweighted moments and their errors will be discussed. The conclusions hold for both cases.

One can argue that for fitting purposes it is necessary to take into account the correlations between factorial moments at different bin-sizes. Therefore, one needs the covariance matrix. Assuming negligible error on the denominator of the normalized factorial moment, the second part of (4.2) yields the following definition of the covariance matrix

$$\begin{gathered}\mathrm{cov}(\left\langle \tilde{F}_q^{(M)} \right\rangle, \left\langle \tilde{F}_q^{(L)} \right\rangle) = \\ \frac{1}{N-1}\left(\left\langle \tilde{F}_q^{(M)} \tilde{F}_q^{(L)} \right\rangle - \left\langle \tilde{F}_q^{(M)} \right\rangle \left\langle \tilde{F}_q^{(L)} \right\rangle\right) = \qquad (4.3) \\ \frac{1}{N-1}\left(\left\langle \left[\frac{n_m^{[q]}}{\langle n_m \rangle^q}\right]_M \left[\frac{n_l^{[q]}}{\langle n_l \rangle^q}\right]_L \right\rangle - \left\langle \left[\frac{n_m^{[q]}}{\langle n_m \rangle^q}\right]_M \right\rangle \left\langle \left[\frac{n_l^{[q]}}{\langle n_l \rangle^q}\right]_L \right\rangle\right).\end{gathered}$$

If the sampling distribution of the averaged factorial moments is assumed to have a Gaussian shape, the error on the factorial moment for a given M is the square root of the corresponding diagonal element of the covariance matrix. Note that for calculation of the covariance, in the vertical case, the bin averaged particle number should be known. This requires therefore an extra run over the events.

Examining the variance for 'bin-size' M more closely, it can be seen that it can be rewritten as

$$\mathrm{var}(\langle F_q \rangle_V^{(M)}) = \frac{1}{M^2}\frac{1}{N-1}\sum_{m=1}^{M}\sum_{m'=1}^{M}\left(\left\langle \frac{n_m^{[q]}}{\langle n_m \rangle^q}\frac{n_{m'}^{[q]}}{\langle n_{m'} \rangle^q} \right\rangle - \left\langle \frac{n_m^{[q]}}{\langle n_m \rangle^q} \right\rangle \left\langle \frac{n_{m'}^{[q]}}{\langle n_{m'} \rangle^q} \right\rangle\right) \qquad (4.4)$$

The first term in this equation measures bin-bin correlations, similar to those studied in the case of the factorial correlators. If these are assumed to be trivial

$$\left\langle n_m^{[q]} n_{m'}^{[q]} \right\rangle = \left\langle n_m^{[q]} \right\rangle \left\langle n_{m'}^{[q]} \right\rangle \qquad (4.5)$$

for $m \neq m'$, then the matrix (4.4) reduces to diagonal elements only and the error on the normalized factorial moment becomes

$$\Delta \langle F_q \rangle_V^{(M)} = \frac{1}{M}\sqrt{\sum_m \frac{\left\langle n_m^{2[q]} \right\rangle - \left\langle n_m^{[q]} \right\rangle^2}{\langle n_m \rangle^{2q}(N-1)}} \qquad (4.6)$$

and will be referred to as histogram error. Note that this corresponds to $R = 1$ in equation (3.23) of the previous chapter.

The horizontally normalized factorial moments are defined by

$$\langle F_q \rangle_H^{(M)} = \frac{\left\langle [n_m^{[q]}]_M \right\rangle}{\langle [n_m]_M \rangle^q} = \frac{M^q}{\langle n \rangle^q}\left\langle [n_m^{[q]}]_M \right\rangle \qquad (4.7)$$

where $\langle n \rangle$ is the average number of particles in the initial interval Δ. The covariance matrix is defined analogously to (4.3) as

$$\mathrm{cov}(\langle F_q\rangle_H^{(M)}, \langle F_q\rangle_H^{(L)}) = \frac{M^q L^q}{\langle n\rangle^{2q}} \frac{\left\langle [n_m^{[q]}]_M [n_l^{[q]}]_L \right\rangle - \left\langle [n_m^{[q]}]_M \right\rangle \left\langle [n_l^{[q]}]_L \right\rangle}{(N-1)} . \qquad (4.8)$$

where, again, the error on the denominator is assumed to be very small. The error on the factorial moments can be calculated from the square root of the variance:

$$\mathrm{var}(\langle F_q\rangle_H^{(M)}) = \frac{M^{2q}}{\langle n\rangle^{2q}} \frac{\left\langle [n_m^{[q]}]_M^2 \right\rangle - \left\langle [n_m^{[q]}]_M \right\rangle^2}{(N-1)} . \qquad (4.9)$$

Once more assuming that there are no correlations between the bins, the error reduces to

$$\Delta \langle F_q\rangle_H^{(M)} = \frac{M^{q-1}}{\langle n\rangle^q} \sqrt{\sum_m \frac{\left\langle n_m^{2[q]} \right\rangle - \left\langle n_m^{[q]} \right\rangle^2}{N-1}} \qquad (4.10)$$

As in (4.6), this error is also referred to as histogram error.

Some remarks:

- The errors plotted in the forthcoming figures will be the histogram errors (4.6) and (4.10). The reason for this is calculational simplicity. The covariance matrix, in the vertical case, demands an extra run and is not used except for this chapter. The errors from the diagonal of the covariance matrix, are somewhat larger than the histogram errors. For the horizontal (vertical) moments, the latter are about 20% (15%) smaller for second order, the difference decreasing for higher order below 10%, in both cases.

- Since in some cases the errors on the factorial moments can be as large as the moments themselves, on a logarithmic plot this would show up as enormous error bars. To avoid this problem, the logarithms of the factorial moments are plotted on a linear scale. The corresponding errors are then

$$\Delta \ln F = \frac{\Delta F}{F} \qquad (4.11)$$

  i.e. the relative errors of the factorial moments.

- From the simulations with a Negative Binomial distribution [LEBC91] (chapter 3) it is found that, especially in small intervals and for higher orders q, the factorial moments are not Gaussian distributed. Thus, the dispersion, as a measure for the error, is only approximately correct. To check the quality of the errors on the data, they are compared to the expected errors from a NBD with the bin-averaged $\bar{n}$ and $1/k$ from the observed F_2 as input. The agreement is found to be satisfactory, taking into account the fact that the NBD is not able to describe the higher-order factorial moments very well (see chapter 6).

4.2 Fitting the power law

Taking the logarithm on both sides, the power law

$$F_q(\delta) = a'_q\, \delta^{-f_q} \tag{4.12}$$

can be written as a linear equation,

$$\ln F_q(\delta) = a_q - f_q \ln \delta \ . \tag{4.13}$$

The parameters a_q (a'_q) and f_q can be determined by χ^2 minimization. The program used is MINUIT [JRMI86].

4.2.1 Definition of χ^2

The χ^2 needed to fit power law (4.12) is

$$\chi^2 = \sum_{L=M_{min}}^{M_{max}} \sum_{M=M_{min}}^{M_{max}} (F_{q,L}^{theor} - F_{q,L}^{exp}) C^{-1}(F_q^L, F_q^M)(F_{q,M}^{theor} - F_{q,M}^{exp}) \ . \tag{4.14}$$

M_{min} and M_{max} denote the range of the fit. The superscripts *theor* and *exp* refer to the function values and the experimentally obtained values, respectively. C^{-1} stands for the inverse of the covariance matrix.

Fitting the linear equation (4.13), the χ^2 becomes

$$\chi^2 = \sum_{L=M_{min}}^{M_{max}} \sum_{M=M_{min}}^{M_{max}} (\ln F_{q,L}^{theor} - \ln F_{q,L}^{exp}) C^{-1}(\ln F_q^L, \ln F_q^M)(\ln F_{q,M}^{theor} - \ln F_{q,M}^{exp}) \ . \tag{4.15}$$

with

$$C(\ln F_q^L, \ln F_q^M) = \frac{C(F_q^L, F_q^M)}{F_{q,L}^{exp} F_{q,M}^{exp}} \ . \tag{4.16}$$

4.2.2 Comparison of fit methods

It is now possible to compare several ways of fitting the power law. The event sample chosen is **p0bad** (not weighted) and will be described in more detail in the next chapter. It is the cleanest and most reliable sample existing in this experiment, since only complete, well-measured events are accepted. Only the one-dimensional (rapidity) vertically normalized factorial moments are discussed, but similar results hold for the horizontal case.

To avoid possible trivial effects, as resonance decay causing correlations for $\delta y > 1$, the start value of the fit is chosen to be $M_{min} = 4$. At the other end, experimental resolution and statistics set a lower limit to the bin-size ($M_{max} = 40$). It is chosen to be $\delta y = 0.1$ corresponding to 40 divisions of the total range. Thus, the maximum number of points used in the fit is 37.

To visualize the difference between the fit results, the lines corresponding to the different fits are plotted in fig. 4.1. In addition, the fitted slopes f_q are listed in tab. 4.1 and the anomalous dimensions $d_q = f_q/(q-1)$ are plotted in fig. 4.2. The different ways of fitting are:

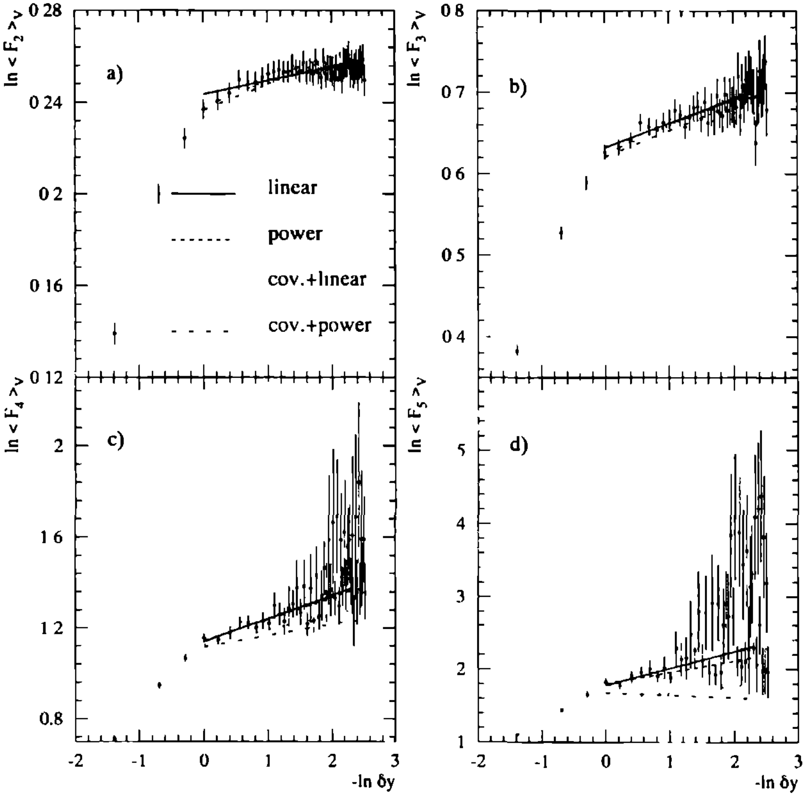

Figure 4.1: *Factorial moments as a function of bin-size. The lines represent the fit results for the methods indicated in a).*

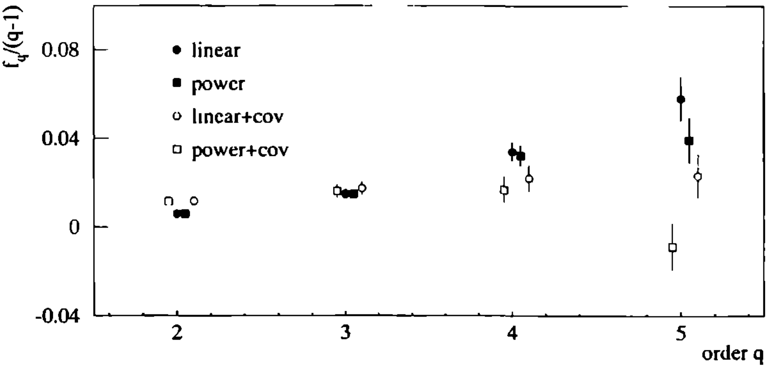

Figure 4.2: *The anomalous dimensions $f_q/(q-1)$.*

q	method	a_q	f_q	χ^2/NDF	corr
2	lin	0.244 ± 0.002	0.006 ± 0.001	13/35	−0.91
	pow	0.244 ± 0.002	0.006 ± 0.002	13/35	−0.91
	lin +cov	0.238 ± 0.005	0.012 ± 0.002	61/35	0.007
	pow +cov	0.237 ± 0.005	0.011 ± 0.002	61/35	0.007
3	lin	0.632 ± 0.005	0.030 ± 0.004	14/35	−0.85
	pow	0.632 ± 0.005	0.030 ± 0.004	14/35	−0.85
	lin +cov	0.62 ± 0.01	0.035 ± 0.006	46/35	0.009
	pow +cov	0.62 ± 0.01	0.033 ± 0.006	46/35	0.006
4	lin	1.14 ± 0.02	0.10 ± 0.02	23/35	−0.77
	pow	1.14 ± 0.02	0.10 ± 0.02	21/35	−0.78
	lin +cov	1.13 ± 0.02	0.07 ± 0.02	57/35	−0.029
	pow +cov	1.12 ± 0.02	0.05 ± 0.02	43/35	−0.056
5	lin	1.78 ± 0.03	0.23 ± 0.04	49/35	−0.72
	pow	1.80 ± 0.04	0.16 ± 0.04	25/35	−0.71
	lin +cov	1.58 ± 0.04	0.09 ± 0.04	1104/35	0.030
	pow +cov	1.68 ± 0.04	−0.03 ± 0.04	51/35	−0.15

Table 4.1: *Fit results for the unweighted* **p0bad** *sample, using the methods explained in the text.*

1. No bin-size correlations taken into account.
   This still leaves the choice of using the histogram errors (4.6) or the square root of the variance, but this turns out to give similar fit values.
   Two further sub-cases are possible:

   a) $F_q(\delta) = e^{a_q}\delta^{-f_q}$, the power law function.
   The higher-order FM's, for example 5th order, suffer from large fluctuations. The large values have large errors, the lower ones have smaller errors. Due to its definition, the largest contribution to the χ^2 is given by the values with the smallest errors. For small bin-sizes the minimization procedure will therefore favor the smaller values. This can be seen from plot d) in fig. 4.1, where the dashed line goes through the lower points

   b) $\ln F_q(\delta) = a_q - f_q \ln \delta$, the linear function.
   Here, the χ^2 has the relative error in the denominator. The higher points become more important, because their relative errors do not differ too much from those of the lower points. Indeed, from the same figure it can be seen that the straight line is steeper. The χ^2 per degree of freedom is 23/35 for 4th order and 48/35 for 5th order. This is larger than for the power law (21/35 and 25/35, respectively). However, the linearly fitted slope gives visually a better impression of the growth of the moments.

   In both cases, there is a strong anti-correlation (-0.7 to -0.9) between the two fit parameters.

2. Using the covariance matrix.
   The correct procedure is to invert only that part of the covariance matrix lying within

the fit boundaries. Using the whole matrix for inversion gives optically better results, but since there is no justification for that procedure it will not be used here. Again, there are the two options of power-law (dot-dashed line) and linear fit (dotted line). Neither of them is able to produce a good fit for the 4th and 5th order. In the case of the 4th order, the line falls below all data. An explanation for that is given by B. Wosiek in [BWAP90]. There, the author demonstrates that negative elements of the covariance matrix (indicating anti-correlations) can produce this paradoxical result. Note the negative slope of the 5th-order power-law fit. This result indicates that there is a serious problem in the 5th-order covariance matrix.

The correlation between the fit parameters is very small when the covariance matrix is taken into account. The difference between inverting the whole covariance matrix, or only the part determined by the begin and end points of the fit, is remarkable. In the former case, the lines describe the data rather well, but as a consequence there is a rather strong anti-correlation between the fit parameters.

4.3 Conclusion

As mentioned already in the introduction, this chapter is meant as a warning against blindly trusting fit values. Since the main reason to fit the data is to give a measure for the behavior of the moments as a function of the bin-size, it is necessary to find a fit procedure that gives a reasonable (visual) description of the data. Therefore, in the next chapters the linear fit without covariance matrix will be used.

4.4 Appendix

The error calculation for weighted moments is more complicated than for the unweighted moments. In [HEN165] it is shown that the error on the weighted event average

$$\bar{x} = \frac{\sum_i w_i x_i}{\sum_i w_i} \quad , \quad \text{with} \quad i = 1, \ldots, N \quad , \tag{4.17}$$

can be calculated from error propagation. Using some approximations the variance is found to be (omitting the event index i)

$$\sigma^2(\bar{x}) = \frac{N}{N-1} \frac{1}{(\sum w)^2} \left[\sum w^2 x^2 + \frac{(\sum wx)^2 \sum w^2}{(\sum w)^2} - 2 \frac{\sum wx \sum w^2 x}{\sum w} \right] \tag{4.18}$$

Note, that this reduces to the usual expression for the variance

$$\sigma^2\left(\frac{1}{N} \sum x\right) = \frac{1}{N-1} \left[\frac{1}{N} \sum x^2 - \left(\frac{1}{N} \sum x \right)^2 \right] \tag{4.19}$$

when all weights are 1.

Bibliography

[BWAP90] B. Wosiek, Intermittency analyses of correlated data, Acta Phys. Pol. B21 (1990).

[HEN165] W. Metzger, Nijmegen note HEN 165-rev. , 1978.

[JRMI86] F. James and M. Roos, Function Minimization and Error Analysis, revised program, CERN Computer Centre GENLIB D506, 1986.

[KSASV1] M.G.Kendall and A.Stuart, The Advanced Theory of Statistics, Vol.1, Charles Griffin & Company Limited, London, 1967.

[LEBC91] P. Lipa, H. Eggers, F. Botterweck and M. Charlet, Z. Phys. C54 (1992) 115.

5

Event selection and biases

The first step in the intermittency analysis is to define an event sample and to see what the consequences of a particular choice are Therefore, two samples are defined and the differences between them concerning one-dimensional factorial moments in rapidity space are discussed

In addition, the influence of the NA22 'spike event' [SPIK87] and the use of event weights are studied and found to be considerable

Biases due to detector limitations are discussed Those due to physics processes like (unseen) Dalitz decay and γ-conversion are estimated by Monte Carlo simulation

5.1 Event samples

In this thesis two main event samples are used **p0bad** and **pMbad** For both, the same quality criteria are used for the particle tracks, but a different limit is applied for the number of tracks allowed to be lost due to these criteria, before an event is rejected

The cuts applied on the data will be given in the order of position in the analysis program Their definition is extensively discussed in [PVHT87] and [HMSN84]

General cuts on event quality:
Only events measured in RCBC are used Reasons for an event not to be measured are too much background due to an interaction upstream, too many other beam tracks close to the interacting beam track, or too faint tracks A small number of events are lost in the reconstruction procedure

Beam:
Events with a bad quality beam track are rejected A beam track is of good quality when it has a hybrid fit (that means it is reconstructed in the upstream wire chambers U1 and U3) and at least two bubble chamber track images are used in the fit The 'fit-probability' parameter of the track should be better than 10^{-5}, and the RMS of the track should be smaller than $400\mu m$ All beam particles satisfying these cuts have a well defined identity (proton, kaon or pion)

Topology:
The number of tracks in an event (the 'topology') after reconstruction must be identical to that found in scanning and measuring No tracks must be lost, but one 'very bad' *extra* track is allowed to be dropped Odd topologies are not allowed The sum of charges of

the outgoing tracks should be 2. However, 0 or 4 are possible if the curvature of a track is determined so badly that a flip of the track's charge restoring the charge balance is possible within errors.

Events with an identified electron are rejected (see below).

The event quality also depends on the number of badly reconstructed tracks. In the quality program, already mentioned in chapter 2, tracks are divided into six categories: Good, Acceptable, Interacting, Suspicious, Very Suspicious and Very Bad [NA22QU]. Tracks belonging to the latter four categories are in general called 'bad'.

For the **p0bad** sample no 'bad' tracks are allowed. There is one exception, a good track that survives the quality cuts, is rejected after all if its momentum is larger than 350 GeV/c or smaller than 0.0005 GeV/c. In the **pMbad** sample events are accepted with 0, 1, 1, 2 and 3 'bad' tracks for a topology of 2, 4, 6, 8 and more than 8, respectively. This is the difference between the two samples, and it is clear that this results in **p0bad** to be a subsample of **pMbad** .

Track quality:

Whether a track is of worse than acceptable quality largely depends on the type of track under consideration. Besides the normal tracks there are some tracks that receive a special label during scanning or measuring. The distinguished track classes are:

S, possibly stopping track.

P, stopping track, mostly very slow protons.

R, decaying pion track: $\pi^{\pm} \to \mu\nu$ and $\mu \to e\nu\bar{\nu}$.

E, electron track, for example from $\pi^0 \to \gamma e^+e^-$

V, neutral decay, for example $K^0_S \to \pi^+\pi^-$

I, interaction on a charged track

N, interaction on a neutral track.

D, decaying charged particle track (kink), for example $K^+ \to \pi^+\pi^0$.

X, track from a confused region.

R and E tracks are always accepted. Heavy ionized S and P tracks are rejected if their charge is negative and their momentum resolution $\Delta p/p > 0.10$ (backward anti-protons are not very probable!).

I,D and X tracks are accepted when their relative momentum resolution is better than 10% or when they are labeled 'reliable', that is when $\Delta p/p < 0.25$ and the sagitta $s > 4.5 * RMS$.

For the normal tracks the relative momentum resolution has to be better than 0.1 (or $\Delta p/p < 0.25$ and $s > 4.5 * RMS$) and the track should be correctly (i.e. within strict matching criteria) hybridized, unless it is completely measured within RCBC.

The idea of selecting tracks only down to acceptable quality is to avoid the possibility of so-called ghost tracks. These can be created by the reconstruction program (GEOHYB). This program is able to create two tracks from one (by combining two pairs of views separately), but then usually gets in trouble with hybridization. On the other hand, badly measured tracks can be matched with anything, and one should be very suspicious about these. Slow tracks cannot be hybridized and, therefore, additional cuts on charge balance, even topology, etc. are applied. Due to the strict criteria described above, *double counting of tracks in the NA22 experiment is virtually excluded.*

Finally, most of the tracks accepted have a relative momentum resolution that is better than 25% and the average value is about 2%. Only tracks with label R, E, S or P may have

$\Delta p/p > 0.25$.

In chapter 2 the relative momentum error has already been shown as a function of the lab momentum, before application of the track cuts. The average momentum resolution $\langle \Delta p/p \rangle$ is better than 2.5% over the whole momentum range. The error on the phase space variables relevant for the analysis is calculated from error propagation of Δp, $\Delta \phi$ and $\Delta \lambda$. The correlation matrices of p, ϕ and λ are not available on the DST, but analogous calculations for NA22 nuclear interactions show that the error on y does not change by taking those correlations into account. For the **p0bad** sample the average resolution in the rapidity region Δy under consideration ($-2 < y < 2$) is shown in fig. 5.1 for rapidity y, azimuthal angle φ and transverse momentum p_T. The number of bins M is 50, corresponding to the largest number of divisions used in the one-dimensional intermittency analysis. Each bin contains the same number of particles (see sec. 7.4) and the local bin-size is indicated by the horizontal bars. For rapidity the resolution is better than 0.02 units in y. The average error on the azimuthal angle φ (here, $\varphi = \arctan(p_z/p_y)$, different from the angle ϕ directly measured in the experiment!) is seen to oscillate between 0.015 and 0.025 rad with minima at 0, π and 2π. This is related to the position of the cameras. In the same figure the resolution of $\ln p_T^2$ (twice the relative resolution of p_T) is plotted. The scale for p_T is given at the top of the sub-plot. The resolution varies from 0.05 to 0.27, far below the corresponding bin-size.

Mass assignment:

Since the moments are calculated with the CMS rapidity variable, knowledge of the mass of the particle is necessary to do the correct transformation from the lab system to the CMS. The bubble chamber is used as a particle identification device and all information comes from the measurement stage and the ionization scan, if available.

All positive particles with momentum larger than 1.2 GeV/c are called pions, except when their momentum is larger than 150 GeV/c, in which case they are given the mass of the beam particle.

Negative tracks are assigned the pion mass, unless the ionization scan result gives a unique electron, or at the measurement stage the electron label was given.

If ionization scan results are available [1], the procedure for positive tracks with momentum smaller than 1.2 GeV/c is:

- unique electron/positron → electron mass
- meson/electron ambiguity → pion mass
- unique proton → proton mass
- meson/proton ambiguity → automatic procedure

In case of the ionization scan being absent, the so-called automatic procedure is invoked:

- if the track label is electron (spiralling track in RCBC) , or pion decay → corresponding mass hypothesis
- if the track is labeled (possible) proton and a proton mass-fit exists → proton mass
- if $p_{lab} > 0.7$ GeV/c → pion mass

---

[1] Ionization scan results are available for the full K^+p sample and for 62% of the π^+p sample.

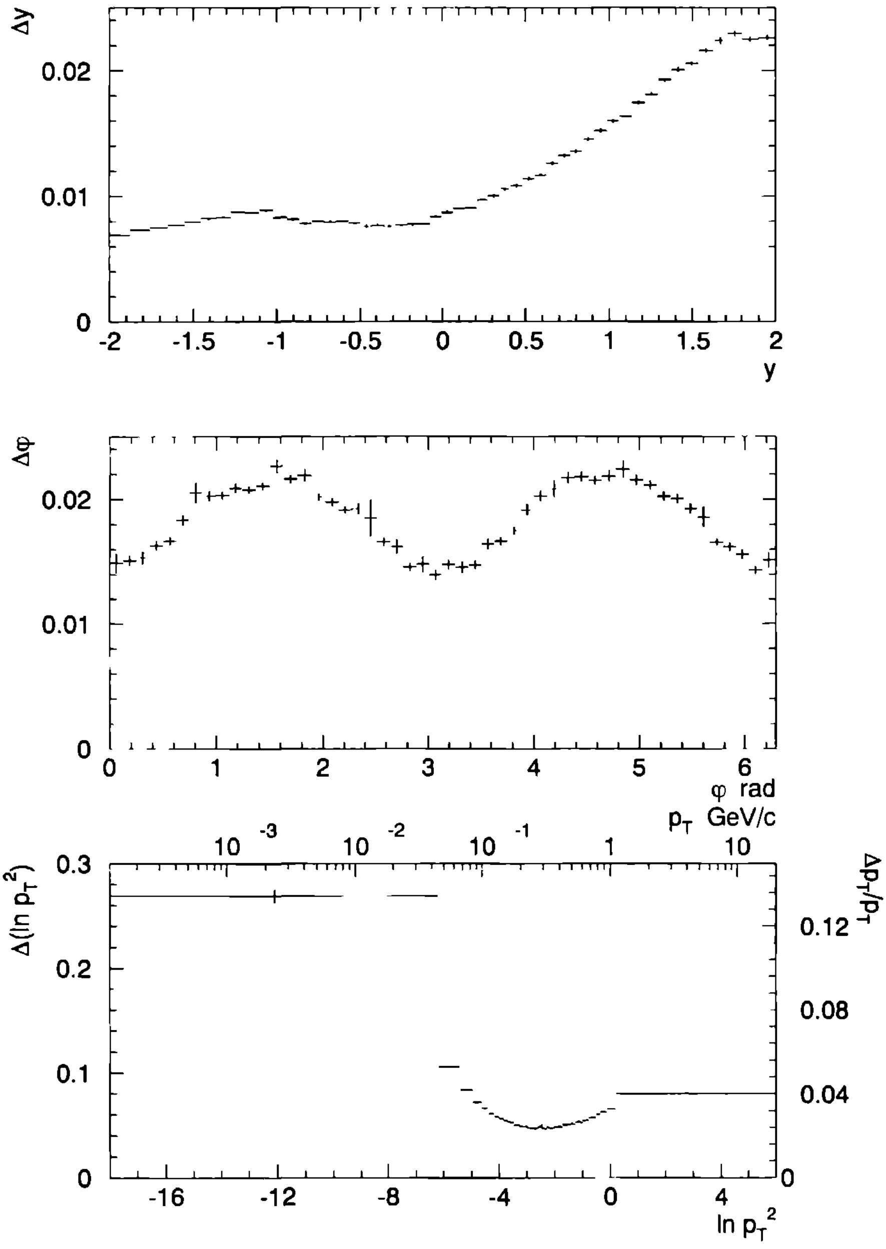

Figure 5.1: *The resolution of the 3 variables y, φ and* $\ln p_T^2$. *The binning corresponds to equal numbers of particles per bin*

	pObad	pMbad
K^+p	15769	29765
π^+p	43463	84639
total	59232	144404

Table 5.1: *The number of events for the* **pObad** *and* **pMbad** *samples.*

- if the probability of the proton hypothesis is 5% larger than the pion probability, the proton mass is used.
- all other tracks are assigned pion mass.

If one of the particles with momentum $p_{lab} < 200$ MeV/c is identified as an electron or positron, the event is rejected. The reason for this is that electrons can only occur in e^+e^- pairs. If one electron is identified, one of the remaining tracks should also be an electron and therefore be excluded from analysis. Since the other electron cannot be found, the whole event is dropped. Still, events with a γ-conversion close to the vertex or a Dalitz decay ($\pi^0 \to e^+e^-\gamma$) with an electron of $p_{lab} > 200$ MeV/c survive. Therefore, it is necessary to estimate their influence on the factorial moments using Monte Carlo simulation. This will be done further on.

Trigger weights:
At this stage trigger weights, mentioned already in chapter 2, are calculated. They are described in detail in [PVHT87] and are applied to correct for event losses due to levels 1 and 2 of the trigger. Events with one fast track suffer from losses due to level 1. To correct for this, x_F and p_T dependent weights obtained from Monte Carlo simulations are applied. For events with more than 1 and less than 4 fast tracks a loss can be expected from level 2. A weight is calculated for these events depending on the vertical position of fast track pairs at W2.

Physics cuts:
Additional cuts are applied to remove events with a specific physical signature. Three classes of events are distinguished: elastic, single-diffractive, and normal inelastic events.

Elastic events are excluded. The most important cut is: if for a two prong event the missing transverse momentum is less than 100 MeV/c and the absolute missing longitudinal momentum (in the lab frame) does not exceed 9 GeV/c the event is assumed to be elastic.

Single-diffractive events have to be rejected in order to be able to compare any of the results with those from e^+e^- and Deep Inelastic Scattering (DIS) experiments. Besides that, it is a widely accepted idea that for these events different mechanisms are at work, not present in multi-particle production of normal events. NA22 data on this topic are presented in [NA22DI]. Diffractive events can be defined in various ways. The cuts used here are based on the Feynman x variable. If the event contains a positive track with $x_F > 0.88$ when it is assigned the mass of the beam particle (or target particle for $x_F < -0.88$) and the total number of particles is less than 8, it is called single-diffractive.

The total number of inelastic non-single-diffractive events left after the selection procedures is given in table 5.1.

Multiplicity weights:
After all event cuts have been applied, the events are given a topology dependent weight C_n according to the topological inelastic cross-section σ_n from [NA22TC]. When an event i of

	pObad		**pMbad**	
topology	weight	number of events	weight	number of events
2	1.22	1837	2.33	1837
4	0.92	7504	1.22	10886
6	0.84	12869	1.05	19830
8	0.96	14755	1.00	27023
10	1.14	10843	1.00	23550
12	1.38	6295	1.06	15660
14	1.66	3122	1.13	8767
16	1.98	1335	1.18	4261
18	2.32	485	1.26	1718
20	4.19	131	1.78	590
22	4.24	41	1.61	205
24	5.72	14	2.22	62
26	6.31	1	2.45	13
28	-		2.39	2

Table 5.2: *The averaged topology dependent event weights and event numbers for the combined π^+p and K^+p interactions for the two event samples* **pObad** *and* **pMbad**.

multiplicity n gets a trigger weight $W^n_{T,i}$, the topology weight C_n is

$$C_n = \frac{\sigma_n}{\sigma} \frac{\sum_n W_n}{W_n}$$

with

$$W_n = \sum_{i=1}^{N_n} W^n_{T,i} \quad \text{and} \quad \sigma = \sum_n \sigma_n \quad .$$

Then, at the stage of determining the factorial moments, an event i of multiplicity n gets the weight

$$W^n_i = C_n W^n_{T,i} \quad .$$

In table 5.2 the final event weights averaged per multiplicity are listed for both samples. The K^+p and π^+p interactions are taken together since for the factorial moment analysis no beam dependence is observed.

For the study of single-particle inclusive distributions also a charge and topology dependent weight is applied to correct for track losses. This extra weight cannot be used for the factorial moments.

5.2 pObad versus pMbad

It is interesting to see how the factorial moments depend on the quality of the sample. The first questions that arise are how much they suffer from track losses and how important the event weights are. The spike event, present in both samples, is another topic, that deserves special attention.

In this chapter, the bin-averaged vertically normalized factorial moments will be used. The definition with the event weights explicitly included was given already in the previous chapter, but here the symbolic notation is recalled

$$\langle F_q\rangle_V^{(M)} = \left[\frac{\langle n_m^{[q]}\rangle}{\langle n_m\rangle^q}\right]_M$$

The $\langle F_q\rangle_V^{(M)}$ are given in figure 5.2 for both event samples, weighted as well as unweighted.

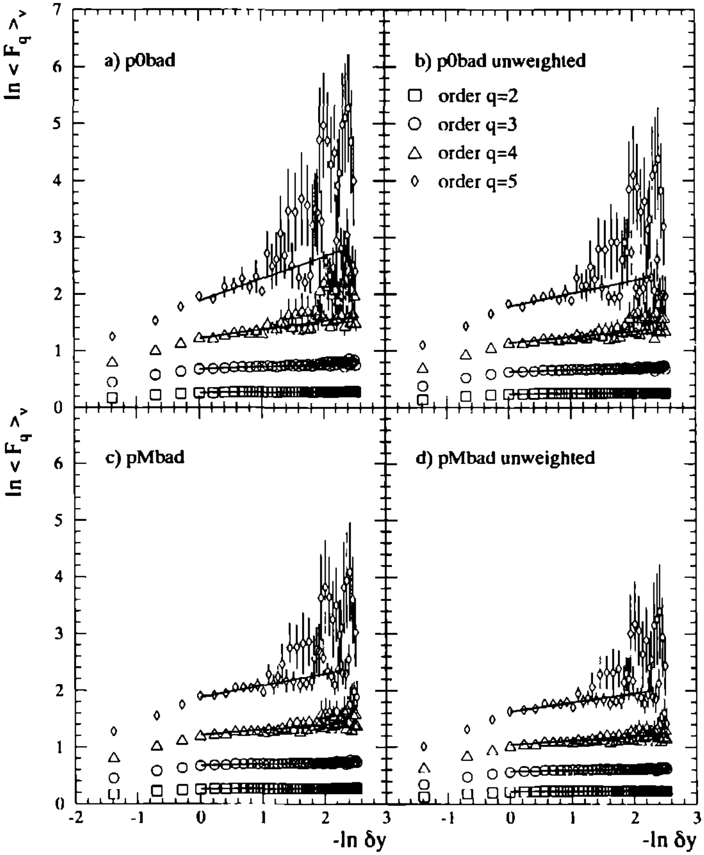

Figure 5.2: *Vertically normalized factorial moments for the* **p0bad** *and* **pMbad** *sample with weights (a and c). Figures b) and d) show the same moments for the case that the event weights are set equal one.*

It can be seen that the rise of the moments is stronger for the weighted events than for the unweighted ones, and that the **p0bad** sample shows a stronger rise than the **pMbad** sample. To understand where the difference comes from, one has to realize that in the NA22 experiment there are 7 events with local rapidity density $\delta n/\delta y \geq 100$. The most prominent spike event (see 7.8) has a charge multiplicity $n = 26$, and a local rapidity density $\delta n/\delta y = 10/0.1$, i.e. 10 particles in a rapidity bin of size 0.1 units. It needs to be stressed that these events have been checked individually on the scanning table. All of the tracks have been identified individually as existent and the most prominent spike event has been measured five times with the same result. All of the tracks are of good quality and in the **p0bad** sample it is the only 26-prong that survives the quality cuts. This means that it gets a rather large weight, almost a factor 3 larger than the 26-prongs of the **pMbad** sample (see tab. 5.2). Of course, this has an influence on the factorial moments. How large this influence is can be seen from fig. 5.3 where the moments are plotted for the **p0bad** and **pMbad** sample without the most prominent spike event. Clearly, the rise of the moments decreases and that relatively more for the **p0bad** sample than for the **pMbad** sample. In the previous chapter it has been shown that the best indication for the rise of the factorial moments is obtained from the straight line fit without covariance matrix. In fig. 5.4 and tab. 5.3 an overview of the fitted slopes is given for second, third and fourth order moments. All slopes are fitted in the range $1 \geq \delta y \geq 0.1$, as indicated by the straight lines in figs. 5.2 and 5.3. Note that in the fig. 5.4 the slopes are given in the form of the 'anomalous' dimension $d_q = f_q/(q-1)$.

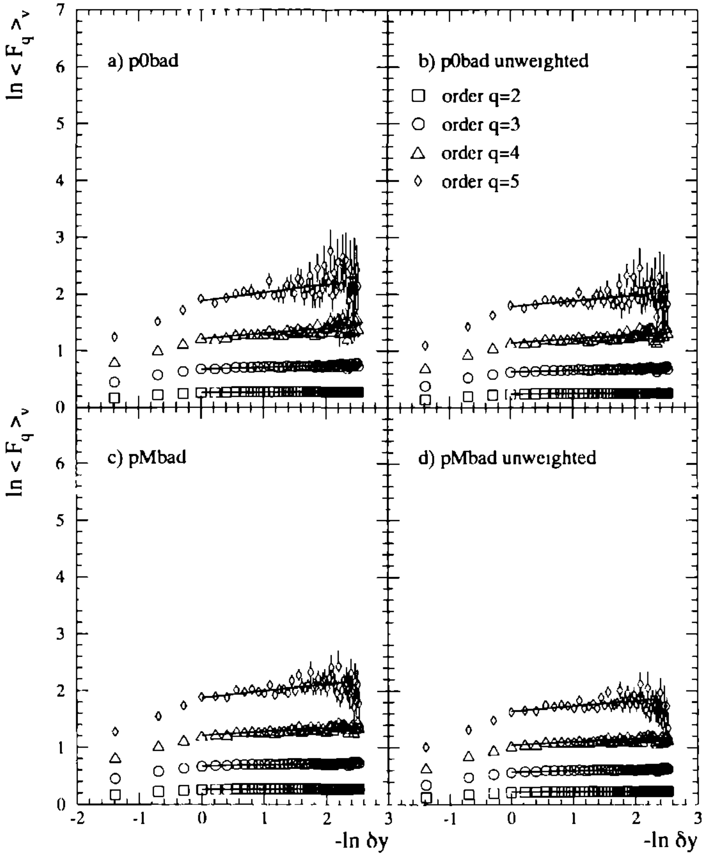

Figure 5.3: *The same as figure 5.2 without the most prominent spike.*

Except for the most prominent spike, there are more events with a local density larger than 100, but with less than 10 particles involved. When these are excluded the slope goes

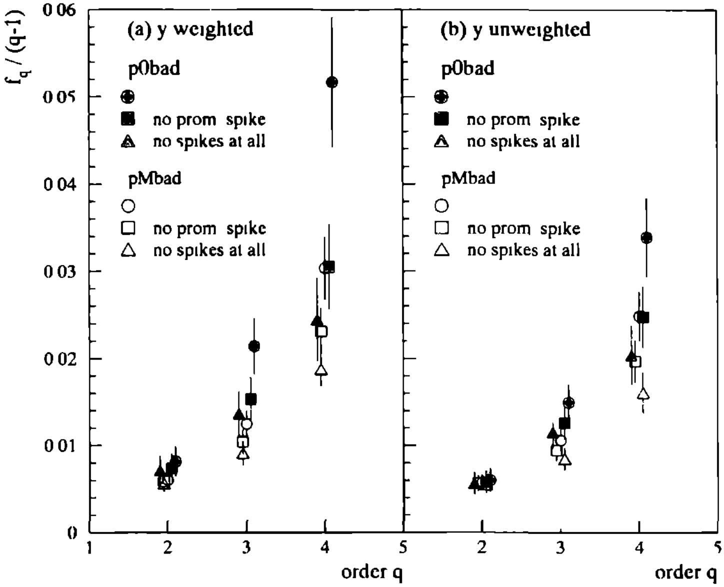

Figure 5.4 *A comparison of the anomalous dimensions d_q for both samples, weighted and unweighted, with and without (all) spike event(s)*

		f_2	f_3	f_4
	weighted			
pObad	all	0.008 ± 0.002	0.043 ± 0.006	0.16 ± 0.02
	no prom spike	0.007 ± 0.002	0.031 ± 0.005	0.09 ± 0.02
	no spikes at all	0.007 ± 0.002	0.027 ± 0.005	0.07 ± 0.02
pMbad	all	0.006 ± 0.001	0.025 ± 0.003	0.09 ± 0.01
	no prom spike	0.006 ± 0.001	0.021 ± 0.003	0.069 ± 0.008
	no spikes at all	0.006 ± 0.001	0.018 ± 0.003	0.056 ± 0.008
	unweighted			
pObad	all	0.006 ± 0.001	0.030 ± 0.004	0.10 ± 0.01
	no prom spike	0.006 ± 0.001	0.025 ± 0.004	0.07 ± 0.01
	no spikes at all	0.006 ± 0.001	0.023 ± 0.004	0.06 ± 0.01
pMbad	all	0.006 ± 0.001	0.021 ± 0.003	0.074 ± 0.009
	no prom spike	0.006 ± 0.001	0.019 ± 0.003	0.059 ± 0.007
	no spikes at all	0.005 ± 0.001	0.017 ± 0.003	0.048 ± 0.007

Table 5.3 *A comparison of the slopes for the samples* **pObad** *and* **pMbad** *with and without weights and spike(s)*

down even more, for **pMbad** as well as for **p0bad** In fig 5 4 these points are represented by the open and filled triangles ('no spikes at all') respectively

From this comparison it would be tempting to conclude that the weighted **p0bad** sample with the spike strongly overestimates the factorial moments However, this is too premature since the spike is a high-quality event and the method is designed just to suppress the non-spiky background under these events The procedure of weighting events is also correct, since the true cross-section has to be recovered On the other hand the **pMbad** sample does suffer from track losses, which for large multiplicity events may go up to 3 tracks This loss can reduce spikes Comparing the unweighted samples in fig 5 4 it can be seen that the **p0bad** slopes are systematically above those of **pMbad** From this it can be concluded that track loss has the biasing effect expected

In any case significantly non-zero anomalous dimensions d_q remain, even for the worst case of unweighted 'non-spiky' events and d_q increases with increasing q

5.3 Biases due to detector limitations

For a factorial moments analysis it is particularly important to have a good knowledge of the detector limitations From the last remarks of the previous section it follows that track loss due to bad reconstruction has a reducing effect on the factorial moments Another important bias can come from a limited two-track resolution However, the hybrid NA22 spectrometer set-up is not expected to suffer from this because of

- its real 4π acceptance without holes
- the fact that tracks are resolved visually in RCBC and matched to spectrometer tracks with very strong criteria

In addition, it is required that the charge balance is correct and that the number of measured tracks is the same as the number of tracks found at the scanning stage

As an illustration, in fig 5 5 the rapidity gap distribution (number of track pairs with a certain difference $|y_i - y_{i+1}|$ in rapidity) is plotted From the left plot, measuring a smallest gap of 0 01 units in rapidity, it can be seen that the gap distribution decreases exponentially with increasing gap size The right plot measures gaps down to 0 001 units In this plot a limited two-track resolution would show up as a serious dip at the smallest values of the gap-size These distributions are integrated over the azimuthal angle φ However, also limiting the analysis to tracks within azimuthal intervals of $\delta\varphi = 2\pi/10$ (the lower distributions in fig 5 5) does not give an indication that the experiment suffers from a limited two-track resolution Therefore, the correction procedure as suggested by E De Wolf (already mentioned in chapter 1) does not need to be applied

A bias that works in the opposite direction could come from double counting of tracks due to track match failure In fig 5 5 this would show up as a sharp increase at the smallest gap sizes In the NA22 experiment it is excluded from the track following and hybridization procedure and the track selection

5.4 Dalitz decay and photon conversion

The advantage of using a bubble chamber as a vertex detector is that part of the neutral particle decays and γ-conversions can be seen Tracks not originating from the primary

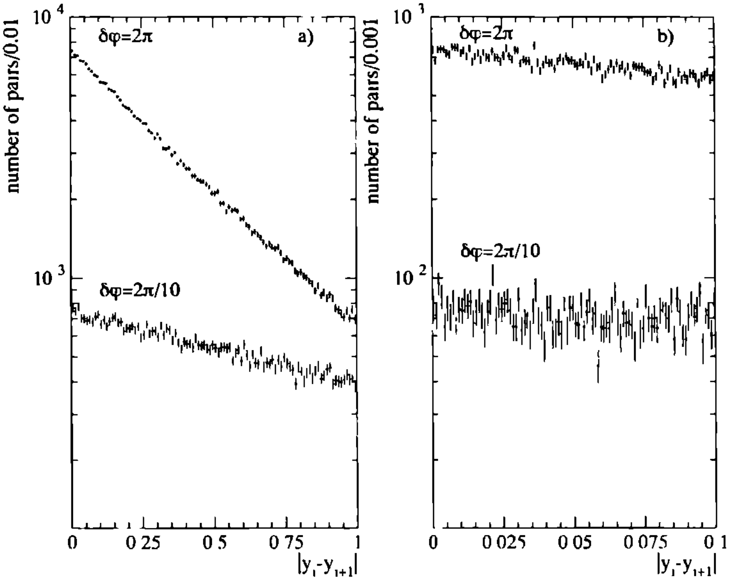

Figure 5.5: *The rapidity gap distribution. The number of track pairs (vertical) are plotted as a function of the gap size. In fig. a) the minimum gap size is* 0.01 *units in rapidity and in b)* 0.001.

vertex are not used in the analysis. It has already been mentioned that when an electron (mainly due to Dalitz decay) is observed, the whole event is rejected. Nevertheless, there is still a possibility that neutral decays or γ-conversions, very close to the primary vertex are not recognized as such. In that case, extra tracks not belonging to the primary vertex are added.

When these tracks are the decay products of a particle such as K^0_S or Λ, there is no reason for the factorial moments in small intervals to increase, since the correlation length is of order 1 in rapidity units. On the contrary, they may be the cause of a decrease of the intermittency index. This has been verified by Monte Carlo simulation.

However, when the tracks are the result of a Dalitz decay or a photon conversion, they can be expected to be very close in phase space. In that case they will give an important contribution to the factorial moments in small intervals, especially for low orders q.

In this section the influence of these biases is studied by means of Monte Carlo (MC) simulations.

When comparing a dynamical MC model like FRITIOF with the data, the usual practice is to generate, for example, 10 times as many MC events as data. This, in order to reduce statistical errors on the model prediction. This method works well for single-particle distributions and probability distributions in large rapidity intervals. However, when looking at factorial moments in small rapidity intervals, the data suffer from the already mentioned empty-bin effect due to the limited particle number in each event, as well as from the limited number of events. This is an effect inherent to factorial moments and cannot be corrected for properly. Thus, in order to have an 'honest' comparison, the same number of MC events as there are real data should be generated

Another aspect which should be mentioned are the weights Though the real data are corrected for losses, the MC does not suffer from track or event losses, especially since no detector tracking has been used and, therefore, no corrections have to be applied

The FRITIOF MC is not able to describe the (tail of the) multiplicity distribution in full rapidity space It is too narrow This results in different moments in large intervals It can be expected that the multiplicity distribution in small intervals of rapidity will not describe the data better This means that the FRITIOF factorial moments are doomed to fall below the data Despite this failure, the MC simulations can be used to study how, for example, a Dalitz decay ($\pi^0 \to \gamma e^+e^-$) responsible for 1 17% of π^0 decay (the rest is $\pi^0 \to \gamma\gamma$) can increase the moments The FRITIOF model uses JETSET 6 3 for the string fragmentation (hadronization) with an optional switch for Dalitz decay Though it has been remarked [OPRC91] that this decay is not correctly implemented in this JETSET version it is used here on an as is basis

Photon conversion ($\gamma \to e^+e^-$) is not a built-in property and has to be estimated from the NA22 data on V^0's [2] [NA22K0] The number of undetected conversions is obtained from the distribution of the distance of the vertex of the measured γ's from the primary vertex (fig 5 6 a) Due to the very small conversion probability, it is reasonable to assume the same number of conversions at each distance from the vertex The hatched area then marks the number of unseen conversions close to the vertex, taking the plateau value between 10 and 20 cm as a reference The fraction of undetected conversions thus estimated is about 10% The conversion probability of a photon along a path of 20 cm in the hydrogen of RCBC is 1 5% [PDGR90] Thus, 0 15% of all produced γ's (mostly from π^0 and η decay) are expected to contribute with 2 particles to the charged multiplicity In the simulation this percentage is increased to 0 25

The 'invariant mass' of the produced e^+e^- pair (fig 5 6 b) as well as the ratio of the maximum and minimum energy of the electrons (fig 5 6 c) is sampled using the distributions from the seen γ's, as an attempt to approximate the behavior of the electrons and positrons Mind that those distributions include the measuring errors on e^+ and e^-

In the FRITIOF simulation, all stable charged particles are given a mass according to the experimental procedure, i e they are all given the pion mass except fast positive particles with momentum larger than 150 GeV/c that are identified as beam particles (only π^+p interactions are generated) and protons with momentum smaller than 1 2 GeV/c

Apart from the parameters mentioned in 1 7, the default FRITIOF and JETSET parameters are used The same setting has, among others, been used in [NA22BA]

The FRITIOF MC is rather 'unstable' in the following sense The slopes depend strongly on the number of events generated This can be seen in fig 5 7 where for the upper 2 plots 60,000 events are generated and for the lower 2 plots 120,000 events The most remarkable fact is that the larger the event number the lower the slopes f_4 and f_5

For the FM's in rapidity, table 5 4 lists the slopes corresponding to the factorial moments from figure 5 7 for the case of 'plain' FRITIOF events and for the case that Dalitz decay and γ-conversion are included The slopes of the weighted **p0bad** and **pMbad** samples are included for comparison None of the FRITIOF samples describes the data It has been recently shown [NA22ET] that the model overestimates η production in the NA22 data by

---

[2] I thank Dr T Haupt for providing the histograms

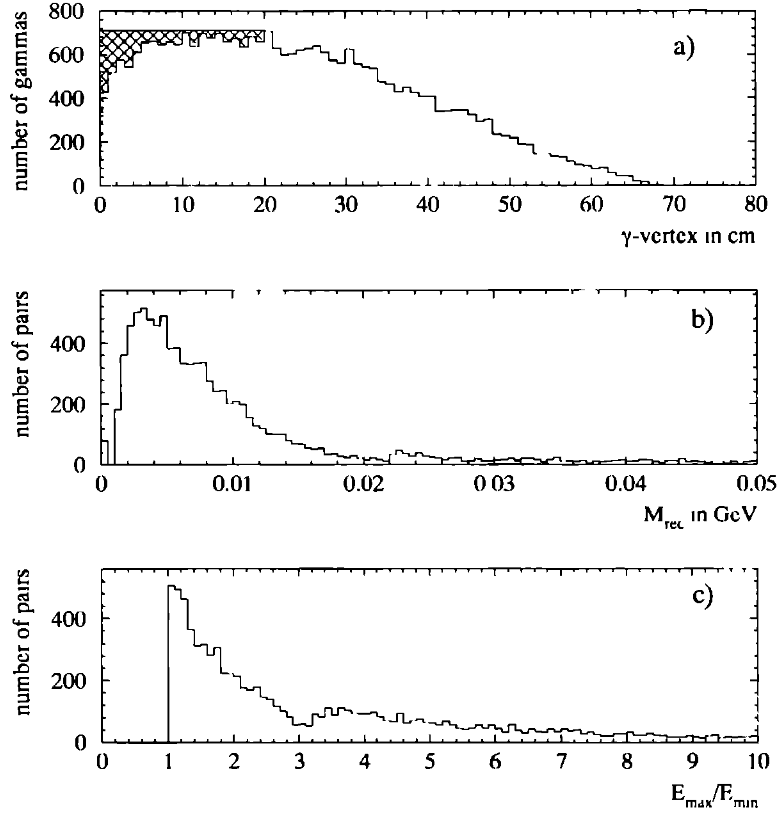

Figure 5.6: *a: The distribution of the distance of the photon vertex from the primary vertex. The dip near the origin is from undetected nearby photons and is used to estimate the fraction of unseen photons (hatched area). The decrease at large distance is due to primary vertices that are near the end of RCBC*

b: The reconstructed invariant mass of the e^+e^- *pair.*

c: The ratio of the maximum and minimum energy of the pair.

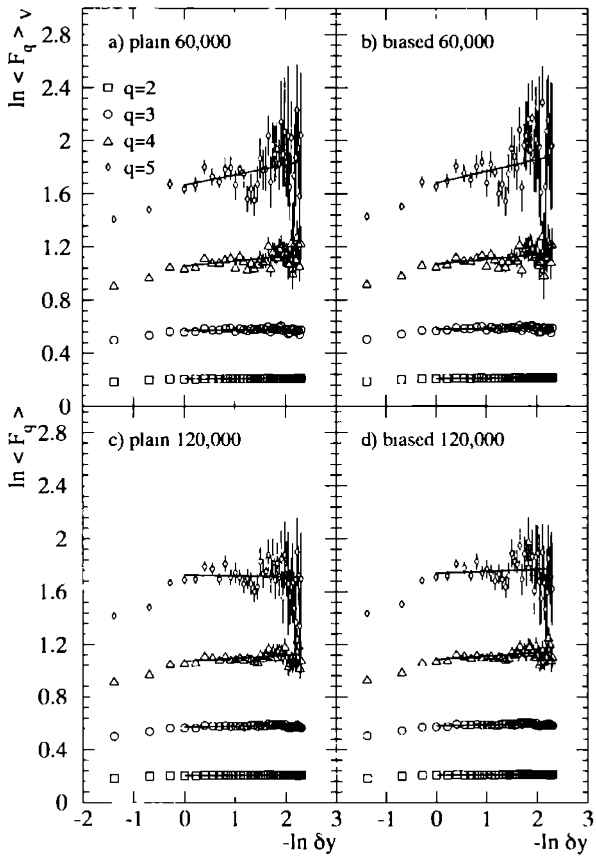

Figure 5 7: *Factorial moments from plain (a,c) and biased (b,d) FRITIOF2.0 events For a) and b)* 60,000 *events were generated, for c) and d)* 120,000 *events. The fitted slopes are indicated. Note the different vertical scale, compared to the data representation*

roughly a factor 2. Since 28% of the η decays yield charged pions, it can be concluded that the signal observed in the data is not due to resonance decay, confirming the remark on K^0 and Λ decays above.

From the figure as well as from the table, it can be concluded that the intermittency effect in the data is not generated by Dalitz decay and photon conversion· Starting from a model not describing intermittency at all it is not possible to simulate intermittency by just adding Dalitz decay or photon conversion

5.5 Summary

In this chapter two event samples are compared. The random track loss in the **pMbad** sample leads to a reduced intermittency signal. The use of event weights to correct for multiplicity dependent event losses increases the intermittency signal, but a significant signal

		f_2	f_3	f_4	f_5
plain	60,000	0.002 ± 0.002	0.005 ± 0.004	0.04 ± 0.01	0.08 ± 0.03
biased	60,000	0.002 ± 0.002	0.005 ± 0.004	0.04 ± 0.01	0.09 ± 0.03
plain	120,000	0.002 ± 0.001	0.005 ± 0.003	0.02 ± 0.01	-0.007 ± 0.02
biased	120,000	0.002 ± 0.001	0.007 ± 0.003	0.027 ± 0.008	0.02 ± 0.02
pObad		0.008 ± 0.002	0.043 ± 0.006	0.16 ± 0.02	0.39 ± 0.06
pMbad		0.006 ± 0.001	0.025 ± 0.003	0.09 ± 0.01	0.21 ± 0.03

Table 5.4 *Comparison of FRITIOF2.0 slopes, in the case of plain and biased events with strangeness suppression factor* $\lambda = 0.3$. *The data are from the weighted* **pObad** *and* **pMbad** *samples.*

remains even when no weights are applied. Exclusion of all events with local density $\delta n/\delta y > 100$ reduces the signal, but a significant rise of the slopes with increasing order remains even then. It should be stressed that the method of factorial moments is in fact designed to study the influence of the high-density events by reducing the non-spiky background.

The NA22 experiment does not suffer from either limited two-track resolution or double counting of tracks. Both facts can be verified from the rapidity gap distribution.

The influence of Dalitz decay and γ-conversion near the vertex is estimated by Monte Carlo simulation, and is found to be negligible and certainly not the cause of the intermittency signal observed in the data.

Bibliography

[HMSN84] P. van Hal, F. Meijers, L. Scholten, Note on the fixup/quality program, Nijmegen note, November 1984.

[NA22BA] I. Ajinenko et al. (NA22 collab.), Z. Phys. C44 (1989) 573.

[NA22DI] M. Adamus et al. (NA22 collab.), Z. Phys. C39 (1988) 301.

[NA22ET] M. Atayan et al. (NA22 collab.), π^0 and η Meson Production in π^+p and K^+p Collisions at 250 GeV/c, Z. Phys. C (to be published).

[NA22K0] I. Ajinenko et al. (NA22 collab.), Z. Phys. C46 (1990) 525.

[NA22QU] Minutes of the 15th NA22 collab. meeting, Serpukhov, May 1989, addendum 15.

[NA22TC] M Adamus et al. (NA22 collab.), Z. Phys. C32 (1986) 475.

[OPRC91] O. Podobrin, Ringberg Workshop on Multiparticle Production, Germany, June 25-28 1991, private communication.

[PDGR90] 'Review of particle properties', Particle Data Group, Phys. Lett. B239 (1990).

[PVHT87] P. van Hal, Particle production in hadron-proton interactions at 250 GeV/c incident beam momentum, Ph.D. thesis 1987.

[SPIK87] M. Adamus et. al. (NA22 collab.), Phys. Lett. B185 (1987) 200.

6

One-dimensional factorial moments

In this chapter several topics are covered concerning one-dimensional factorial moments. The first section describes a number of general aspects of the factorial moments in the one-dimensional rapidity variable. In the second section, the influence of Bose-Einstein correlations will be checked by limiting the analysis to like-sign particles. The last section deals with the aspect of transverse momentum cuts and their influence on the intermittency index.

6.1 General aspects of one-dimensional moments

In the previous chapter, the difference between the two samples **p0bad** and **pMbad** has been discussed. Now, it is interesting to see the influence of the different ways of averaging the factorial moments. In table 6.1 a comparison of the slopes is given for **p0bad** and **pMbad**, using the linear fit (4.13) as described in chapter 4. For the vertically normalized factorial moments (4.2) the histogram errors (4.6) are used. The same holds for the horizontally normalized factorial moments (equations (4.7) and (4.10)). The slopes of the horizontal moments are larger than those of the vertical ones. This is due to the introduction of extra 'correlations' from a non-flat rapidity spectrum. To correct for this effect, Fiałkowski et al. [FWAP89] suggest the so-called R-factor, yielding the reduced factorial moments

$$\langle F_q\rangle_R^{(M)} = \frac{[\langle n_m^{[q]}\rangle]_M}{[\langle n_m\rangle^q]_M} = \frac{[\langle n_m^{[q]}\rangle]_M}{[\langle n_m\rangle]_M^q}\,\frac{[\langle n_m\rangle]_M^q}{[\langle n_m\rangle^q]_M} = \frac{\langle F_q\rangle_H^{(M)}}{R_q^{(M)}}\,. \tag{6.1}$$

	p0bad		**pMbad**	
	vertical	horizontal	vertical	horizontal
f_2	0.008 ± 0.002	0.013 ± 0.002	0.006 ± 0.001	0.011 ± 0.001
f_3	0.043 ± 0.006	0.065 ± 0.007	0.025 ± 0.003	0.044 ± 0.004
f_4	0.16 ± 0.02	0.21 ± 0.03	0.09 ± 0.01	0.13 ± 0.01
f_5	0.39 ± 0.06	0.50 ± 0.06	0.21 ± 0.03	0.28 ± 0.04

Table 6.1: *A comparison of horizontal and vertical normalization. The linear fit with histogram errors is used. The fit region is* $1 \geq \delta y \geq 0.1$, *corresponding to* $M = 4, \ldots, 40$.

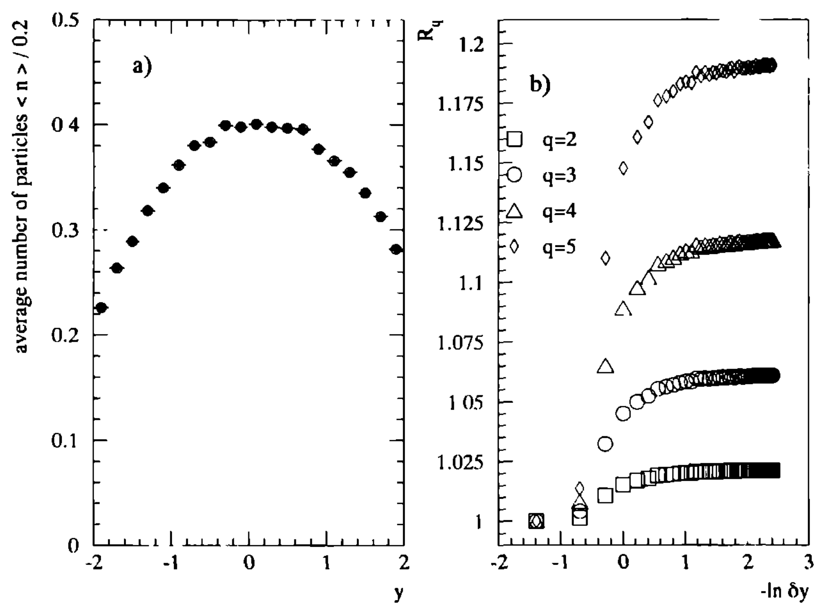

Figure 6.1: *a) The average number of particles corresponding to 20 divisions of the initial rapidity interval. b) The correction factor R_q for orders 2 to 5. In both cases the weighted* **p0bad** *sample is used.*

The authors find a sizeable effect only when starting with a very large initial rapidity interval. Investigations of NA22 data confirm their result. In fig. 6.1 the inclusive rapidity distribution in the interval $-2 < y < 2$ is shown together with the R-factor. The R-factor does not significantly change the value of the slope when a central region of 4 units in rapidity is taken: The slopes of the reduced moments are lower than those from the horizontal moments, but always within errors. The method only approximately corrects for the variation of the average over the rapidity interval. To avoid the trivial correlations, in the following only the vertically normalized factorial moments will be used.

In his thesis [EGGETH], Eggers shows that correlations from resonance decays may be expected to reach down to bin-sizes of 0.5 units in rapidity. Indeed, the slopes f_2 and f_3 decrease when the fit interval is changed from $M = 4, \ldots, 40$ to $M = 8, \ldots, 40$. The increase of f_4 and f_5 is due to the strong fluctuations in the data. The comparison is given in table 6.2.

6.1.1 Smaller initial interval

To see the influence of the initial interval size Δy, the slopes of the factorial moments for $-1 < y < 1$ are listed in tab. 6.3 and can be compared to those for $-2 < y < 2$ listed in tab. 6.2. in table 6.3. The fit region is chosen between $1 \geq \delta y \geq 0.1$ which for the decreased initial interval coincides with $M = 2, \ldots, 20$. The smaller initial interval of 2 rapidity units gives larger slopes than the original interval of 4 units in rapidity. This can be at least partially explained by the fact that the spike event remaining in the reduced interval is even

	pObad		pMbad	
	4-40	8-40	4-40	8-40
f_2	0.008 ± 0.002	0.006 ± 0.003	0.006 ± 0.001	0.003 ± 0.002
f_3	0.043 ± 0.006	0.04 ± 0.01	0.025 ± 0.003	0.019 ± 0.005
f_4	0.16 ± 0.02	0.18 ± 0.04	0.09 ± 0.01	0.10 ± 0.02
f_5	0.39 ± 0.06	0.6 ± 0.1	0.21 ± 0.03	0.26 ± 0.06

Table 6.2: *A comparison of fits for the vertically averaged factorial moments for the* **pObad** *sample, for the intervals* $M = 4, \ldots, 40$ *and* $M = 8, \ldots, 40$.

	pObad	pMbad
f_2	0.020 ± 0.002	0.017 ± 0.001
f_3	0.070 ± 0.004	0.056 ± 0.003
f_4	0.198 ± 0.009	0.147 ± 0.006
f_5	0.43 ± 0.02	0.32 ± 0.02

Table 6.3: *The slopes of the vertically normalized factorial moments for* **pObad** *and* **pMbad** *for* $-1 < y < 1$. *The fit region is* $1 \geq \delta y \geq 0.1$.

more stressed there.

Due to the smaller number of bins used in the averaging, the statistics is decreased, which results in larger errors on the factorial moments. Therefore, the larger initial interval is preferred in the following.

6.1.2 The Negative Binomial and factorial moments

As mentioned in chapter 1, several authors have tried to describe the rise observed in the factorial moments using short-range correlations. Though a better way to check those assumptions is to use the factorial cumulant moments instead of the factorial moments, here a first result on this test will be given.

In fig. 6.2 the factorial moments and the fitted slopes are plotted separately for orders q = 2 to 5, using the weighted **pObad** sample. For the second order the dashed curve represents a fit by the short-range form [CSPR89]

$$F_2 = 1 + \gamma_2 \frac{1 - e^{-\delta/2L}}{\delta/2L} . \tag{6.2}$$

The correlation length L and the correlation strength γ_2 are listed in table 6.4. An attempt was made to obtain fit values for the bin-size independent ratios A_q (1.70) predicted by the Linked-Pair Approximation [CSPR89]. The dashed curves in the figure show the result and the parameters are listed in tab. 6.4. For orders 4 and 5 it can be best seen that the LPA does not describe the rising data. This is most probably due to the fact that the ratios A_q are not bin-size independent (see M.Charlet [CHARTH] and forthcoming publication).

For third and higher orders, the dashed-dotted curves represent the negative binomial prediction

$$F_q = \prod_{j=2}^{q-1} (1 + j(F_2 - 1)). \tag{6.3}$$

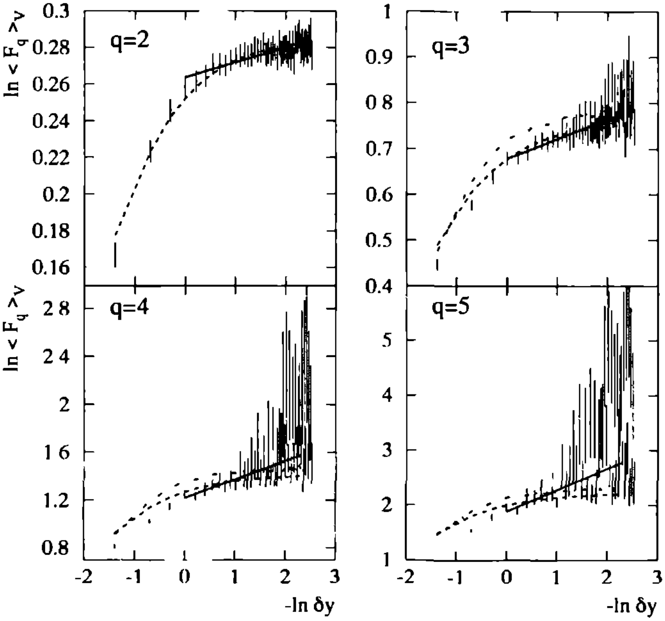

Figure 6.2: *The factorial moments for the* **p0bad** *sample. For all orders q the straight lines represent the usual power-law fit (4.13). The dashed curves represent the short-range fit (6.2) for order 2 and the corresponding linked-pair fit for orders 3 to 5. The dashed-dotted curves for orders* $q = 3, 4$ *and* 5 *are obtained from the NBD assumption using* F_2 *from the data as input.*

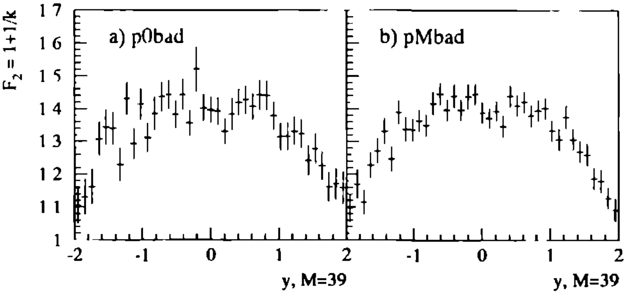

Figure 6.3: *The dependence of the NBD parameter* $1/k$ *on the position in rapidity for* $M = 39$.

	pObad		pMbad	
	$-2 < y < 2$	$-1 < y < 1$	$-2 < y < 2$	$-1 < y < 1$
L	1 7 ± 0 1	1 6 ± 0 2	1 83 ± 0 08	1 7 ± 0 2
γ_2	0 331 ± 0 002	0 412 ± 0 005	0 325 ± 0 001	0 408 ± 0 003
A_3	1 3 ± 0 1	1 9 ± 0 2	1 06 ± 0 05	1 55 ± 0 07
A_4	6 ± 2	6 ± 3	4 8 ± 0 9	5 ± 1
A_5	17 ± 35	5 ± 33	19 ± 17	13 ± 18

Table 6 4 *Short-range correlation length L and strength γ obtained from a fit of the data to (6 2) A_3, A_4 and A_5 are the fitted Linked Pair parameters (1 70)*

with F_2 from the data (not from the fit to (6 2)) as input Clearly, at large δy the NBD prediction overestimates the factorial moments in absolute value, but very quickly saturates, contrary to the data The same effect is seen for the **pMbad** sample The reason for the bad behavior could be the fact that the NBD parameter $1/k$ is not a constant over the whole rapidity region Indeed, from fig 6 3 it can be seen that there is a strong bin dependence for $1/k$ However, using the $1/k$ expansion (6 3) per bin leads to a similar result

Limiting the initial interval to $-1 < y < 1$ gives a NBD prediction closer to the data at larger bin-sizes, but below the data for smaller bin sizes Here too the NBD saturates faster than the data

From explicit comparison of the NB multiplicity distribution with the data, it can be seen that the NBD does not correctly describe the tail of the experimental multiplicity distribution This possibly explains the failure of equation (6 3) to describe the higher-order factorial moments However, the NBD can be conveniently used as a possible parametrization to try to estimate the empty-bin effect, as was done in chapter 3

6.2 Bose-Einstein contribution

When first results became available on intermittency, the obvious question was whether the rise of the moments with decreasing bin-size was not to be explained by the Bose-Einstein interference (BE) between identically charged particles [GYLH89] Besides many other experiments [BOSEEX], Bose-Einstein interference has also been observed in NA22 [NAZP88] If, indeed, intermittency originates from BE, the slopes are expected to rise by roughly a factor 2 when the analysis is restricted to particles of identical charge [1] According to ref [GYLH89], deviations from this rule in e^+e^- and π^+p collisions would give the strongest evidence against the BE origin

To illustrate the effect of limiting the analyses to like-charge tracks, firstly the behavior of the factorial moments as a function of δy is shown for all charged tracks, for positives only and for negatives only in fig 6 4, for the weighted **pObad** sample The fitted power law (4 13) is represented by the straight lines The absolute values of the factorial moments are lower in the case of like-charge tracks However, the slopes are not very different This can be seen from fig 6 5, where a comparison is made for four samples as indicated There is no strong indication that the like-charge slopes would be twice as large as those of the

---

[1] If Bose-Einstein is the source for intermittency, in the all charged case two independent intermittent sources (positive positive and negative-negative) are added leading roughly to a decrease by a factor 1/2

all-charged sample One exception is the slope of the fourth-order moment for the negatives of the weighted **p0bad** sample [2] (0 29±0 06), almost twice that for the all charged case (0 16±0 02), see tab 6 5 This exceptional value, is probably due to the influence of the spike event (6 negatives out of 10 spike particles)

		f_2	f_3	f_4
p0bad	all	0 008 ± 0 002	0 043 ± 0 006	0 16 ± 0 02
	positives	0 010 ± 0 002	0 050 ± 0 009	0 18 ± 0 03
	negatives	0 007 ± 0 003	0 06 ± 0 02	0 29 ± 0 06
pMbad	all	0 006 ± 0 001	0 025 ± 0 003	0 09 ± 0 01
	positives	0 008 ± 0 002	0 034 ± 0 005	0 10 ± 0 02
	negatives	0 009 ± 0 002	0 036 ± 0 008	0 08 ± 0 04

Table 6 5 *A comparison of the slopes for all-charged, positives and negatives for rapidity The weighted* **p0bad** *and* **pMbad** *samples are used*

In the next chapter a study of higher dimensional factorial moments will be presented Therefore, it is interesting to have a look at their behavior in one-dimensional azimuthal angle φ, already here Transverse momentum conservation causes an anti-correlation at large relative φ This results in an initial decrease of factorial moments A rise of the moments begins approximately at $2\pi/8$, therefore used as start value for fitting However, slopes in φ should not be taken too seriously, as can be seen from the large fluctuations in the data in figure 6 6

The dramatic consequence of using positive particles only is illustrated in fig 6 6b where the unweighted **p0bad** sample is shown for φ The factorial moments not only decrease, but for $\delta\varphi < \pi$ the higher-order moments are *below* the lower order ones In the NA22 experiment the incoming particles are positive This implies that, in general, two of the positive particles are anti-correlated in φ

In conclusion, no clear evidence can be seen for a strong influence of the Bose-Einstein interference, in these one-dimensional variables

6.3 p_T cuts

To see from which region in phase space the intermittent behavior originates, it is useful to undertake a more differential study This has been done in the NA22 experiment, where cuts on the transverse momentum of the tracks are applied The sample used in ref [LPPL91] was **p0bad** The factorial moments for this sample are shown in fig 6 7 In figure 6 8 a collection of anomalous dimensions $d_q = f_q/(q-1)$ is given for several samples

It is difficult to derive very strong conclusions from these figures since the behavior of the slopes seems to be largely dependent on the use of weights and on the presence of a specific event However, some points can be noted

From fig 6 8a it follows that there is an increased intermittency effect when the sample

---

[2] The factorial moments of this sample have been published in [NAPL90] with a different normalization Only events contributing with tracks in the initial interval were taken In this thesis all events are included for normalization The difference lies in an overall, bin independent factor $(N_{all}/N_{>0})^{q-1}$ The values of the slopes remain unchanged

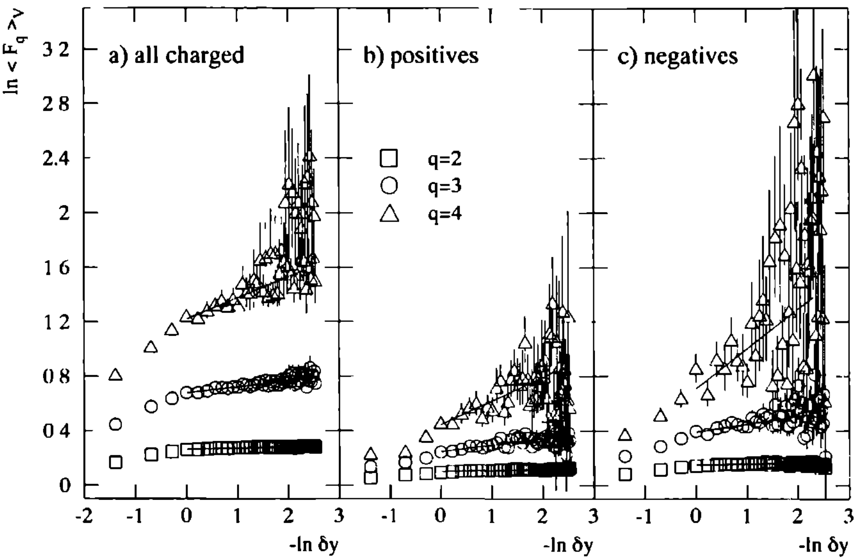

Figure 6.4: *The factorial moments for all charged tracks (a), positive tracks only (b) and negative tracks only (c), as a function of rapidity.*

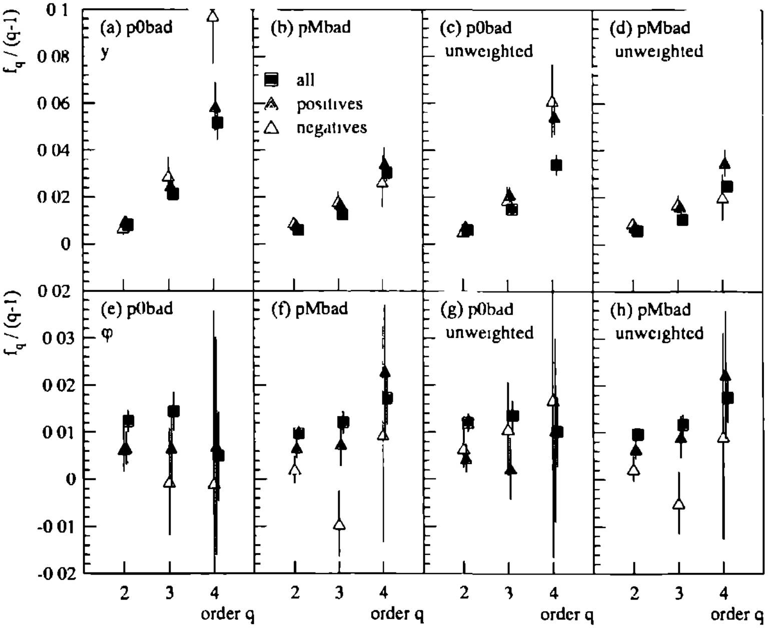

Figure 6.5: *The top four figures show the anomalous dimensions* $d_q = f_q/(q-1)$ *in rapidity for all charged, negative tracks only, and positive tracks only, for four samples as indicated. The lower plots give slopes, not to be taken too seriously, in azimuthal angle* φ.

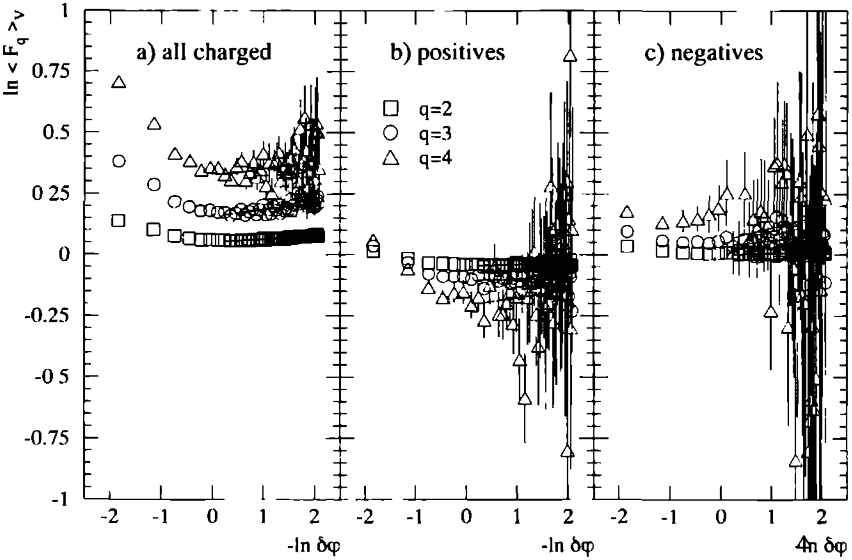

Figure 6 6: *The factorial moments for all charged tracks (a), positive tracks only (b) and negative tracks only (c), as a function of azimuthal angle* φ. *The sample shown is the unweighted* **p0bad** .

is limited to low transverse momentum tracks (filled triangles and circles) and a decreased effect, when the sample is limited to higher p_T tracks (open triangles and circles), compared to the all-track sample (filled squares). For the weighted **pMbad** sample (d) all cut samples are above the all-track sample. For fourth order, the tracks with $p_T > 0.3$ GeV/c even show a stronger effect, than those with $p_T < 0.3$ GeV/c.

For the unweighted samples the differences become much smaller. In fact, within errors, no special behavior can be noticed. If the most prominent spike [SPIK87] is excluded (weighted or unweighted) the third- and fourth-order slopes even become negative for $p_T < 0$ 15 GeV/c, probably due to the empty-bin effect. Exclusion of other high-density events does not change this picture.

The average number of particles in the considered phase-space intervals are listed in tab. 6.6. One notices that, indeed, the number of particles contributing to the $p_T < 0.15$ GeV/c is rather small, and the higher-order factorial moments can easily suffer from the empty-bin effect.

What remains in all samples is a larger second-order slope for the lowest transverse momentum tracks. The question is whether this effect is due to e^+e^- pairs from Dalitz decay or γ-conversion. As mentioned before, FRITIOF can be parametrized to give (almost) any result wanted and a more reliable check has to be searched for.

If, indeed, the γ-conversion or Dalitz decay is responsible for the large second-order slopes for low transverse momentum tracks, restricting the sample to like-charge tracks only, would be expected to spoil the effect. In table 6.7, for the weighted **p0bad** sample the second-order slopes are given for all-charged, positives only and negatives only, in the five regions of transverse momentum. In all cases, like-charge and all-charge, the slope for the low p_T

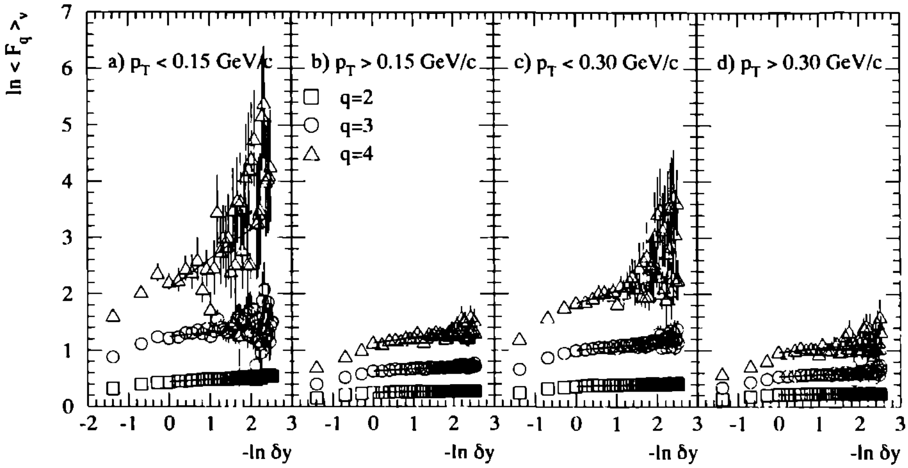

Figure 6.7: *The vertically averaged normalized factorial moments for the weighted* **p0bad** *sample limiting the tracks to the transverse momentum regions as indicated.*

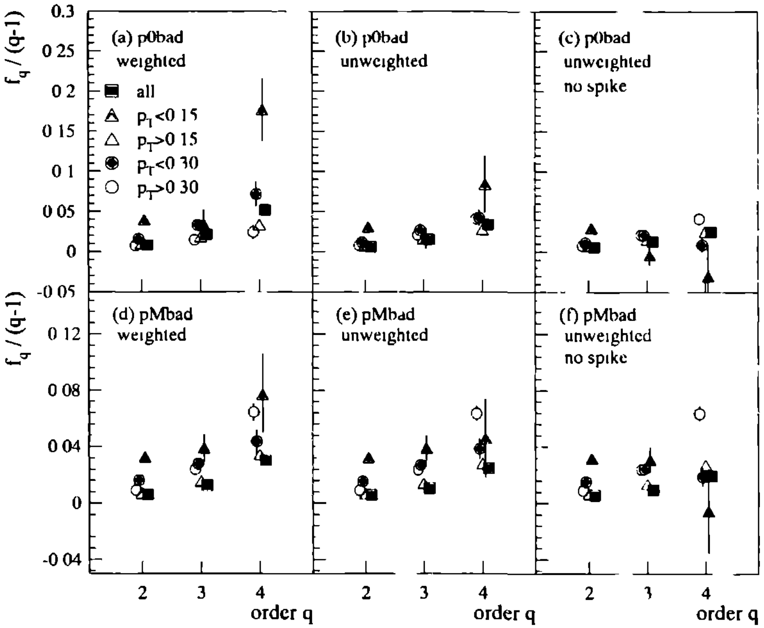

Figure 6.8: *The fitted slopes f_q for tracks with momentum as indicated in (a). In figure (a) the weighted* **p0bad** *sample is used (as in* [LPPL91]*) in (b) the same sample but without weights and in (c) the same as (b) but without the most prominent spike. In figures (d)-(f) the same procedure has been followed for the* **pMbad** *sample. Note the change of scale.*

p_T in GeV/c	all	$p_T < 0.15$	$p_T > 0.15$	$p_T < 0.30$	$p_T > 0.30$
weighted					
p0bad	6.98 ± 0.02	1.174 ± 0.006	5.81 ± 0.02	3.28 ± 0.01	3.70 ± 0.01
pMbad	6.47 ± 0.01	1.087 ± 0.004	5.38 ± 0.01	3.042 ± 0.007	3.430 ± 0.007
unweighted					
p0bad	6.19 ± 0.02	0.998 ± 0.005	5.19 ± 0.02	2.831 ± 0.009	3.359 ± 0.009
pMbad	6.53 ± 0.01	1.081 ± 0.004	5.446 ± 0.009	3.041 ± 0.007	3.486 ± 0.007

Table 6.6: *The average particle numbers in the p_T regions indicated for the rapidity interval* $-2 < y < 2$.

	all p_T	$p_T < 0.15$	$p_T > 0.15$	$p_T < 0.30$	$p_T > 0.30$
all	0.008 ± 0.002	0.039 ± 0.007	0.010 ± 0.002	0.016 ± 0.003	0.007 ± 0.002
pos	0.010 ± 0.002	0.03 ± 0.01	0.013 ± 0.003	0.015 ± 0.005	0.006 ± 0.004
neg	0.007 ± 0.003	0.05 ± 0.02	0.005 ± 0.004	0.026 ± 0.006	0.003 ± 0.005

Table 6.7: *Second-order slopes f_2, for the weighted* **p0bad** *sample with restrictions on transverse momentum (p_T in GeV/c) and charge. Fits are obtained in the region* $1 \leq \delta y \leq 0.1$ *for the vertical factorial moments, as usual.*

region is larger than the all p_T case. This proves that the low-p_T effect is real and not due to γ-conversions or Dalitz decays.

6.4 Conclusion

The most important conclusion from this chapter is that an effect, intermittency, does indeed exist in the NA22 data. However, the one-dimensional analysis in rapidity depends very much on the presence of the spike event. Limiting the analysis to specific regions in p_T, in fact stresses the spike even more. Therefore, a more sample independent analysis has to be looked for. Due to the nature of the spike event (a more or less isotropic spreading of the tracks in azimuthal angle φ) it can be expected that a multidimensional analysis is less dominated by its presence.

Bibliography

[BOSEEX] For a review of experimental results, see: W. Zajc, Bose-Einstein Correlations: From statistics to dynamics, Hadronic Multiparticle production, ed. P. Carruthers et al. World Scientific Press (1987).

[CHARTH] M. Charlet, Ph.D. thesis Univ. of Nijmegen, in preparation.

[CSPR89] P. Carruthers and I. Sarcevic, Phys. Rev. Lett. 63 (1989) 1562.

[EGGETH] H. Eggers, Intermittency, moments and correlations in distributions of particles created in high energy collisions, Ph.D. thesis Univ. of Arizona 1991.

[FWAP89] K. Fiałkowski, B. Wosiek and J. Wosiek, Acta Phys. Pol. B20 (1989) 639.

[GYLH89] M. Gyulassy, Is intermittency caused by Bose-Einstein interference?, Festschrift Léon Van Hove, eds. A. Giovannini and W. Kittel (World Scientific, Singapore, 1989) 479.

[LPPL91] N. Agababyan et al. (NA22 collab.), Phys. Lett. B261 (1991) 165.

[NAPL90] I. Ajinenko et al. (NA22 collab.), Phys. Lett. B235 (1990) 373.

[NAZP88] M. Adamus et al. (NA22 collab.), Z.Phys. C 37 (1988) 347.

[SPIK87] M. Adamus et al. (NA22 Collab.), Phys. Lett. B185 (1987) 200.

7

Multidimensional factorial moments

The previous chapters were devoted to the one dimensional intermittency analysis However, there are several important reasons to extend the analysis to two and three dimensions

Pencil jets

Is there a reason to assume that intermittency comes from particles strongly collimated in rapidity y and azimuthal angle φ? First experimental results on this have been published in [NAPL90] Updated results will be given in section 7 1

Projection effect

Since multiparticle production is a process in three-dimensional momentum space, one has to expect that part of the information is lost by studying only one or two dimensions This loss of information will reduce the intermittency signal

Bose-Einstein correlations

Though the one-dimensional factorial moments do not support the idea that intermittency is caused by B-E interference, the situation may change in a three dimensional analysis The last section of this chapter is dedicated to this topic

As is the case for the one-dimensional analysis, biases are also expected in higher dimensions Due to the higher dimension of the grid, and the larger number of intervals considered, the empty-bin effect will be larger This cannot be corrected for, but imposes constraints on the size of the grid to be chosen

Furthermore, it will be necessary to study the influence of Dalitz decays and photon conversions, once more Due to the instability of the Monte Carlo (FRITIOF) already mentioned, it will be difficult to draw conclusions from the simulations

The variables y and φ used in the one-dimensional analysis show a reasonably flat inclusive density distribution However, the three-dimensional analysis requires an additional variable the transverse momentum p_T The inclusive single particle distribution in this variable has an exponential shape and thus is far from being flat Both ways of averaging the factorial moments (horizontal and vertical) would suffer from this defect The horizontally normalized factorial moments would suffer from the strong correlation introduced by the non-flat inclusive p_T distribution, the vertically normalized factorial moments from the very small average particle number expected in certain bins The latter would lead to very unstable calculations due to limited computational precision Therefore, new variables connected to the original ones have to be invented to circumvent these problems

The topics listed above will be discussed in the following sections Since only vertical averaging is used, the brackets <> and the subscript V will be omitted in the following

7.1 Pencil jets

The interest in studying the behavior of the (factorial) moments in higher dimensions has first been pointed out by Ochs and Wosiek [OWPL88] From a simple scale-invariant branching model inspired by [POLY71], the authors expected a typical behavior of the factorial moments in the two-dimensional $y - \varphi$ space

In short, the model can be described as follows An initial state of total energy W decays into two masses m_1 and m_2 distributed according to the relation $dn/d{\mu_1}^2 d{\mu_2}^2 = F({\mu_1}^2, {\mu_2}^2)$, with $\mu_i = m_i/W$ being the scaled masses The scale invariant kernel function F is specific to the particular model At the next step, the energy W is replaced by m_i, and each particle again decays into two particles, according to the same distribution The cascade stops when all particles have a mass smaller than two times the hadron mass Each decay is assumed to be isotropic

For a kernel function peaking near small masses, the model indeed gives an approximate power law behavior $F_q(\delta y) \approx (\delta y)^{-f_q}$ The effect is the stronger the larger the energy The levelling-off observed for the lower moments is explained by the authors as due to non-asymptotic effects of short cascades

A strong effect is found with a kernel function singular in μ_i^2 ($F = (\mu_1 \mu_2)^{-2}$) leading to strongly collimated jets In these 'pencil jets' the particles will not only be clustered in rapidity, but also in azimuthal angle φ One therefore expects the rise of the moments to be stronger in a two-dimensional $y - \varphi$ grid than in a one-dimensional binning in, for example, rapidity y Indeed, for second order Ochs and Wosiek find in two dimensions a slope six times larger than in one dimension

To confront the pencil jet hypothesis with the data, a two-dimensional analysis of the NA22 data is presented in the following

The vertically normalized one-dimensional y and φ and two-dimensional $y - \varphi$ factorial moments are shown in fig 7 1 as a function of δy, $\delta\varphi$ and $\delta\omega = \delta y \delta\varphi$, respectively The weighted **pMbad** sample has been used The initial interval $\Delta y \Delta\varphi$ has size 8π At each step, both Δy and $\Delta\phi$ are divided into an equal number of intervals The finest grid contains 22^2 boxes of size $\delta\omega = 0\ 052$ units As in chapter 6, $\Delta y = 4$ and $\Delta\varphi = 2\pi$ is used for the one-dimensional moments

The two-dimensional factorial moments remain rather constant down to $\ln \delta\omega = 0$, corresponding to a grid of 25 boxes This can be explained from the combination of a strong rise of the rapidity moments with a decrease of the φ moments at large intervals

NA22 statistics does not allow to calculate the fifth moment at the relevant $\delta\omega$ range This is a first hint that intermittency is not due to pencil jets in these data, since no events are left with a sufficiently large number of tracks in a small two-dimensional area Also the fourth-order moment should be taken with great care In fact, only second- and third-order fits can be trusted

The slopes for both the one-dimensional y and φ and the two-dimensional $y - \varphi$ factorial moments are given in table 7 1 The corresponding anomalous dimensions are plotted in fig 7 2

A comparison between the samples **pObad** and **pMbad** , weighted as well as unweighted, leads to the following results for the slopes from the two-dimensional analysis (see table 7 1 and fig 7 2)

- There is almost no difference between the slopes for the weighted and unweighted

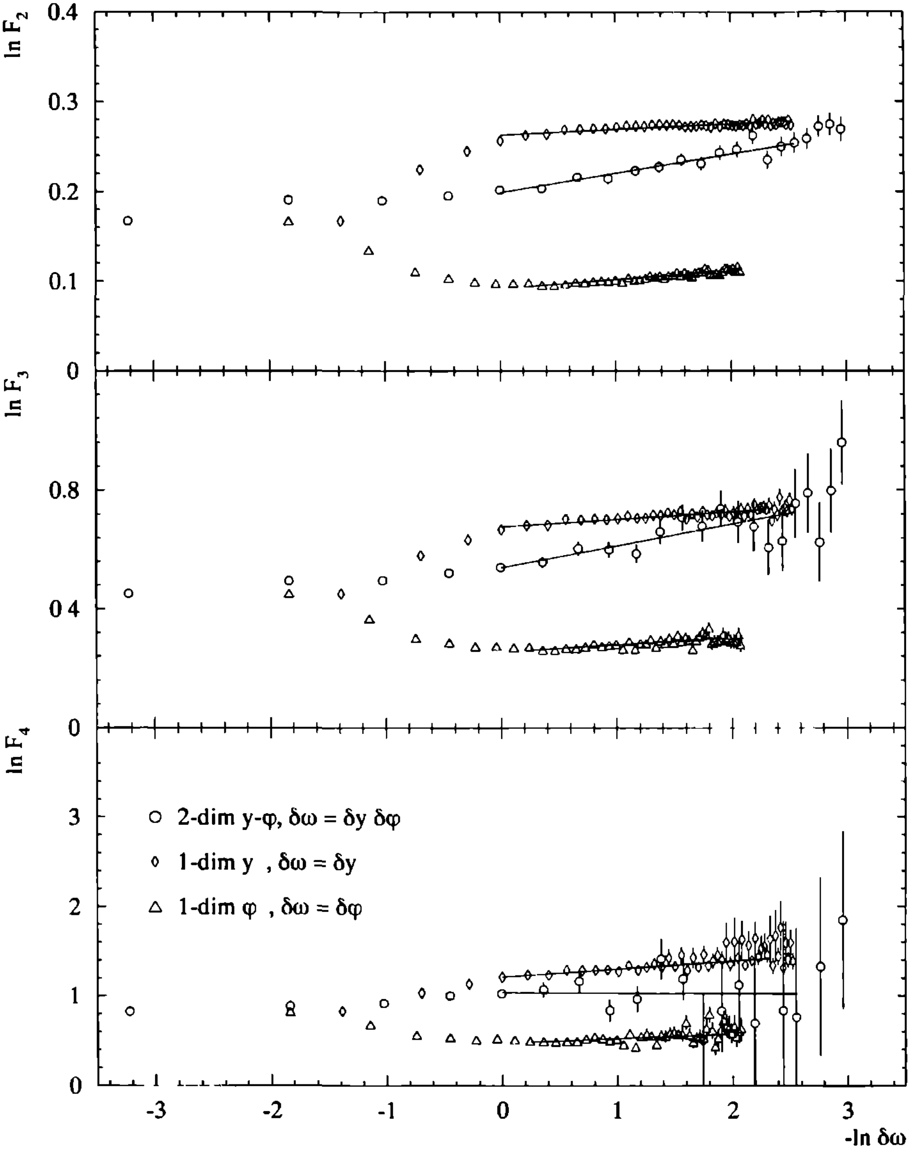

Figure 7.1: *The vertically normalized factorial moments F_q in a two-dimensional $y-\varphi$ grid. For comparison, the one-dimensional moments in y and φ are also shown. The weighted* **pM-bad** *sample is used. The straight lines indicate the fitted slopes for the intervals* $0.1 \leq \delta y \leq 1$, $\pi/20 \leq \delta\varphi \leq \pi/4$, *and* $8\pi/324 \leq \delta y \delta\varphi \leq 8\pi/25$.

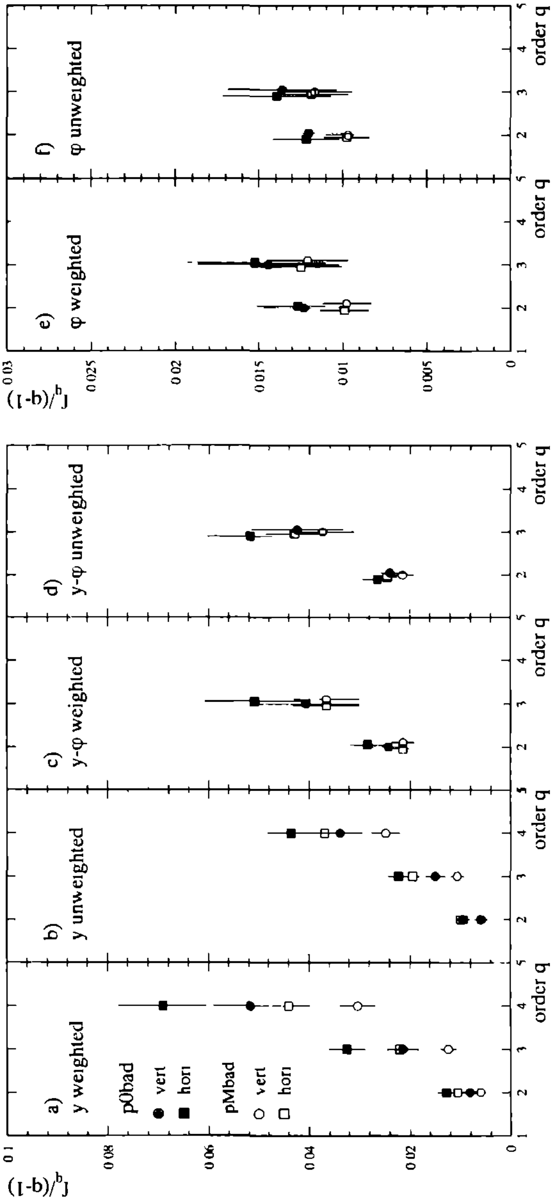

Figure 7.2: *The anomalous dimensions $d_q = f_q/(q-1)$ as a function of the order q for the variables indicated. Both samples* **p0bad** *and* **pMbad** *are presented by the symbols indicated in sub-fig. a).*

		pObad		pMbad	
		weighted	unweighted	weighted	unweighted
f_2	y	0.008 ± 0.002	0.006 ± 0.001	0.006 ± 0.001	0.006 ± 0.001
	φ	0.012 ± 0.002	0.012 ± 0.002	0.010 ± 0.002	0.010 ± 0.002
	$y\varphi$	0.024 ± 0.004	0.024 ± 0.003	0.021 ± 0.002	0.021 ± 0.002
f_3	y	0.043 ± 0.006	0.030 ± 0.004	0.025 ± 0.003	0.021 ± 0.003
	φ	0.029 ± 0.008	0.027 ± 0.007	0.024 ± 0.005	0.023 ± 0.005
	$y\varphi$	0.08 ± 0.02	0.08 ± 0.02	0.07 ± 0.01	0.07 ± 0.01

Table 7.1: *The slopes f_2 and f_3 from the one- and two-dimensional (vertical) analysis for the samples indicated. The fit ranges indicated in fig. 7.2 correspond to the numbers of bins* $M = 4 - 40$ *for* y, $M = 8 - 40$ *for* φ, *and* $M = 5 \cdot 5 - 18 \cdot 18$ *for* $y - \varphi$.

samples. This means that the influence of the most prominent spike event is reduced. A similar observation has been made for the one-dimensional φ slopes.

- Within errors, the **p0bad** and **pMbad** samples yield the same slopes.

Combining these results gives confidence that the higher-dimensional analyses will yield more stable results than the one-dimensional ones. As expected, the horizontally normalized moments are always slightly larger than the vertically normalized ones.

Although the slopes for the two-dimensional case are larger than those for the one-dimensional ones, they do not increase as dramatically as predicted by the pencil-jet model. Moreover, the ten tracks found in the bin $\delta y = 0.1$ in the most significant event [NAPL87] are spread in φ. A similar observation has been made in other events with high local density and from a selection in φ [EDBE89].

The conclusion is that pencil jets cannot be the main source for the intermittent behavior in the NA22 data.

7.2 Projection effect

Independently of each other, Ochs [OCPL90] as well as Bialas and Seixas [BSPL90] have pointed out that intermittency, if present in three dimensions, does not automatically lead to an effect of the same strength in fewer dimensions. Instead of reproducing the detailed calculations given in the papers, the so-called projection effect will be demonstrated on the α-model with same weights and probabilities as used in [OCPL90].

First, the α-model characteristics are recalled in short. At each step in the cascade, a d-dimensional interval with density $X_{\nu-1}$ is divided into λ^d 'boxes'. For each box a random weight W_ν is generated with probability b to find $W_\nu = \beta_+ > 1$ and probability $a = 1 - b$ to find $W_\nu = \beta_- < 1$. The parameters are chosen such that the sample-averaged weight $\{W_\nu\} = a\beta_+ + b\beta_-$ is one. The density in a box then obtains the value $X_\nu = W_\nu X_{\nu-1}$. Starting from an initial density X_0, the density in one of the $M_d = \lambda^{d\nu}$ boxes after ν steps in the cascade becomes

$$X_\nu = W_\nu W_{\nu-1} \cdots W_1 X_0 \ . \tag{7.1}$$

The normalized moments then are

$$C_q^\nu = \frac{\langle X_\nu^q \rangle}{\langle X_\nu \rangle^q} \sim M_d^{f_q} \quad , \tag{7.2}$$

with slope f_q defined as

$$f_q = \frac{\ln \langle W^q \rangle}{\ln \lambda^d} \quad . \tag{7.3}$$

A two-dimensional version of the α-model is shown in fig. 7.3. The parameters are chosen such that the uncorrected two-dimensional TASSO [TASSO] data are described correctly. Ochs shows that the one-dimensional projection also follows the trend in the experimental data, although the latter saturate much faster. The figure has been obtained from 2000 events with a fixed multiplicity of 100. It can be clearly seen that the two-dimensional data follow the theoretical curve (the straight line) and that the one-dimensional projection immediately starts to bend and almost saturates.

Fig. 7.4 shows a realization of the three-dimensional α-model . The number of events generated is 256. To save computer time, in this case the *densities* generated in the grid are used. Therefore, the normal moments have to be used instead of the factorial moments. All data are normalized such that $C_q(\nu = 0) = 1$. The unprojected (three-dimensional) moments follow the theoretical curve exactly, whereas the two-dimensional projection indeed stays well below the straight line and the one-dimensional moments become flat.

7.3 The modified power law

The deviation from a power-law behavior of the factorial moments in lower-dimensional variables might suggest that there is no intermittency at all in projected variables. However, in [OWPL88, OCPL90] it is suggested that the projections may still 'remember' their intermittent origin. Therefore, one has to assume a modified power-law behavior of the factorial moments

$$F_q(\delta y) = b_q(g(\delta y))^{\alpha_q} \quad . \tag{7.4}$$

Taking the logarithms of both sides yields the relations

$$\begin{aligned} \ln F_q(\delta y) &= \ln b_q + \frac{\alpha_q}{\alpha_2}(\ln F_2(\delta y) - \ln b_2) \\ &= \tilde{b}_q + \frac{\alpha_q}{\alpha_2} \ln F_2(\delta y) \; . \end{aligned} \tag{7.5}$$

Thus, the modified power law corresponds to a straight line in a $\ln F_q(\delta y)$ versus $\ln F_2(\delta y)$ plot, a so-called Ochs-plot.

The Ochs-plot for the three-dimensional α-model (with densities instead of multiplicities) is presented in fig. 7.5. The linear relation is fulfilled very well. Apart from the α-model , this relation has been found valid [OCPL90, OCZP91] in the hadronic scale-invariant branching model described above [OWPL88] and in a QCD parton cascade model with hadronization (HERWIG [MWNP84]).

Note from fig. 7.5, that for this α-model the slope ratios α_q/α_2 are not exactly the same for the one-, two- and three-dimensional moments.

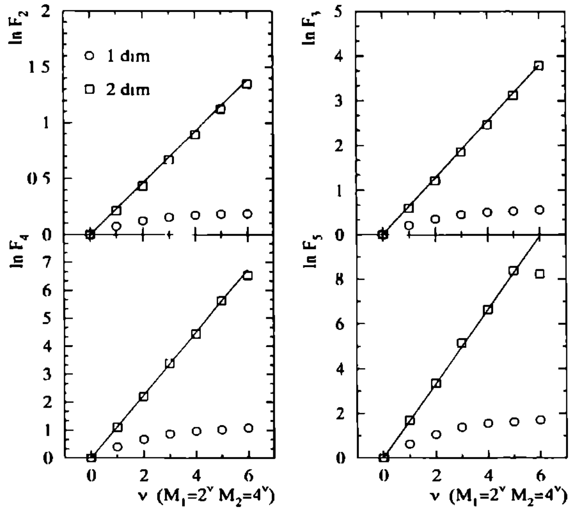

Figure 7.3: *The two-dimensional α-model with $a = 0.68$ and $\beta_- = 0.65$. The line indicates the theoretical expectation.* 2000 *events were generated with a fixed multiplicity of* 100. *The horizontal axis gives the number of divisions of the original interval. For two dimensions this yields 4^ν bins, while for one dimension the binning is defined by 2^ν.*

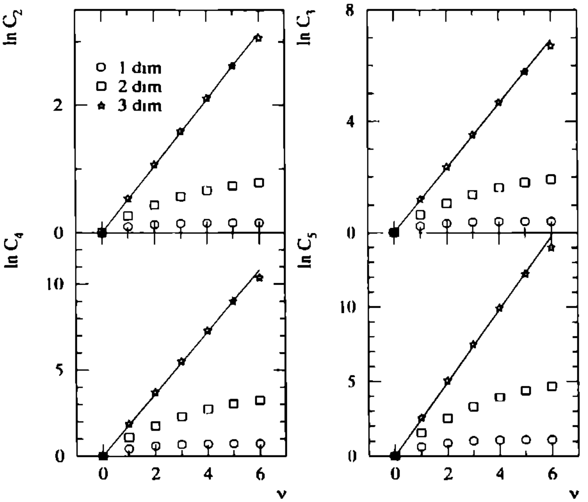

Figure 7.4: *The three-dimensional α-model with $a = 0.55$ and $\beta_- = 0.25$, as chosen in* [OCPL90]. *Here, the densities were used instead of real event realizations. Therefore, the normal moments are used and normalized to $C_q(\nu = 0) = 1$. The three-dimensional moments again follow the theoretical predictions perfectly, while the two-dimensional ones deviate from a power-law behavior. The one-dimensional moments saturate and become a flat line in the* ln − ln *plot.*

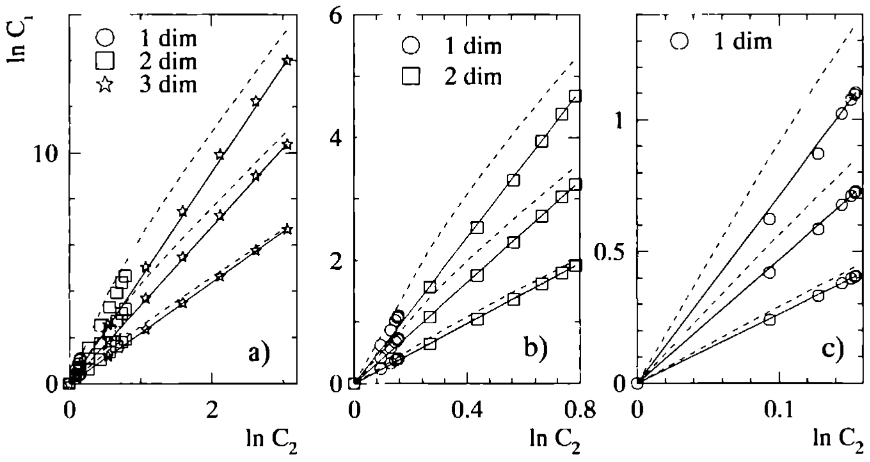

Figure 7.5: *The Ochs plot for the three-dimensional α-model with $a = 0.55$ and $\beta_- = 0.25$, as in 7.4. Again, only densities are used. Figure a) shows the one-, two- and three-dimensional moments, plot b) only the one- and two-dimensional projections and c) solely the one-dimensional moments (note the change of scale). The projections follow a straight line. The dashed lines indicate the NBD prediction using F_2 of the highest dimension indicated as input.*

If the underlying multiplicity distribution would be Negative Binomial (NBD) for all bin-sizes, the factorial moments (expressed in $1/k = F_2 - 1$)

$$F_q = (1 + 1/k) \cdots (1 + (q-1)/k) \tag{7.6}$$

would not yield a straight line in the Ochs plot. This is shown by the dashed lines in the figures, where from left to right F_2 from 3-D, 2-D, and 1-D is used as input.

Assuming that $1/k \ll 1$ and making some crude approximations, the Log-Normal result (chapter 1)

$$\frac{\alpha_q}{\alpha_2} = q(q-1)/2 \tag{7.7}$$

is retrieved. In a following section, the NA22 data will be compared with this approximation and with results from other experiments.

7.4 Transformed variables

As already pointed out at the beginning of this chapter, one cannot perform a three-dimensional analysis in the usual variables rapidity y, azimuthal angle φ, and transverse momentum p_T, since the distribution in especially the latter is far from flat. Therefore, Ochs in [OCZP91] and Białas and Gaździcki in [BGPL90] have proposed methods to overcome this problem. In both papers, the authors suggest to use a normalized cumulative variable

$$X(y) = \frac{\int_{y_{min}}^{y} \rho(y')\mathrm{d}y'}{\int_{y_{min}}^{y_{max}} \rho(y')\mathrm{d}y'} \qquad (7.8)$$

Here, the initial interval is defined from y_{min} to y_{max}. From the definition follows

$$0 \leq X(y) \leq 1 \qquad (7.9)$$

The cumulative variable $X(y)$ has a flat density distribution (by construction)

$$\rho(y)dy = \rho(y(X)) \left| \frac{\partial y}{\partial X} \right| dX = \rho'(X)dX, \qquad (7.10)$$

since the Jacobian is given by

$$\left| \frac{\partial y}{\partial X} \right| = \left| \frac{\partial X}{\partial y} \right|^{-1} = \frac{C}{\rho(y)} \qquad (7.11)$$

yielding

$$\rho'(X) = C, \qquad (7.12)$$

independent of X.

Though in both cases this cumulative distribution is the basic idea, the higher-dimensional treatment differs. First, the Ochs method will be described, then the more elaborate Bialas and Gazdzicki technique will be shown to yield similar results.

7.4.1 Multidimensional intermittency analysis according to Ochs

The calculation of factorial moments for a transformed variable in one dimension requires two runs over the data sample. In the first run the density distribution $\rho(y)$ is calculated in a very fine grid. In the second run, y is used for each particle in the event and the corresponding cumulative variable $X(y)$ is determined for each particle.

An equal binning in $X(y)$ results in small y bins for large $\rho(y)$ and large y bins for small $\rho(y)$. In fig. 7.6 this is demonstrated for the p_T-transform. Fig. 7.6a shows the p_T distribution varying over 5 orders of magnitude. In fig. 7.6b the corresponding $\ln p_T^2$ distribution is the bell-shaped dashed curve. The solid line is the cumulative distribution. The horizontal lines divide $X(\ln p_T^2)$ into four equal intervals and the vertical lines indicate the corresponding intervals in $\ln p_T^2$.

To calculate the factorial moments the same procedure as for the usual one-dimensional case is followed. The range of the new variable, which is now between 0 and 1, is divided into M bins, and for each event the number of particles within such a bin is determined.

It is important to realize that, due to the fact that the inclusive distribution in the new variable is flat, horizontal and vertical averaging are equivalent. This has been verified experimentally.

It is found to be sufficient to use 100,000 bins in the original variable to obtain stable results on the factorial moments.

Weights can be easily taken into account. When in the initial run the density distribution is calculated with an event weight for each particle of a certain event, then the same should

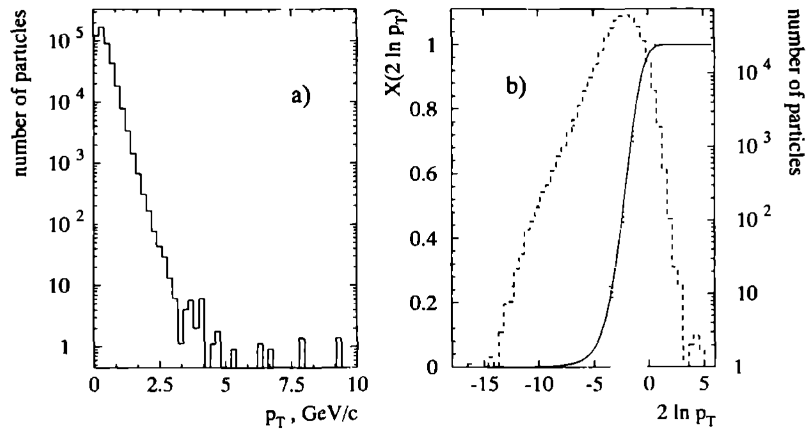

Figure 7.6: *a): The inclusive* p_T *distribution. b): The inclusive* $\ln p_T^2$ *distribution (dashed curve, right scale) and its cumulative counterpart* $X(\ln p_T^2)$ *(solid curve, left scale). The dotted lines show the correspondence between intervals in* X *and intervals in* $\ln p_T^2$.

be done in the second run, where the moments should be calculated with the corresponding event weight.

To go to higher dimensions, Ochs assumes that the density function in three dimensions factorizes,

$$\rho(y, \varphi, p_T) = \rho(y)\rho(\varphi)\rho(p_T). \tag{7.13}$$

Using this rather strong assumption, it is sufficient to calculate the cumulative distribution for the three variables, independently.

Ochs has studied two different ways to calculate the factorial moments. In the first, all variables are divided simultaneously into the same number of intervals. The alternative method consists of an azimuthal angle dependent division of the transverse interval, leading to bins with similar radial and azimuthal extension. It turns out that both yield approximately the same result, and therefore the easier first method is used here.

From fig. 7.7 it can be seen that assumption (7.13) is only approximately correct. In this figure, the transformed three-dimensional space is subdivided into $10 \cdot 10 \cdot 10$ boxes, and the number of particles in each box is counted. The large vertical bars (at positions 100, 200 etc.) indicate the 10 intervals in $X(y)$. Each such interval is divided into 10 intervals in $Y(\varphi)$, indicated by the smaller vertical bars. Finally, these intervals are subdivided once more in 10 $Z(\ln p_T^2)$ intervals. In this way the $10 \cdot 10 \cdot 10$ cube is projected onto one dimension. The lower figure is an enlarged detail of the second $X(y)$ interval. Though relatively flat, there is some structure visible, indicating that the method is not perfect. Therefore, Białas and Gazdzicki suggested another way of treating the higher-dimensional analysis. This will be described and compared to the Ochs method in the following subsection.

7.4.2 The Białas and Gazdzicki method

Independently from Ochs [OCZP91], Białas and Gazdzicki [BGPL90] investigated the possibility of using a transformed variable to study intermittency in three dimensions. Like Ochs, they found that the normalized cumulative distribution would best fit their purpose.

To show the influence of the choice of variables on the intermittency behavior in one dimension, they used the one- and two-particle density distributions. Assuming a singularity in the two-particle correlation function (or the two-particle density distribution) and various shapes for the single particle inclusive distributions, the authors found that the intermittent behavior in the new variable followed exactly the theoretically expected slope.

The higher-dimensional treatment of Białas and Gazdzicki is different from that of Ochs in that they do not assume factorization of the variables. Indeed, fig 7.7 discussed above shows that the three-dimensional inclusive distribution, using the factorization assumption, is only approximately constant.

To overcome this problem, the authors introduce three 'new' probability densities

$$P(x,y,z) = \frac{\rho(x,y,z)}{\int\int\int \mathrm{d}x\mathrm{d}y\mathrm{d}z\rho(x,y,z)} \tag{7.14}$$

$$P(x,y) = \int \mathrm{d}zP(x,y,z) \tag{7.15}$$

$$P(x) = \int \mathrm{d}y\mathrm{d}zP(x,y) \ . \tag{7.16}$$

Next, the transformation of (x,y,z) to (X,y,z) is performed,

$$X(x) = \int_{a_x}^{x} P(x)\mathrm{d}x \ . \tag{7.17}$$

Then (X,y,z) to (X,Y,z) by

$$Y(y) = \int_{a_y}^{y} P(x,y)\mathrm{d}y/P(x) = \int_{a_y}^{y} P(X,y)\mathrm{d}y \ , \tag{7.18}$$

and finally (X,Y,z) to (X,Y,Z), equivalently to the previous step,

$$Z(z) = \int_{a_z}^{z} P(x,y,z)\mathrm{d}z/P(x,y) = \int_{a_z}^{z} P(X,Y,z)\mathrm{d}z \ . \tag{7.19}$$

The Jacobian of this transformation is

$$\left|\frac{\partial(x,y,z)}{\partial(X,Y,Z)}\right| = \begin{vmatrix} \frac{\partial x}{\partial X} & \frac{\partial y}{\partial X} & \frac{\partial z}{\partial X} \\ \frac{\partial x}{\partial Y} & \frac{\partial y}{\partial Y} & \frac{\partial z}{\partial Y} \\ \frac{\partial x}{\partial Z} & \frac{\partial y}{\partial Z} & \frac{\partial z}{\partial Z} \end{vmatrix} = \frac{1}{P(x,y,z)} \ , \tag{7.20}$$

yielding

$$\rho'(X,Y,Z) = \text{constant.} \tag{7.21}$$

To apply this method to the data, a sorting algorithm [PODO90] has been used [1]. Two steps are necessary to determine the borders of the three variables y, φ and $\ln p_T^2$. First, four

---

[1] Thanks are due to O.Podobrin from the CELLO collaboration for supplying the program.

arrays, the particle number being the index, are filled with the rapidity y, the azimuthal angle φ, the transverse momentum $\ln p_T^2$, and the event number of the particle. Then, the particles are sorted in rapidity y. Next, the y-row is divided into M intervals of equal particle number. The particles in each interval of y are then sorted in φ and the resultant row is divided again into M parts of equal particle number. Finally, the particles in each of the M^2 intervals are sorted in $\ln p_T^2$, and M intervals of equal particle number are constructed.

To obtain the factorial moments, for each event the position of the particles in the new three-dimensional grid is determined, and the number of particles in each box is counted.

A drawback of the method is that weights cannot be taken into account. Therefore, a comparison has to be performed with the Ochs method without weights. Furthermore, due to computer memory limitations, the method can only be applied to the smaller, but cleanest, **p0bad** sample.

It is interesting to notice, that the size of the boxes, when expressed in the original variables, differs from one box to the other. This is a consequence of the fact that the density distribution is forced to be completely flat. An attempt to illustrate this difference with the Ochs procedure is made in fig. 7.8. There, the three-dimensional phase space is projected onto a surface. An interval in y and φ is marked by four solid horizontal and vertical lines. The initial $\ln p_T^2$ interval is scaled to fit a y interval. Then, one box in a certain $y - \varphi$ region is defined by two dashed lines (indicating the $\ln p_T^2$ interval) and two solid horizontal lines. The right figure corresponds to the Ochs method. The four φ intervals have the same borders in each y interval. In the left figure however, where the Białas and Gaździcki method is used, the φ borders are slightly shifted.

7.4.3 Comparison of the methods

Before proceeding to the more detailed description of the multidimensional data, a comparison between the two transformation methods is made.

In figure 7.9 the three-dimensional data are compiled. At each step, the three initial intervals are divided simultaneously into M bins ($M = 1, \ldots, 10$) yielding $M_3 = M^3$ boxes. The black squares represent the Ochs method for the weighted **p0bad** sample. The full triangles represent the unweighted Ochs method. The latter are always slightly lower, but exhibit the same trend.

The circles are the data obtained with the Białas and Gaździcki method (in the following denoted by B&G method). Originally, these data were normalized using the number of events that contribute with at least one particle to the initial interval ($N_{>0}$). The Ochs method is normalized using all events N_{all} as for the analysis in the original one- and two-dimensional variables. This results in a shift of the moments

$$F_q^{>0} = \left(\frac{N_{>0}}{N_{all}}\right)^q F_q^{all} \tag{7.22}$$

In the plot the $\ln F_q$ for the B&G method are shifted upward by $q \ln(N_{all}/N_{>0})$. The three-dimensional data (circles) correspond to $M_3 = 2^{(3\nu)}$ boxes, with $\nu = 0, \ldots, 6$. In addition, the two-dimensional data for B&G are plotted (open boxes) with $M_2 = 4^\nu$ and $\nu = 0, \ldots, 6$. Only for F_2 it makes sense to go to very small intervals ($\nu = 5, 6$).

The figure shows that the three-dimensional B&G method perfectly agrees with the unweighted Ochs method (in order to be able to distinguish the circles from the triangles,

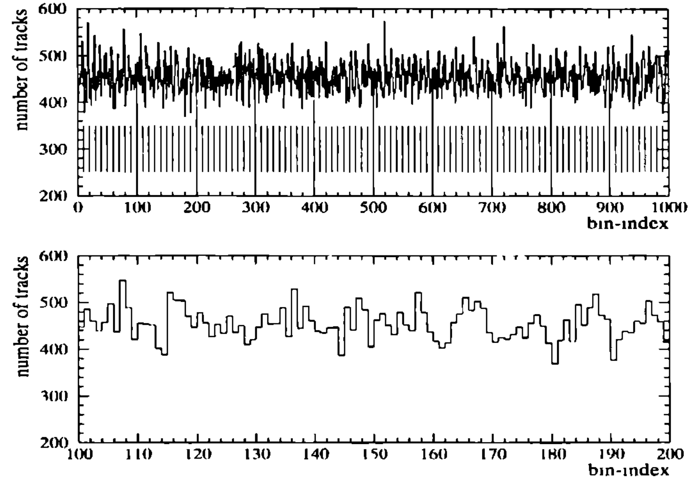

Figure 7.7: *The inclusive transformed three-dimensional particle distribution. The primary intervals between the large vertical bars correspond to 10 divisions in $X(y)$. The secondary intervals, indicated by the smaller vertical bars correspond with the division in $Y(\varphi)$ and are subdivided into 10 $Z(\ln p_T^2)$ intervals. The lower plot shows an enlarged version of bin 2 in $X(y)$. The sample used is* **p0bad** .

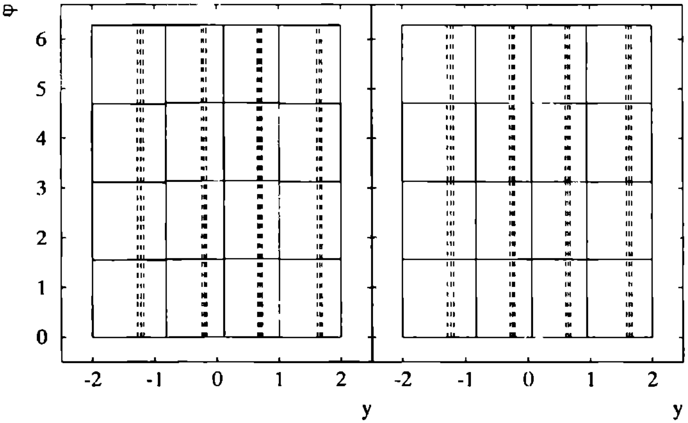

Figure 7.8: *The borders of bins in the original variables y, φ and $\ln p_T^2$. The left plot is for the Bialas and Gazdzicki method, where each box contains exactly the same number of particles. The right plot is for the Ochs method, where each variable is transformed independently of the other two. The solid vertical lines divide the rapidity interval into 4 parts. Each y interval is divided into 4 φ intervals by the solid horizontal lines. The initial $\ln p_T^2$ interval is scaled to fit a y interval, and the four subintervals are marked by the dashed vertical lines. The difference between the two methods can best be seen from the small shift in horizontal lines from one y interval to the other in the left diagram.*

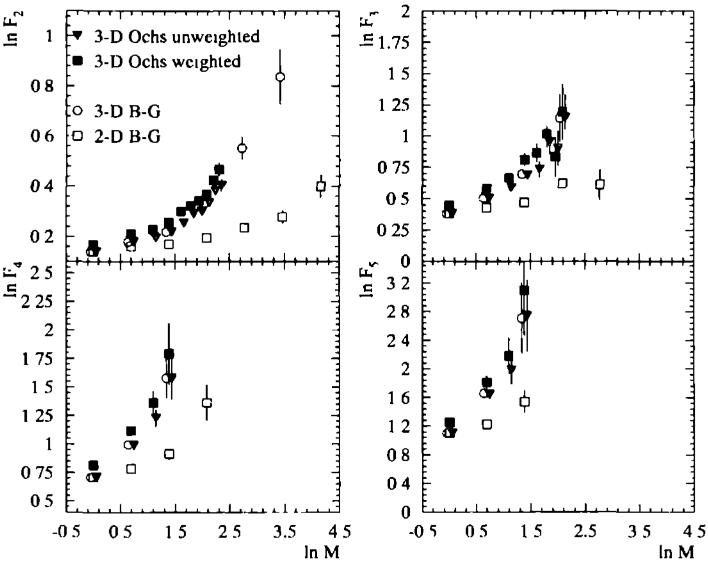

Figure 7.9: *The normalized factorial moments as a function of the bin-size. The Ochs data are vertically normalized. The binning is* $1^3, 2^3, \ldots, 10^3$ *in the cumulative variables. For the Bialas and Gazdzicki data, the binning is* 8^ν, $\nu = 0, \cdots, 6$ *at the maximum. All data exhibit the same rising trend, which is not a power-law behavior. In addition the two-dimensional data are plotted for the B&G method. The* **p0bad** *sample has been used.*

a small horizontal shift has been applied). A similar observation has been made for the two-dimensional data. This is expected, since for the Ochs method the difference between horizontal and vertical averaging has been found to be very small, in spite of the fluctuations in the inclusive spectrum (fig. 7.6).

7.5 Multidimensional factorial moments

In the previous section, it has been shown that there is almost no difference between the results obtained with the Ochs and B&G methods. Here, a comparison of data will be given in the various dimensions using the Ochs transform. In all cases, the sample used is **p0bad** with weights and the transformed variables will be referred to by their 'parent' symbol.

In fig. 7.10 a compilation is shown of the factorial moments F_2 to F_5 using the Ochs transform. The reliability of the errors has been checked using the method proposed in chapter 3 and found to be good. For each order, in the first point ($\ln M = 0$) the moments have the same value for the one-, two- and three-dimensional case. This is due to the fact that the same cuts are used on the initial interval in all cases:

$$\begin{gathered} -2 < y < 2 \\ 0 \leq \varphi \leq 2\pi \\ -18 < \ln(p_T^2) < 6 \\ (0.0012 \text{ GeV/c} < p_T < 20 \text{ GeV/c}) \ . \end{gathered} \tag{7.23}$$

The horizontal axis corresponds to the number of divisions M in one variable, thus $M_1 = M$, $M_2 = M^2$, and $M_3 = M^3$

It can be seen that the three-dimensional data rise fastest The two-dimensional $y - p_T$ data (asterisks) are also rising very fast This can be explained from the rise of the one-dimensional y as well as p_T data

From F_2 it follows that the three-dimensional moments (black squares) rise much faster than expected from a power law To study this in more detail, $\ln F_2$ and $\ln K_2 = \ln(F_2 - 1)$ are plotted in fig 7 11 a and b, respectively On the horizontal axis the logarithm of the inverse bin-size ($-\ln \delta\omega = \ln M_d = d \ln M$) is plotted, since in that case, a better comparison of the rise of the moments is possible For F_2 the power-law fits are shown (solid lines) and the fit regions are $M = 4$, ,40 for the one-dimensional moments (8 40 for φ), $M = 5$, ,18 for the two-dimensional moments, and $M = 1$, ,10 for the three dimensional F_2 In particular from the latter it becomes clear that there is a serious deviation from a straight line

In an attempt to explain this apparently too strong rise in three dimensions, Fiałkowski [FIALKO] and Eggers [EGGETH] (see also section 1 5 2) have suggested that the factorial *cumulant* moments rather than the factorial moments obey a power law To demonstrate that this is not the case, K_2 is plotted in fig 7 11b [2] However, in the same paper Fiałkowski [FIALKO] suggests to add a constant term c, representing possible long-range correlations, such that the second-order cumulant moment becomes

$$K_2(M_d) = aM_d^{\phi_2} + c \qquad (7\ 24)$$

This prediction has been tested for the three-dimensional K_2 using all 10 points in the fit The power ϕ_2 and the 'long-range' constant c are found to be 0 38 ± 0 07 and 0 16 ± 0 02, respectively [3] In the case of the unweighted **p0bad** sample, these values are $\phi_2 = 0\ 38 \pm 0\ 07$ and $c = 0\ 13 \pm 0\ 02$ In both cases the χ^2/NDF is better than one

It is remarkable that these powers correspond closely to those found in other experiments For example, in μp [IDMP91] Fiałkowski finds $\phi_2 = 0\ 45$ (the long-range correlation being 0) Similar values are found in pAu, OAu and SAu from [NA3591]

To investigate the modified power-law assumption of Ochs, the Ochs-plot is given in fig 7 12 for the indicated variables While in [OCZP91] data at small scales, where F_2 does not vary significantly, are rejected, here all points are presented This leads to a somewhat messy, but honest plot Notice the fact that, in rapidity third- and higher-order moments vary stronger than second order ones This is illustrated by the accumulation of the data at $\ln F_2 = 0\ 3$ Data for φ are not given, but it has been checked that they are on a straight line, even for the larger intervals This is remarkable, since from fig 7 10 it can be seen that the F_q themselves decrease for these interval sizes Thus, even the anti-correlations follow a modified power law

To be able to compare the NA22 results with other experiments, the modified power law has been fitted to the data To obtain meaningful results, only factorial moments in the larger intervals (down to $\delta\omega = 1/10^d$ for dimension d) are used, where F_2 still grows significantly For the useful variables (thus not for one-dimensional φ and two-dimensional $\varphi - p_T$), the Ochs plots are given in fig 7 13 The lines correspond to individual fits to

---

[2] A detailed analysis of factorial cumulant moments and the connection with the LPA will be given by M Charlet in [CHARTH] and in a NA22 paper [NA22KM]

[3] Including the bin-size correlations in the fit of the weighted data, ϕ_2 becomes 0 30 ± 0 04 and c decreases to 0 13 ± 0 01 [NA22KM]

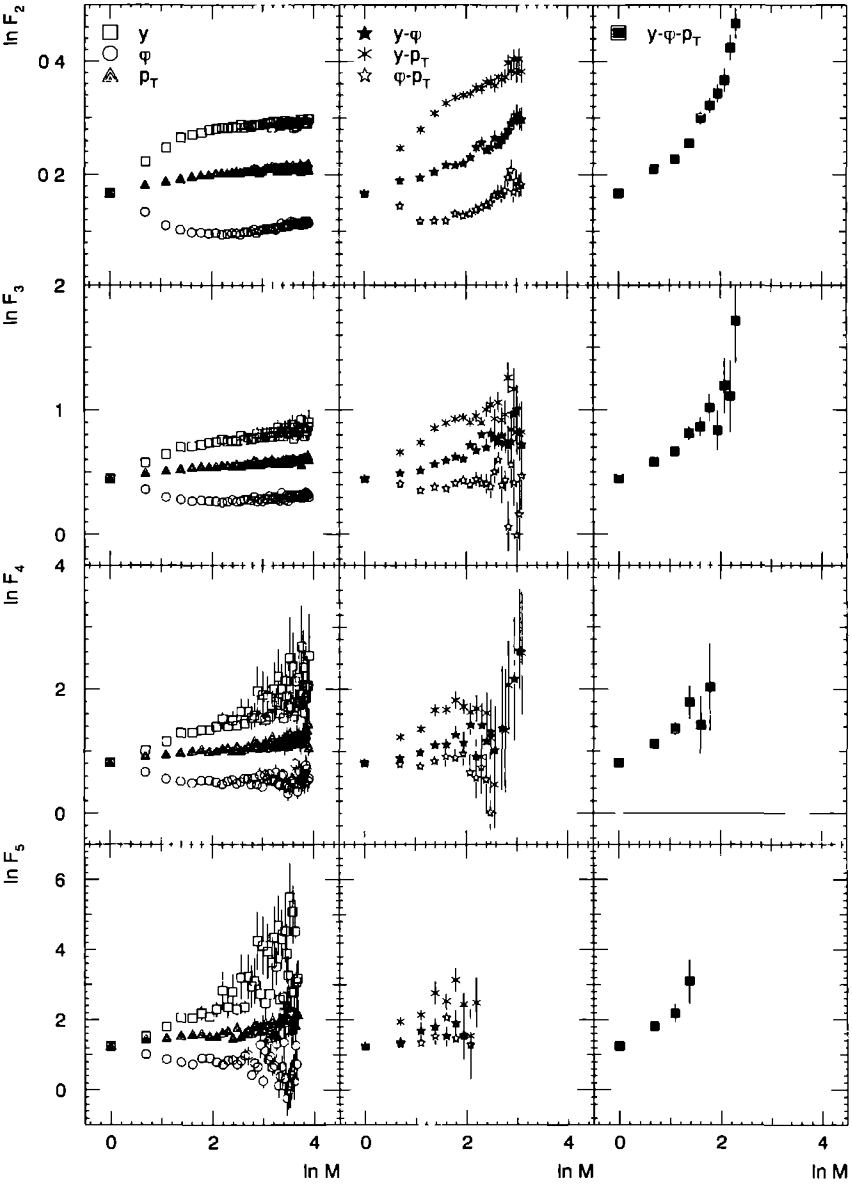

Figure 7.10: F_2, F_3, F_4 *and* F_5 *for one, two and three dimensions in the Ochs-transformed variables as indicated. The weighted* **p0bad** *sample has been used*

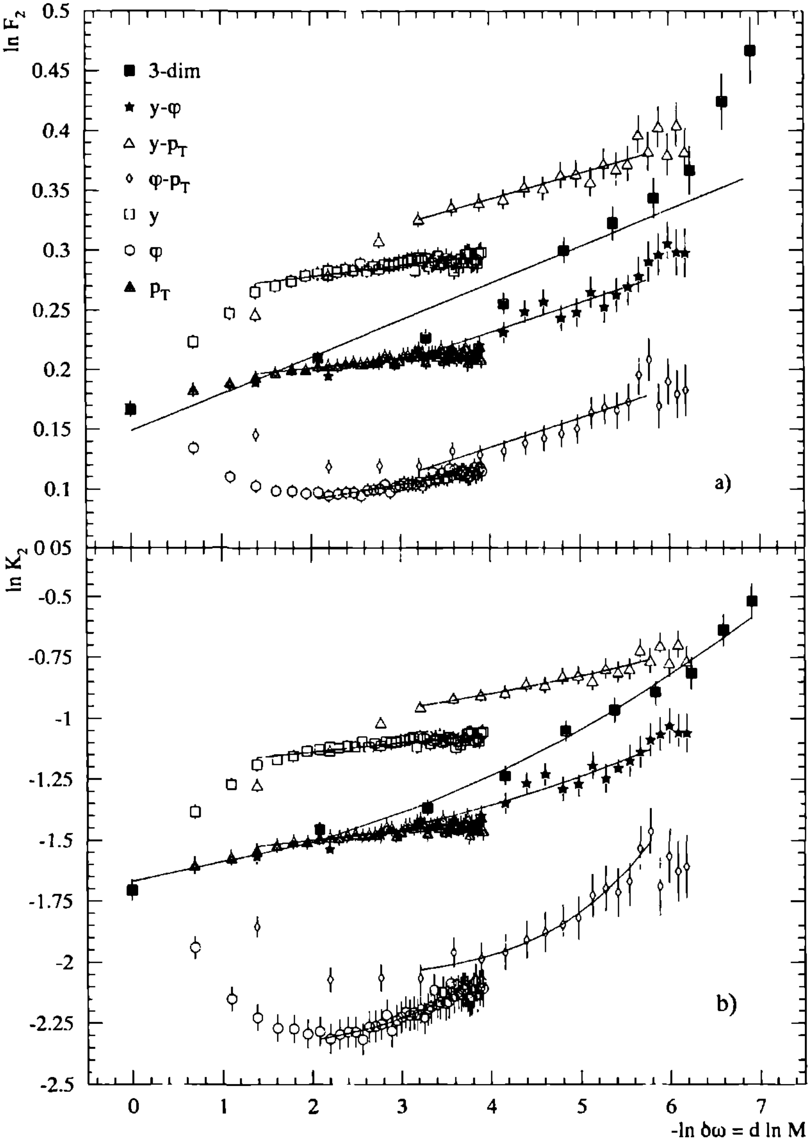

Figure 7.11: *F_2 and K_2 as a function of the 'box'-size $\delta\omega$ for the samples of fig. 7.10.*

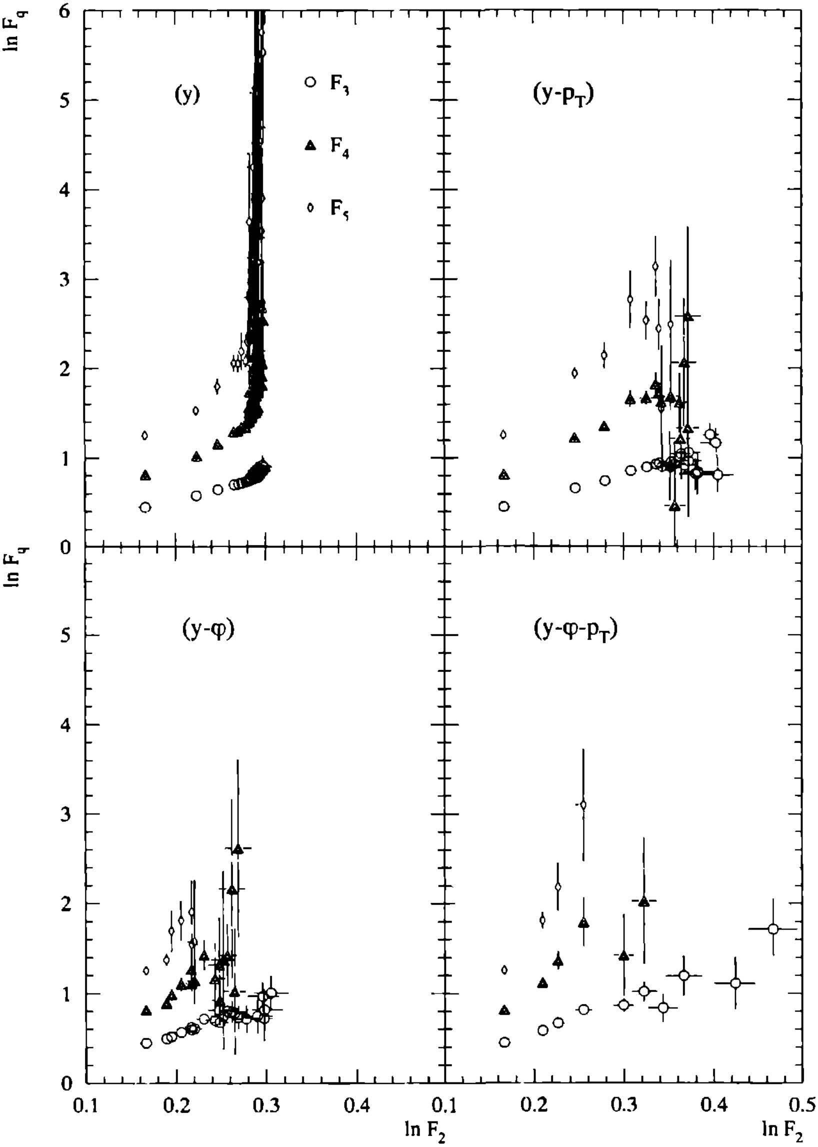

Figure 7.12: *Illustration of the modified power-law behavior, for each dimension separately: one-dimensional y, two-dimensional $y-\varphi$ and $y-p_T$ and three-dimensional $y-\varphi-p_T$, as indicated in the figure. The circles are F_3, triangles F_4 and the diamonds F_5.*

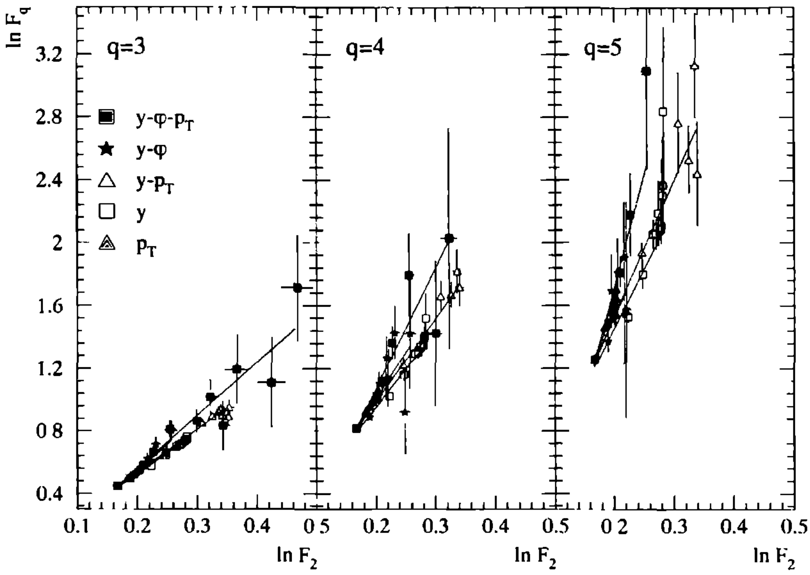

Figure 7.13: *The Ochs plot revisited. Only the divisions up to $M = 10$ are used. The lines represent the individual fits for the variables indicated*

these data according to (7.5). Contrary to the observation in [OCZP91], the slope $r_q = \alpha_q/\alpha_2$ depends on the dimension and is largest for the three-dimensional data. This changes when the fits are forced to have $\tilde{b}_q = 0$. Then, all slopes are similar.

The influence of biases (Dalitz decay and γ-conversion) has been studied using the FRITIOF Monte Carlo generator. The correction factor obtained from the 'plain' and the 'biased' FRITIOF (see chapter 5) data has been applied to the NA22 data. This is shown in fig. 7.14 for the three-dimensional data for orders two and three. Clearly the corrected data are lower than the original data, but the upward bending of the factorial moments is not changed. To see the influence of the correction procedure on the ratio r_3, in fig. 7.15 the Ochs-plot is shown for F_3 versus F_2. Due to the smaller variations of the corrected data in F_2 as well as F_3 (see fig. 7.14) the corrected data are concentrated in a smaller region. However, the slope r_3 obtained from the corrected and uncorrected data is approximately the same.

Because of the large uncertainties in FRITIOF the correction procedure has not been applied to higher-order moments. In the remaining part of this chapter only uncorrected data will be used.

A comparison of the slopes r_q for the different variables as well as for the combined sample (all five variables taken together) and for the weighted average is given in table 7.2. The fits of the other experiments are from [OCZP91]. From this table it can be concluded that the weighted average slopes are similar to those found from one-dimensional DELPHI data ($\sqrt{s}$ = 91 GeV) [DELPHI] and from one- and two-dimensional TASSO data ($\sqrt{s}$ = 35 GeV) [TASSO]. The fit of the combined NA22 sample corresponds more or less with the one- and two-dimensional EMC data ($\sqrt{s} = 4 - 20$ GeV) [DJSS90]. None of the samples agree with the *hh* data quoted by Ochs. This might be due to the fact that those early results

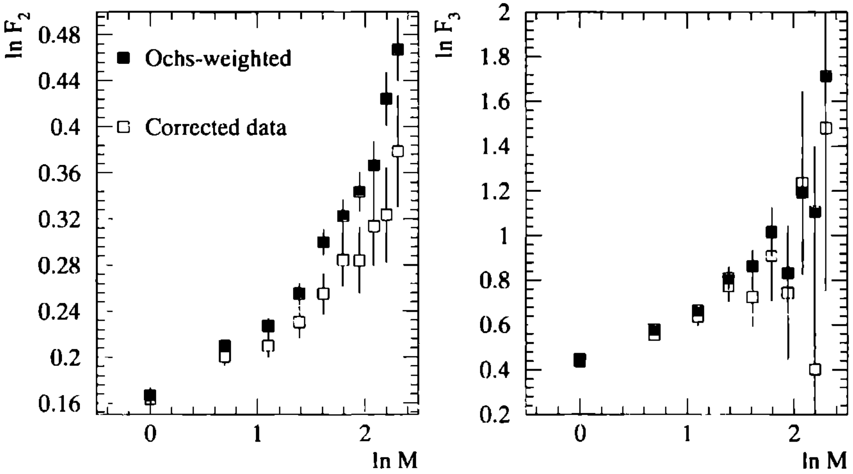

Figure 7.14: *The full squares are the uncorrected three-dimensional NA22 data, as shown in fig 7.10. The open squares are the data obtained after subtraction of bias from unseen Dalitz decay and γ-conversion.*

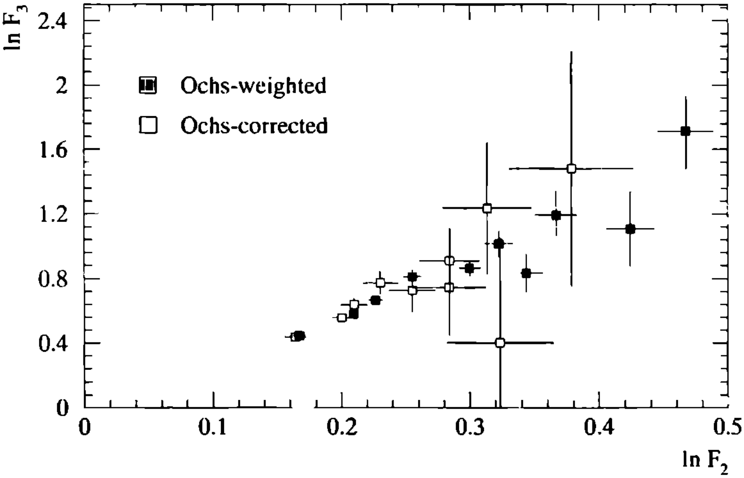

Figure 7.15: *The Ochs-plot for the uncorrected (full squares) and the corrected (open squares) three-dimensional NA22 factorial moments.*

		r_3	χ^2/NDF	r_4	χ^2/NDF	r_5	χ^2/NDF
NA22	y	2.63 ± 0.09	0.6	4.9 ± 0.2	3.6	7.7 ± 0.3	8.3
NA22	p_T	3.0 ± 0.3	0.1	6.2 ± 0.5	0.5	10.4 ± 0.7	1.3
NA22	$y - \varphi$	3.4 ± 0.2	1.8	6.1 ± 0.6	3.3	9 ± 2	1.9
NA22	$y - p_T$	2.75 ± 0.07	1.1	5.2 ± 0.2	2.8	8.6 ± 0.4	2.0
NA22	$y - \varphi - p_T$	3.4 ± 0.2	1.4	7.8 ± 0.5	1.2	14 ± 1	0.6
NA22	combined fit	2.64 ± 0.04	2.0	4.87 ± 0.09	3.9	7.8 ± 0.2	4.6
NA22	average	2.81 ± 0.04		5.29 ± 0.07		8.4 ± 0.1	
e^+e^-	TASSO,DELPHI	2.83 ± 0.11		5.32 ± 0.20		8.33 ± 0.33	
μp	EMC	2.60 ± 0.10		4.76 ± 0.22		7.9 ± 0.3	
hh	UA1, UA5, NA22	2.43 ± 0.10		4.3 ± 0.2		6.9 ± 0.3	
pA, AA	KLM,EMU01	2.86 ± 0.07		5.22 ± 0.22		8.2 ± 0.3	

Table 7.2: *Fits to the modified power law from equation (7.5). The values labeled average are the weighted averages of the results from the separate fits. Combined fit stands for all NA22 data fitted together. The lower four rows are from* [OCZP91].

have been obtained from y using no transformation.

The slopes r_q become of theoretical importance when they are related to the anomalous dimensions d_q (see equation (1.30))

$$\frac{d_q}{d_2} = \frac{\alpha_q}{\alpha_2(q-1)} = \frac{r_q}{q-1} . \tag{7.25}$$

Brax and Peschanski have shown in [BPPL91] that the Lévy-stable law can be used as an approximation to the final density distribution in the case of a self-similar multiplicative cascade process, as for example the α-model. The order dependence of the ratio (7.25) is then parametrized by

$$\frac{d_q}{d_2} = \frac{q^\mu - q}{2^\mu - 2}\frac{1}{q-1} . \tag{7.26}$$

The Lévy index μ in principle determines the shape of the density distribution. However, it has already been mentioned in 1.4.4 that only for few cases the distribution is expressible in analytical form. An important case is the Gaussian distribution with $\mu = 2$. If the central limit theorem is applied to the calculation of the moments for a cascade process, which was shown to be only a very first approximation [ABZP91], the ratio reduces to

$$\frac{d_q}{d_2} = \frac{q}{2} . \tag{7.27}$$

If the self-similarity is not due to a cascade process, but due to a second-order phase transition (e.g. quark-gluon plasma to hadrons) at the critical temperature, a monofractal behavior is expected [SANP89, BHPL91], resulting in a constant ratio. This would correspond to $\mu = 0$, a value not in the allowed range for the Lévy index ($0 < \mu \leq 2$).

In fig. 7.16a the ratio d_q/d_2 is plotted for the three-dimensional data and for the combined and average fits from table 7.2. The lines represent (7.26) with the μ values indicated. The three-dimensional data have $\mu > 2$ which is not allowed in the sense of Lévy-stable laws. The combined sample and the weighted average are close to the fit of [OCZP91]. The new

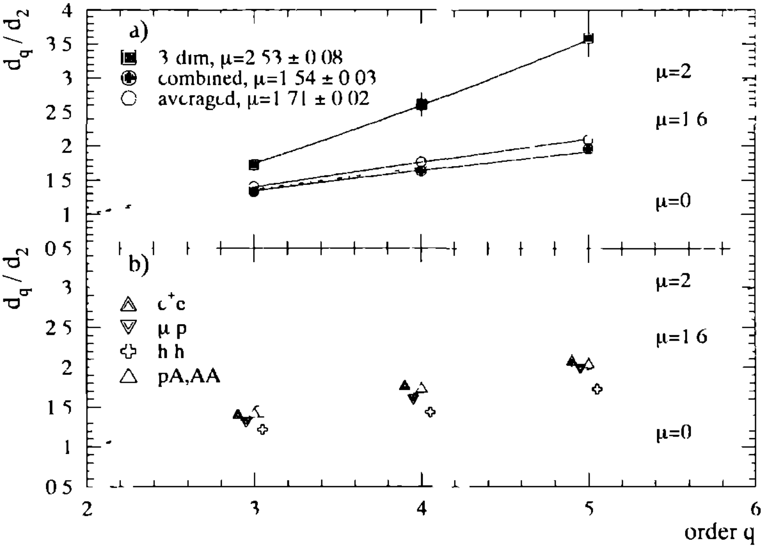

Figure 7.16 *a) The ratio d_q/d_2 for the three-dimensional data, the combined sample, and fit average. b) Data from experiments indicated. The dashed lines correspond to (7.27), the dotted lines to the mono fractal behavior. The dashed-dotted line is a fit from* [OC/P91] *with* $\mu = 1.6$

NA22 data are higher than the *hh* data quoted in the same paper and shown in fig. 7.16b. All results exclude the option of a second-order phase transition as a possible mechanism of multiparticle production, even in the case of *AA* interactions.

The conclusion of this section is that, to a certain extent, the data follow a modified power law. However, the slope r_q obtained from the Ochs-Wosiek relation is not independent of the dimension in which the factorial moment analysis is performed. For the three-dimensional data, this results in a value for the Levy index that is beyond the theoretically allowed region. Thus, the combination of the Ochs-Wosiek relation to describe the experimental data and the Levy-stable law to determine the shape of the underlying distribution is not very well suited to give a decisive conclusion about the origin of the multiparticle production process. The suggestion of Fialkowski, that a long-range correlation constant has to be added to a power-law behavior of the second-order factorial cumulant, works well for the three-dimensional data.

7.6 Bose-Einstein effect

To get a feeling for the influence of Bose-Einstein interference on the behavior of the factorial moments, the three-dimensional analysis has been repeated for particles of the same charge. In fig. 7.17 the second- and third-order moments are plotted. From this figure it is difficult to tell whether the rise of moments is stronger for like-sign particles than for all charged particles. This indicates that even the three dimensional data, in this form, fail to allow decisive conclusions.

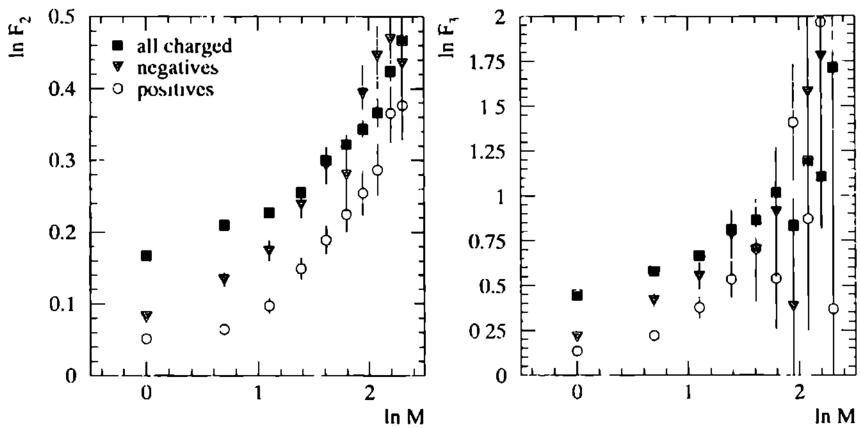

Figure 7.17: *The three-dimensional factorial moments for the weighted* **p0bad** *sample, using the Ochs transform. The data are calculated using all charged particles (squares), only negatives (triangles) and only positives (circles).*

7.6.1 The Density Integral and Bose-Einstein correlations

A better variable to analyse a three-dimensional phenomenon is used in explicit Bose-Einstein correlation studies. It is the 'momentum transfer' $Q^2 = -(p_1 - p_2)^2$ where p_1 and p_2 are four-momentum vectors. The variable Q^2 is related to the invariant mass of a pion pair by $M^2 = (p_1 + p_2)^2 = Q^2 + 4m^2$. The advantage of Q^2 is that it combines the features of a three-dimensional analysis with the larger statistics of the one-dimensional projection. To use this variable in the intermittency analysis, a modified procedure of calculating the factorial moments has to be applied. This procedure, called Correlation Integral Method [4] is extensively described in [LICI91, LCEB91]. The additional advantage over the usual bin-averaged normalized factorial moments is that the integration area is extended. This is illustrated in fig. 7.18 for the one-dimensional variable y. In fig. 7.18a the grey area indicates the integration domain for the usual second-order correlation function $C_2(y_1, 0)$ In fig 7.18b the second-order factorial moment domain is indicated. The total integration area is the sum over the boxes $\Omega_B = \sum_{m=1}^{M} \Omega_m$. The area in fig. 7.18c is a strip. All particles within this strip Ω_S have a pair-wise distance $|y_1 - y_2| < \delta y$. Then the usual normalized factorial moment turns into

$$F_q^S(\delta y) = \frac{\int_{\Omega_S} \prod_i dy_i \rho_q(y_1, \ldots, y_q)}{\int_{\Omega_S} \prod_i dy_i \rho_1(y_1) \cdots \rho_1(y_q)} \tag{7.28}$$

The consequence of extending the integration to a strip is that the normalization procedure is no longer straightforward. The denominator does not factorize anymore and to solve this problem, a 'track-pool' is used. This procedure is described in [LICI91] and in a forthcoming publication [NA22KM].

The actual determination of the moments F_q^S in any variable is just the counting of the number of particles that have a distance smaller than a certain resolution. Mathematically,

---

[4] The correct name should be Density Integral Method.

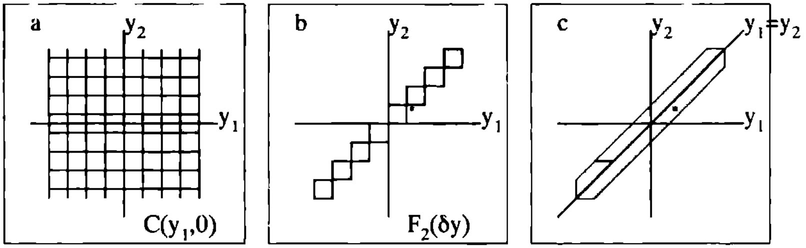

Figure 7.18: *Integration domains for a) the second-order correlation function, b) the second-order factorial moment, and c) the second-order density integral. The cross in b) indicates the position of a particle pair with $|y_1 - y_2| < \delta y$ that is excluded from the F_2 calculation due to the binning. In c) the point is included.*

this is expressed by

$$F_q^S(\delta y) = \frac{1}{\text{Norm}} \left\langle q! \sum_{i_1 < \dots < i_q} \theta\left(\delta y - \text{distance}(y_{i_1}^{ev}, \dots, y_{i_q}^{ev})\right)\right\rangle . \qquad (7.29)$$

The summation stands for the sum over all ordered q-tuples [5] and the brackets $\langle\rangle$ once more indicate the event average. Using the four-momentum as a variable and defining the distance as

$$\text{distance}(p_{i_1}^{ev}, \dots, p_{i_q}^{ev}) = \underset{\substack{\text{all pairs} \\ k_1, k_2}}{\text{Max}} \left\{-(p_{i_{k_1}}^{ev} - p_{i_{k_2}}^{ev})^2\right\} , \qquad (7.30)$$

for Q^2 the normalized density integral becomes

$$F_q^S(Q^2) = \frac{1}{\text{Norm}} \left\langle q! \sum_{i_1 < \dots < i_q} \prod_{\substack{\text{all pairs} \\ k_1, k_2}} \theta\left(Q^2 - Q^{2\,(ev)}_{i_{k_1}, i_{k_2}}\right)\right\rangle . \qquad (7.31)$$

Preliminary results are shown in fig. 7.19. Due to the absence of the arbitrary bin-splitting the curves are very smooth compared to the usual factorial moments. With this largely improved method, it is now clear that in the given range of Q^2 the like-sign (negative) data (triangles) show a much stronger rise than the all-charged data (black squares). For the second order it is possible to calculate the contribution of mixed (+−) pairs (circles). They are much flatter than the other two cases. Notice also the very small errors, even for the moments of higher order. These results are consistent with (preliminary) results from the UA1 collaboration [UA1C91].

From first Monte Carlo simulations with FRITIOF2.0 the following results are obtained. The 'plain' version is not able to describe the all-charged data, but the 'biased' version (Dalitz decay on and 0.25% undetected γ-conversions) reproduces these data rather well. However, as expected, both versions fail completely in describing the like-sign data. It would be very

---

[5] For n particles, there are $\binom{n}{q}$ ordered q-tuples. The factor $q!$ takes into account the number of permutations within a q-tuple

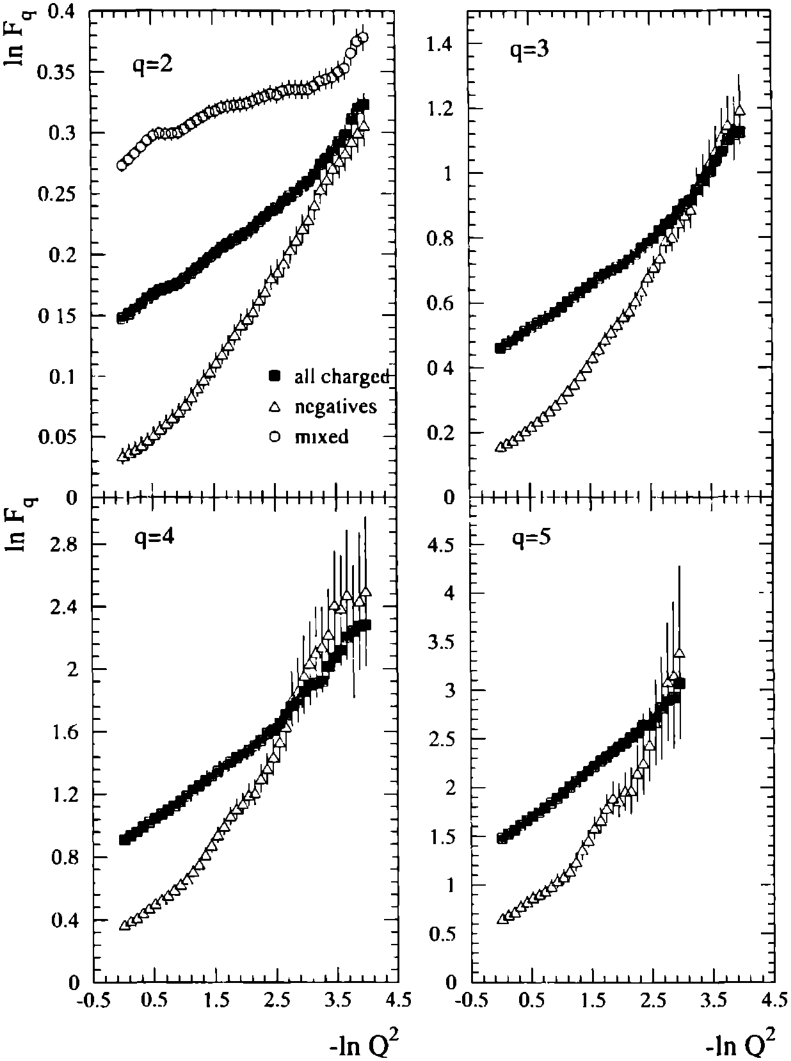

Figure 7.19: *The Density Integral Method applied to the unweighted* **p0bad** *sample. For each* Q^2 *value the number of clusters for which the pair-wise particle distance is smaller than the given value is counted. To get a feeling for the values on the horizontal axis:* $-lnQ^2 = 0.65$ *corresponds to the peak of the* ρ *meson,* 1.77 *is the value corresponding to the* K^0 *mass, Dalitz pairs and* γ*-conversion sets in for the mixed sample at* $-\ln Q^2 \approx 4$ [PODO90].

interesting to see whether Monte Carlos like JETSET 7.3 with and without Bose-Einstein are able to describe e^+e^- data of this kind.

If the observed effect is real, it might support a recently developed view by Bialas. In [ABPP92] Białas explains intermittency from Bose-Einstein correlations between (like-sign) pions. The power-law behavior is then obtained from the assumption that the size of the source, which is usually assumed to be fixed, fluctuates in a power-like manner. This fluctuation could be from event to event, with a regular shape of the interaction region in each event. However, another possibility is that the interaction region itself is a self-similar fractal extending over a very large volume. Though at this moment only speculative, it is an interesting new view because this explanation is not troubled by fragmentation and the decay of resonances.

7.7 Conclusion

The multidimensional factorial moment analysis is an improvement compared to the one-dimensional analysis. If an intermittency effect exists, it can be studied very well in three dimensions. The data do not yet allow a conclusion about the production process. The Ochs-Wosiek relation is not very well suited for three-dimensional data, at least not when the Lévy-stable law parameters have to be determined. The relation introduced by Fiałkowski turns out to describe the second order factorial cumulant very well. The parameter α_2, measuring the singularity strength, is found to be similar for a wide range of experiments. This indicates a sort of universal behavior in the multiparticle production process. The reason for this universality, however, is not yet clear.

In the last section a new, promising, method of correlation study is shortly introduced. The results support the idea that a large part of the observed intermittency effect can be attributed to the existence of Bose-Einstein correlations between pions of like charge, but with strongly fluctuating radius of the production zone.

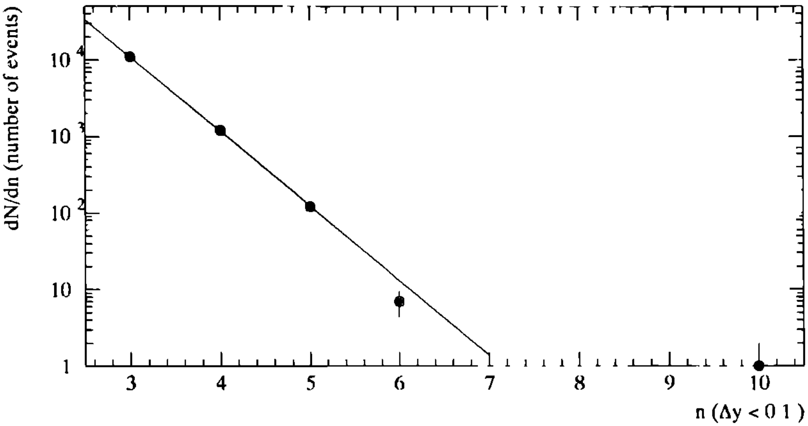

Figure 7 20 *The number of events N with a maximum of n particles within* $\Delta y = 0\ 1$

7.8 Appendix: The spike event

Some characteristics of the most prominent spike event will be given here This event was described in [NAPL87] In fig 7 20 the distribution of the number of events N, with a maximum of n charged particles inside 0 1 units of rapidity of the combined π^+ and K^+p **pMbad** sample is given Only the tracks with good quality are taken into account The anomalous event is indicated, and lies at n=10 It has been shown that from an extrapolation of the smooth behavior of the other events the probability to find an event with 10 particles inside a rapidity region of 0 1 units, corresponds to about 10^{-3} expected events in our sample

In fig 7 21 the anomalous event is plotted in two ways As a scatter plot in y and azimuthal angle φ, and as a projection onto the rapidity axis This event is one of 13 (12 for π^+p and 1 for K^+p) events with a charged topology of 26 in the **pMbad** sample, where in the **p0bad** sample it is the only 26 prong

The charged particles carry 57% of the total available energy All tracks are well measured in the bubble chamber or reconstructed in the downstream spectrometer, and have the best possible quality

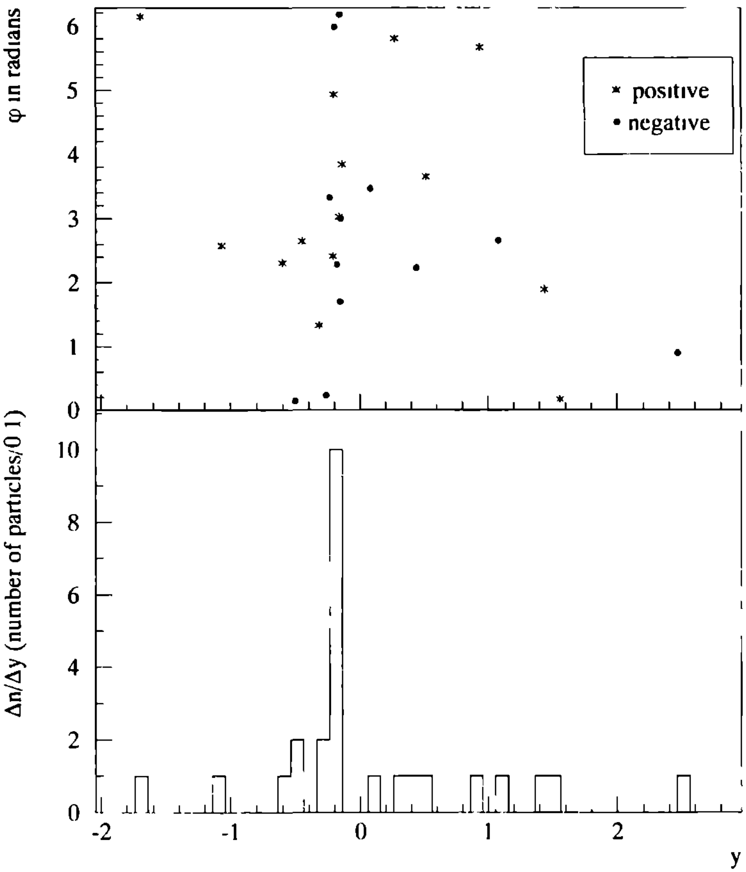

Figure 7.21: *The most prominent spike event. The left scale indicates the number of particles per tenth of rapidity units, and corresponds to the histogram bars The rights scale showing the azimuthal angle from 0 to 2π, corresponds to the scatter plot The dots stand for the negative particles, and the stars for the positives*

Bibliography

[ABZP91] J Alberty and A Białas, Z Phys C50 (1991) 315

[ABPP92] A Białas, Acta Phys Pol B23 (1992) 561

[BGPL90] A Białas and M Gazdzicki, Phys Lett B252 (1990) 483

[BHPL91] A Białas and R Hwa, Phys Lett B253 (1991) 436

[BPPL91] Ph Brax and R Peschanski, Phys Lett B253 (1991) 225

[BSPL90] A Białas and J Seixas, Phys Lett B250 (1990) 161

[CHARTH] M Charlet, Ph D thesis Univ of Nijmegen, in preparation

[DELPHI] P Abreu et al (DELPHI collab), Phys Lett B247 (1990) 137

[DJSS90] I Derado G Jansco, N Schmitz and P Stopa (EMC collab), Z Phys C47 (1990) 306

[EDBE89] E Den Bekker, Intermittency patterns in hadron-proton interactions at 250 GeV/c, diploma thesis Univ of Nijmegen HEN-324 (1989)

[EGGETH] H Eggers, Intermittency, moments and correlations in distributions of particles created in high-energy collisions, Ph D thesis Univ of Arizona, 1991

[FIALKO] K Fiałkowski, Phys Lett B272 (1991) 139

[FWAP89] K Fiałkowski, B Wosiek and J Wosiek, Acta Phys Pol B20 (1989) 639

[GYLH89] M Gyulassy, Is intermittency caused by Bose-Einstein interference?, Festschrift Léon Van Hove, eds A Giovannini and W Kittel (World Scientific, Singapore, 1989) p 479

[IDMP91] I Derado et al A study of fluctuations and correlations in deep inelastic muon-nucleon scattering at 280 GeV, MPI-PhE/91-08 (1991)

[LCEB91] P Lipa P Carruthers, H Eggers and B Buschbeck, The correlation integral as a probe of multiparticle correlations, AZPH-TH/91-53 (1991)

[LICI91] P Lipa, On the measurement of correlations and intermittency, AZPH-TH/91-45 (1991)

[MWNP84] G Marchesini and B R Webber, Nucl Phys B238 (1984) 1, B310 (1988) 461

[NAPL87] M Adamus et al (NA22 collab), Phys Lett B185 (1987) 200

[NAPL90] I Ajinenko et al (NA22 collab), Phys Lett B235 (1990) 373

[NA22KM] NA22 collab , Factorial moments, cumulants, correlators and correlation integrals in π^+p and K^+p interactions at 250 GeV/c, Nijmegen preprint HEN-353 in preparation

[NA3591] I. Derado (NA35 collab.), Proc. of the Ringberg workshop on Multiparticle production.

[OCPL90] W. Ochs, Phys. Lett. B247 (1990) 101.

[OCZP91] W. Ochs, Z. Phys. C50 (1991) 339.

[OWPL88] W. Ochs and J. Wosiek, Phys. Lett. B214 (1988) 617.

[OWPL89] W. Ochs and J. Wosiek, Phys. Lett. B232 (1989) 271.

[PODO90] O. Podobrin, Private Communication. I am very much indebted to this member of CELLO, for his fancy algorithm.

O. Podobrin, Cello results on multiparticle production, DESY 91-111, invited talk at Ringberg Workshop on Multiparticle Production, Germany, June 25-28 1991.

[POLY71] A. M. Polyakov, Sov. Phys. JETP 32 (1971); ibid. 33 (1971).

[SANP89] H. Satz, Nucl. Phys. B236 (1989) 613.

[TASSO] W. Braunschweig et al. (TASSO collab.), Phys. Lett. B231 (1989) 548.

[UA1C91] N. Neumeister et al. (UA1-MB collab.), CERN preprint PPE/91-156 (1991). I thank A. Białas for bringing these data to my attention.

8

Summary

The aim of this thesis is to gain a bit more understanding of the multiparticle production process by means of π^+/K^+ p interactions at 250 GeV/c beam momentum.

The experiment, described in chapter 2, makes use of a bubble chamber, used as target and vertex detector, and the European Hybrid Spectrometer, used for charged- and neutral-particle measurement. Two magnets allow for precise determination of charged-particle momentum. The 4π acceptance, the visual vertex detection and the long spectrometer lever arm provide for a good two-particle track resolution and minimize the possibility of track double-counting.

The goal is to describe recently discovered event-to-event fluctuations of charged-particle multiplicities in ever-decreasing regions of phase space. In chapter 1 it is shown that if these fluctuations were purely statistically (i.e. Poissonian) distributed, the normalized factorial moments of all orders would have to be equal to one, for all sizes of phase-space intervals δ considered.

However, if the underlying *dynamical* distribution is due to a self-similar cascade (for example in the particle density, as in the α-model), then the normalized factorial moments will rise according to a power law with decreasing size of the phase-space interval. In elementary-particle physics this behavior has been named *intermittency* by Białas and Peschanski, in analogy to the setting in of turbulence in hydrodynamics.

Chapter 3 describes the problems from which experiments with low average multiplicity and rather low statistics may suffer when using factorial moments. This so-called empty-bin effect is found not to play an important rôle in this experiment, except possibly for fifth order in small intervals.

In chapter 4 the method to determine the intermittency index is explained and the error calculation is described.

Since there is a one-to-one relation between factorial moments and multiparticle density distributions, a power-law behavior of the former shows up as a singularity in the latter. In chapters 5 and 6, describing the one-dimensional factorial moments, it is shown that, indeed, there is evidence for such a singularity. The attempt to reduce all higher-order correlations to merely (short-range) two-particle correlations, ultimately resulting in a Negative Binomial description of the data, is not successful in this experiment. Neither is there a strong indication that these experimental data can be explained by the correlations due to Bose-Einstein interference between like-sign particles.

In chapter 7 it is demonstrated that if intermittency is an effect in three-dimensional momentum space, much of the information is lost in a one- or two-dimensional projection, just as the shadow of a tree does not reveal much of the fractal structure of the branches Therefore, the analysis has been repeated in three dimensions, using the technique of transformed variables This results in a more than linear rise of the factorial moments in a double-logarithmic plot, not accounted for by experimental defects such as double counting of tracks or physical biases as Dalitz decay or nearby γ-conversions

It is shown that the upward bending of the second-order factorial moment can be parametrized by a power-law-behaved factorial *cumulant* plus a constant (possibly representing long-range effects), thus indicating a singularity in the two-particle correlation The remarkable fact is that a similar power law seems to hold for different experiments, with a similar value for the power The reason for this experimentally observed *universality*, however, is not yet known

A modified power-law behavior, predicting linearity in a double logarithmic plot of second- versus higher-order factorial moments, has also been tested Contrary to earlier observation, it is found not to be independent of the dimension Assuming that the underlying distribution can be described by a Lévy-stable function, the relation between the slope and the order can be parametrized with only one parameter For the three dimensional factorial moments this parameter is found to be larger than mathematically allowed The conclusion that can be drawn from these data is that a second-order phase-transition from a quark-gluon plasma to hadrons is excluded as a possible source of intermittency

Drawbacks of the standard method to determine factorial moments are the strong fluctuations due to the change of binning and the limited accessible integration region Therefore, the so-called Correlation Integral method has been introduced The results of this method are presented in the last paragraph of chapter 7 for the four-momentum transfer variable Q^2 A significant difference is observed between like-charged and all-charged data The latter can be described reasonably well by the FRITIOF Monte Carlo with γ-conversions and Dalitz decay The former however, showing a stronger rise than the all charged sample, are not described at all This can be understood from the absence of Bose Einstein correlations in the model

The pronounced difference between like-charged and all-charged data is not found using the conventional factorial moments, neither in one-, nor in two- or three dimensional analysis Therefore, special care should be taken in interpreting these earlier data

If, indeed, Bose Einstein correlations play such an important rôle, one is faced with the problem that standard B-E parametrizations with a constant source size do not predict a power law behavior This has given rise to speculations about a production zone with strongly fluctuating radius Since this should be typically an effect showing up in hadronic interactions, it would be very interesting to repeat the analysis for e^+e^- interactions

It is clear that the last word about *intermittency* in high-energy physics has not yet been spoken A more detailed study of the phenomenon is necessary for all types of interactions, the correlation integral being a step in the right direction Also other observables, such as the factorial correlators and cumulants, may reveal interesting properties

Samenvatting

Dichtheidsfluctuaties in π^+/K^+p wisselwerkingen bij 250 GeV/c

In dit proefschrift zijn bepaalde resultaten weergegeven van een hoogenergetisch botsings experiment, NA22 genaamd In dit experiment, dat in het kort in hoofdstuk 2 beschreven is, wordt een bundel van geladen mesonen (π^+ en K^+) met een impuls van 250 GeV/c op de protonen in een bellenvat geschoten Tijdens de wisselwerking tussen deze deeltjes worden vele nieuwe deeltjes (geladen en ongeladen) geproduceerd De impuls van de geladen deeltjes kan men zeer nauwkeurig meten met behulp van twee magneten, het bellenvat en een veelvoud aan detectoren Het experiment is zodanig geconstrueerd dat in principe ieder deeltje gemeten wordt, dat twee deeltjes die zich zeer dicht bij elkaar bevinden onderscheiden kunnen worden, en dat de kans op het dubbel tellen van één deeltje te verwaarlozen is

Om iets meer van de aard van de veeldeeltjesproductie te weten te komen, worden per botsing de deeltjes geteld die zich in een bepaald gebied van de impulsruimte bevinden De aantallen deeltjes zullen van gebeurtenis tot gebeurtenis verschillen Om er achter te komen of deze schommelingen afhankelijk zijn van de grootte δ van het impulsgebied, wordt deze gevarieerd Uit de deeltjesaantallen kunnen de factoriele momenten van verschillende ordes q berekend worden In hoofdstuk 1 is aangetoond dat, wanneer de fluctuaties puur statistisch van aard zijn, de genormeerde factoriele momenten van iedere orde en voor alle waarden van δ constant en gelijk aan één zullen zijn Een afwijking van dit gedrag impliceert de aanwezigheid van een bepaalde onderliggende dynamica

Indien deze dynamica het gevolg is van een splitsingsproces, waarbij iedere vertakking min of meer een kopie van de voorgaande is, dan zullen de genormeerde factoriele momenten stijgen als een machtsfunctie van de afnemende intervalgrootte δ Białas en Peschanski hebben dit gedrag intermittency genoemd

Experimenten met een gemiddeld klein aantal geproduceerde deeltjes en/of met een niet al te groot aantal gebeurtenissen kunnen problemen ondervinden bij het gebruik van de factoriele momenten als maat voor de fluctuaties Het 'lege doosjes' effect dat dan optreedt wordt beschreven in hoofdstuk 3 Voor het NA22 experiment is er geen serieus probleem, behalve wellicht voor de factoriele momenten van vijfde orde in kleine intervallen

In hoofdstuk 4 wordt beschreven hoe de fouten op de factoriele momenten berekend zijn en hoe de sterkte van het intermittency effect bepaald kan worden

Uit hoofdstuk 1 blijkt dat een factorieel moment van orde q gelijk is aan de geintegreerde dichtheidsverdeling van q deeltjes Dat betekent dat een machtsafhankelijkheid van de eerste overeenkomt met een singulariteit in de dichtheidsfunctie Uit de ééndimensionale factoriele momenten zoals beschreven in de hoofdstukken 5 en 6 blijkt inderdaad dat er een aanwijzing is voor een singulariteit. De poging om alle correlaties van hogere dan tweede orde terug te brengen brengen tot combinaties van tweedeeltjescorrelaties, hetgeen, bij benadering, resulteert in een Negatief Binomiaal verdeling van de deeltjesaantallen, blijkt voor de NA22 data niet succesvol te zijn. In de ééndimensionale data is er geen sterke aanwijzing dat het geobserveerde intermittency effect volledig is terug te voeren op Bose-Einstein interferentie van pionen met gelijke lading.

In hoofdstuk 7 is aangetoond dat, wanneer intermittency een proces is dat zich in de driedimensionale impulsruimte afspeelt, veel van het oorspronkelijke effect verloren gaat wanneer geintegreerd wordt over een of twee van de drie onafhankelijke variabelen: de schaduw van een boom geeft over het algemeen ook weinig informatie over de fijne structuur van de takken. Derhalve is de hele analyse herhaald in drie dimensies, waarbij echter, om bepaalde problemen te omzeilen, de oorspronkelijke variabelen getransformeerd dienen te worden. Het resultaat is dat, in een dubbellogaritmische grafiek, de factoriele momenten sterker dan lineair stijgen. Dit gedrag kan niet worden verklaard door experimentele onvolkomenheden zoals het dubbel tellen van deeltjes of door fysische effecten zoals Dalitz verval of γ-conversies nabij het wisselwerkingspunt.

Het blijkt dat de opwaartse kromming van het genormeerde factorieel moment van tweede orde verklaard kan worden door aan te nemen dat de tweedeeltjescorrelatie singulier is en door een extra constante in te voeren die mogelijke langedrachtscorrelaties beschrijft. Het opmerkelijke van deze parametrizatie is dat voor verschillende experimenten ongeveer gelijke machten gevonden worden. Het hoe en waarom van deze universaliteit is echter nog niet duidelijk.

Nadere bestudering van de data toont aan dat er een lineair verband bestaat tussen de logaritmen van de tweede-orde en derde- en hogere-orde factoriele momenten. De richtingscoefficienten zijn afhankelijk van de dimensie, en hun afhankelijkheid van de orde sluit een tweede-orde fase overgang van een quark-gluonplasma naar hadronen als mogelijke oorzaak van intermittency uit.

De standaard methode om de factoriele momenten te bepalen heeft twee nadelen: er treden sterke fluctuaties op wanneer de intervalgrenzen veranderd worden en er is, vanwege de verdeling in intervallen, slechts een beperkt gebied beschikbaar voor integratie. Bij de zogenaamde Correlatie Integraal methode treedt het eerste nadeel niet op en wordt het integratiedomein vergroot. Het resultaat van deze nieuwe methode is in de laatste paragraaf van hoofdstuk 7 getoond voor de variabele Q^2. De momenten stijgen veel sterker indien de analyse beperkt wordt tot deeltjes van gelijke lading dan wanneer alle geladen deeltjes gebruikt worden. De FRITIOF Monte Carlo blijkt het laatste geval redelijk te kunnen beschrijven, maar het eerste geval absoluut niet. Een verklaring hiervoor is dat FRITIOF geen Bose-Einstein correlaties bevat.

Het feit dat dit opmerkelijke verschil niet is waargenomen bij de 'conventionele' factoriele momenten in de één- en twee-dimensionale variabelen duidt er op dat men voorzichtig moet zijn met het interpreteren van deze data.

Het is duidelijk dat het laatste woord over intermittency in de hoge-energiefysica nog niet gesproken is. Een meer gedetailleerde studie van het fenomeen is noodzakelijk. Naast de Correlatie Integraal zijn er ook nog andere observabelen, zoals de factoriele correlatoren en cumulanten, die interesante eigenschappen van het productieproces bloot kunnen leggen.

Curriculum Vitae

Frank Botterweck

Geboren 28 december 1963 te Geleen. Gymnasium β doorlopen aan scholengemeenschap St. Michiel, eveneens te Geleen, in de periode van 1976 tot 1982. Volgde in Nijmegen de natuurkundestudie met als bijvak informatica, in de periode van 1982 tot 1987. Afgestudeerd bij de afdeling theoretische hoge-energiefysica. Vanaf 1987 tot 1991 officieel in dienst bij de afdeling experimentele hoge-energiefysica. De onderwijs taak bestond uit het geven van werkcolleges in de vakken kernfysica en electrodynamica.

Een deel van het onderzoek dat gedurende de vier en een half jaar in samenwerking met de NA22 collaboratie is gedaan, is weergegeven in dit proefschrift.

Een studie naar de detectie mogelijkheden van het W' deeltje in de Large Hadron Collider is gepubliceerd in de Proceedings van de Large Hadron Collider Workshop in Aken, oktober 1990.

Vanaf 1 mei 1992 in dienst bij het Max-Planck-Institut für Physik in München.